Präparation und Analyse organischer Schichten mittels clusterinduzierter Desorption/Ionisation

Preparation and analysis of organic molecular layers by means of cluster-induced desorption/ionization

Kumulative Dissertation zur Erlangung des Doktorgrades der Naturwissenschaften (Dr. rer. nat.)

von

Karolin Pluschke geb. Bomhardt

November 2023

JUSTUS-LIEBIG-UNIVERSITÄT GIESSEN

Fachbereich 07
Institut für Angewandte Physik

Eingereicht am:	09.11.2023
Als Dissertation angenommen am:	14.11.2023
Tag der mündlichen Prüfung:	20.12.2023
Erstgutachter:	Prof. Dr. Michael Dürr
Zweitgutachter:	Priv.-Doz. Dr. Marcus Rohnke

Zusammenfassung

In dieser kumulativen Dissertation wurde die Desorption/Ionisation durch neutrale Cluster (engl.: Desorption/Ionization induced by Neutral Clusters, kurz: DINeC) zum einen zur Präparation dünner Filme organischer Moleküle (kurz: DINeC-Depo) und zum anderen in Kombination mit Massenspektrometrie (kurz: DINeC-MS) zur Analyse unterschiedlicher organischer Systeme verwendet. Grundlage der Experimente ist dabei die fragmentationsfreie und oberflächenempfindliche Desorption organischer Moleküle von Oberflächen durch neutrale SO_2-Cluster.
Für die mittels DINeC-Depo präparierten Schichten konnte mittels DINeC-MS gezeigt werden, dass sie aus intakt abgeschiedenen Biomolekülen bestehen. Dabei können sie aus einer oder mehreren unterschiedlichen Molekülsorten aufgebaut sein. Ein Vergleich mit verwandten Depositionsmethoden demonstriert, dass der Anteil intakter Moleküle nur bei der Elektrospray-Ionenstrahl-Deposition in der gleichen Größenordnung liegt.
Die fragmentationsfreie Desorption ist auch für die Identifikation von Farbstoffen in Textmarkertinten von entscheidender Bedeutung, da sich die verschiedenen Farbstoffe ähnlicher Farbe oft nur durch einzelne Alkylgruppen unterscheiden, die bei Zersetzungsprozessen oder auch unter harten Desorptionsbedingungen abgespalten werden können. Des weiteren konnte die Zersetzung von Farbstoffmolekülen durch Wärmezufuhr bzw. UV-Strahlung auf der Basis der DINeC-Massenspektren unterschieden werden, da keine zusätzlichen Fragmente durch den Desorption/Ionisationsprozess induziert werden.
Die Oberflächenempfindlichkeit der Methode wurde zum einen genutzt, um die Oberflächenzusammensetzung verschiedener ionischer Flüssigkeiten zu bestimmen. Dabei wurde in Übereinstimmung mit der Literatur beobachtet, dass Kationen mit langen Alkylketten sich bevorzugt an der Oberfläche anlagern; die Tendenz nimmt mit steigender Größe des Anions ab. In dünnen Filmen auf SiO_2-Substraten ist die Anreicherung der Kationen an der Oberfläche durch den Einfluss des Substrats verstärkt.
Mittels DINeC-Depo hergestellte dünne Schichten aus organischen Molekülen zeigen ebenfalls eine starke Beeinflussung durch das Substrat, allerdings mehr in Bezug auf die chemischen Eigenschaften. Die deponierten Moleküle reagieren beispielsweise mit Oberflächenadsorbaten, nachweisbar in Form von Adduktpeaks in den Massenspektren. Weitere Reaktionen der durch DINeC-Depo abgeschiedenen Moleküle, zum Teil ausgelöst durch Wechselwirkungen mit dem Substrat, konnten ebenfalls untersucht werden. So wurden Oxidationsreaktionen verschiedener Peptide auf die Aktivierung des Substrats oder leicht oxidierbare Aminosäuren zurückgeführt. Für die mittels DINeC-Depo präparierten Proben wurde im Allgemeinen eine höhere Reaktivität beobachtet, die darauf zurückzuführen ist, dass die einzelnen Moleküle auf der Oberfläche stärker isoliert vorliegen. Dies wurde auch bei der Metallisierung von Porphyrinen durch DINeC-Depo ausgenutzt, bei der ein Metallion aus der Oberfläche, in den Ring des deponierten Porphyrins

eingebaut wurde.

Abstract

In this thesis, desorption/ionisation induced by neutral clusters (short: DINeC) was on the one hand used to prepare thin films of organic molecules (short: DINeC-Depo) and on the other hand, it was applied in combination with mass spectrometry (short: DINeC-MS) for the analysis of different organic systems. The experiments are based on the fragmentation-free and surface-sensitive desorption of organic molecules from surfaces by means of neutral SO_2 clusters.
For thin films prepared by means of DINeC-Depo, it was shown by means of DINeC-MS that biomolecules were transferred intact onto the substrate surface. Films of mixed molecules were deposited when using two different types of source molecules. A comparison with related deposition methods shows that only electrospray ion beam deposition allows for the deposition of intact molecules in comparable concentration.
Fragmentation-free desorption is also crucial for the identification of dyes e.g., in highlighter inks, as the various dyes of similar colour often differ only by individual alkyl groups which can be cleaved during decomposition processes or under harsh desorption conditions. In addition, the decomposition of dye molecules by heat or UV light could be distinguished in the DINeC mass spectra based on the fragment peaks observed, as no additional fragments are induced by the desorption/ionisation process as such.
The surface sensitivity of the method was used to determine the surface composition of various ionic liquids. It was observed that cations with long alkyl chains tend to accumulate on the surface; this tendency decreases with increasing size of the anion. In thin films on SiO_2 substrates, this accumulation of cations on the surface is enhanced by the influence of the substrate.
Thin films of organic molecules prepared via DINeC-Depo were shown to exhibit a strong influence of the substrate but rather with respect to their chemical properties. For example, the molecules deposited via DINeC-Depo were observed to react with surface adsorbates which were detected in the form of adduct peaks in the mass spectra. Reactions of the molecules deposited by DINeC-Depo, to some extend triggered by interactions with the substrate, were also studied. E.g., oxidation reactions of various peptides were attributed to the activation of the substrate or amino acids which can be readily oxidized. A higher reactivity was typically observed for samples prepared via DINeC-Depo due to the high degree of isolation of the individual molecules on the surface. This was also exploited in the metallisation of porphyrins, where a metal ion of the surface was incorporated into the ring of the deposited porphyrin.

Liste der Publikationen

Artikel I bis **III** wurden im Rahmen der kumulativen Dissertation in Fachzeitschriften publiziert. Die Kernaussagen der Publikationen und die Eigenleistung der Autorin werden im folgenden dargestellt:

I Cluster-induced desorption/ionization mass spectrometry of highlighter ink: unambiguous identification of dyes and degradation processes based on fragmentation-free desorption
K. Bomhardt, P. Schneider, M. Rohnke, C. R. Gebhardt, and M. Dürr; *Analyst* **147**, 333 - 340 (2022).

In **Artikel I** wird die Desorption/Ionisation mittels neutraler Cluster in Kombination mit der Massenspektrometrie verwendet, um die Zusammensetzung von Textmarkertinten zu untersuchen und die darin enthaltenen Farbstoffe eindeutig zuzuordnen. Die Zersetzung dieser Farbstoffe durch Wärmezufuhr oder UV-Licht kann aufgrund der fragmentationsfreien Natur der Desorptionsmethode untersucht und in den jeweiligen Spektren durch unterschiedliche Zersetzungsprodukte unterschieden werden. Bei Proben mit sukzessiv aufgetragener Tinte kann durch die hohe Oberflächenempfindlichkeit der Methode die oberste Tintenschicht identifiziert werden.

KB führte die DINeC-MS Experimente durch und realisierte mit Hilfe von MR die SIMS Messungen. Die Ergebnisse wurden von KB und MD interpretiert. KB verfasste eine erste Version des Manuskripts, welches anschließend mit Unterstützung von PS, MR, CRG und MD ergänzt und verbessert wurde.

II Surface Properties of Ionic Liquids: A Mass Spectrometric View Based on Soft Cluster-Induced Desorption
K. Bomhardt, P. Schneider, T. Glaser, and M. Dürr; *J. Am. Soc. Mass Spectrom.* **33**, 974 - 980 (2022).

In **Artikel II** wird die molekulare Oberflächenzusammensetzung verschiedener ionischer Flüssigkeiten mittels DINeC-MS untersucht. Je nach Zusammensetzung der ionischen Flüssigkeit lagern sich unterschiedliche Ionen bevorzugt an der Oberfläche an. So neigen Kationen mit langen Alkylketten in Kombination mit kleinen Anionen zur Aggregation an der Oberfläche; diese Tendenz nimmt mit zunehmender Größe der Anionen ab. In dünnen Filmen der ionischen Flüssigkeit kann die Anreicherung einer Ionensorte an der Oberfläche durch Wechselwirkung mit der Substratoberfläche weiter verstärkt werden.

KB führte die Experimente durch und interpretierte anschließend die Ergebnisse zusammen mit PS und MD. KB verfasste eine erste Version des Manuskripts, welches anschließend mit Unterstützung von PS, TG, und MD ergänzt und verbessert wurde.

III Soft deposition of organic molecules based on cluster-induced desorption for the investigation of on-surface and surface-mediated reactions

K. Pluschke, A. Herrmann, and M. Dürr; *ACS Omega* **8**, 40639 - 40646 (2023).

In **Artikel III** wird die Deposition verschiedener organischer Moleküle durch Desorption der Moleküle aus einem Volumenfilm mittels clusterinduzierter Desorption untersucht. Massenspektren und Quarzkristall-Mikrowaagen-Messungen der Proben zeigen qualitativ und quantitativ den intakten Transfer weniger Monolagen der Moleküle. Gemischte Schichten wurden durch die Deposition mittels Desorption zweier Peptide erzeugt und das Mischungsverhältnis mittels DINeC-MS analysiert. Reaktionen der abgeschiedenen Moleküle mit Adsorbaten der Oberflächen und Oxidationsreaktionen eines Peptids wurden untersucht und der Einfluss der Präparationsmethode auf die jeweiligen Prozesse diskutiert.

KP konstruierte die verwendete Kammer und führte die Experimente mit Hilfe von AH durch. Die Ergebnisse wurden von KP und MD interpretiert. KP verfasste eine erste Version des Manuskripts, welches anschließend zusammen mit MD und AH ergänzt und verbessert wurde.

Inhaltsverzeichnis

1 | Einleitung

Biomolekulare Oberflächenbeschichtungen werden aufgrund ihrer spezifischen Oberflächeneigenschaften in einer Vielzahl von Anwendungen eingesetzt bzw. auf ihre Anwendungsgebiete hin getestet [1, 2]. So kann eine biomolekulare Schicht beispielsweise die Biokompatibilität von Implantaten erhöhen [3] oder Oberflächen vor Korrosion schützen [4]. Als dünne Schicht zwischen zwei Elektroden können Biomoleküle in Resistive Random Access Memory (RRAM) durch Änderung des elektrischen Widerstands zur Informationsspeicherung eingesetzt werden [5]. Ebenso werden bei der Herstellung von Biosensoren [6, 7] dünne Schichten verschiedener Biomoleküle zur biologischen Erkennung unterschiedlicher Substanzen verwendet [8]. Diese Schichten können durch nasschemische Verfahren [9–11], aber auch durch verschiedene Arten der chemischen [12–14] oder physikalischen [15, 16] Gasphasenabscheidung erzeugt werden. Einige der Methoden erfordern eine erhöhte Temperatur der abzuscheidenden Moleküle, was insbesondere bei Biomolekülen zur Zersetzung führen kann [17–19].
Die im Rahmen dieser Arbeit entwickelte Depositionsmethode verwendet die Desorption/Ionisation mittels neutraler SO_2-Cluster (DINeC) für die Abscheidung verschiedener (bio)organischer Moleküle auf unterschiedlichen Substraten und wird im ersten Teil der Arbeit beschrieben. Eine schematische Darstellung des als DINeC-Depo abgekürzten Prozesses ist in Abb. 1.1(a) dargestellt. Die SO_2-Cluster desorbieren die Biomoleküle aus einem Volumenfilm. Dabei übertragen sie im Stoß mit der Oberfläche nicht nur die Energie für die Desorption der Moleküle, sondern bilden auch eine transiente Matrix, in der die zu desorbierenden Moleküle gelöst werden können. Die desorbierten Spezies können anschließend auf einem beliebigen Substrat abgeschieden werden. Das Verfahren ist durch den stattfindenden Lösungsprozess besonders schonend für Biomoleküle, sodass mehr als 98% der Moleküle intakt übertragen werden. Je nach Dauer des Depositionsprozesses können einzelne Moleküle in Submonolagen (Abb. 1.2(a)) bis hin zu mehreren Monolagen auf einem Substrat abgeschieden werden. Wenn die Molekülquelle während des Depositionsprozesses durch eine andere ersetzt wird, können gemischte Schichten hergestellt werden, wie in Abb. 1.2(b) schematisch gezeigt. Es wird generell eine erhöhte Reaktivität gegenüber anderen Oberflächenadsorbaten und der umgebenden Gasphase beobachtet (Abb. 1.2(c)), die darauf zurückgeführt wird, dass die Moleküle isoliert auf der Oberfläche vorliegen.
Für die Analyse dieser organischen Schichten und auch anderer empfindlicher Probensysteme ist eine Technik erforderlich, die ausreichend sanft ist, um die Oberflächeneigenschaften genau widerzuspiegeln. Auch hierfür kann die Desorption/Ionisation mittels neutraler SO_2-Cluster, jetzt in Kombination mit Massenspektrometrie, eingesetzt werden. Die Grundlagen für die massenspektrometrische Analyse wurden bereits Anfang des letzten Jahrhunderts gelegt [20–23] und ver-

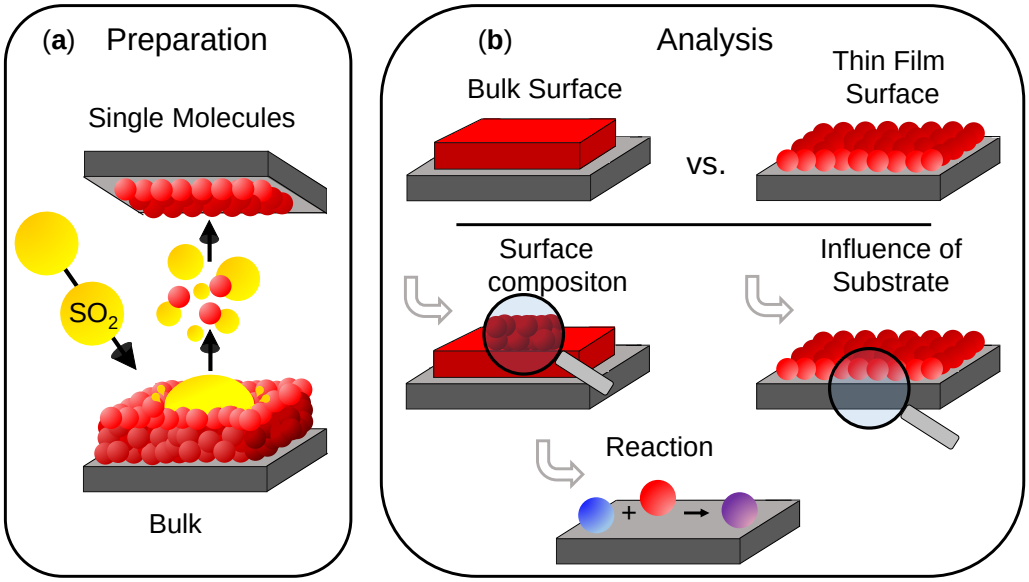

Abbildung 1.1: Schematische Darstellung der in dieser Arbeit thematisierten Teilgebiete der Präparation und Analyse organischer Schichten mittels clusterinduzierter Desorption. (a) Schematische Darstellung des DINeC-Depo Prozesses zur Abscheidung intakter Biomoleküle mittels clusterinduzierter Desorption von einem dicken Molekülfilm auf ein beliebiges Substrat. (b) Schematische Darstellung der mittels DINeC-MS untersuchten Aspekte (Oberflächenzusammensetzung, Substrateinfluss und Reaktionen) an unterschiedlichen Probensystemen.

schiedene Aspekte der Methode wurden mit Nobelpreisen gewürdigt (1922: F.W. Aston, 1989: W. Paul, 2002: J. B. Fenn und K. Tanaka). Insbesondere mit der Einführung sanfter Ionisationsmethoden wie der Elektrospray-Ionisation [24, 25] und der Matrixgestützten Laser Desorption/Ionisation [26, 27] hat sich die Mas-

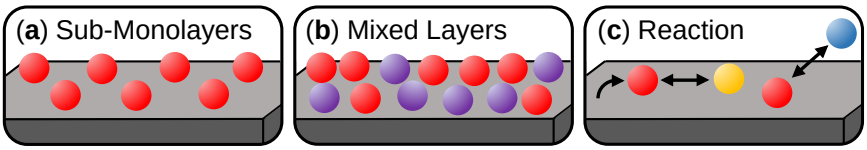

Abbildung 1.2: Schematische Darstellung der durch DINeC-Depo präparierten Schichten. Die Schichtdicke der durch Desorption mittels SO_2-Cluster deponierten Proben reicht von Submonolagen (a) bis zu Multilagen. Sie können aus einer oder mehreren Molekülarten aufgebaut sein (b). Reaktionen der deponierten Moleküle beispielsweise mit Adsorbaten der Oberfläche können untersucht werden (c).

senspektrometrie zu einer wichtigen Analysemethode in vielen Bereichen der chemischen Biologie entwickelt und wird vielfältig in der Qualitätskontrolle [28,29], der Medizin [30–32], der Forschung [33–35] und anderen Lebensbereichen [36,37] eingesetzt.
In diesem Zusammenhang zeichnet sich DINeC-MS als besonders sanfte *Desorption*smethode aus, mit welcher fragmentfrei die molekulare Zusammensetzung einer Oberfläche ohne weitere Probenpräparation bestimmt werden kann [38,39]. Die sanften Bedingungen, die durch den Lösungsprozess des Analyten im Cluster entstehen, wurde anhand der Massenspektren zahlreicher fragiler Moleküle nachgewiesen [40–46]. Ein Überblick über die in dieser Arbeit mittels DINeC-MS untersuchten organischen Systeme ist schematisch in Abb. 1.1(b) gezeigt; dabei sind einige der untersuchten Eigenschaften von Volumensproben und dünner Filme gegenübergestellt. Die sanften Desorptionsbedingungen von DINeC wurden z.B. genutzt, um verschiedene Textmarkertinten und deren Zusammensetzung (**Artikel I**) bzw. die Oberflächenzusammensetzungen von Volumensproben ionischer Flüssigkeiten (**Artikel II**) zu untersuchen. Darüber hinaus wurde ein Einfluss des Substrats auf die Oberflächenzusammensetzung von dünnen Filmen dieser ionischen Flüssigkeit beobachtet. Mittels DINeC-Depo hergestellte dünne Schichten aus organischen Molekülen zeigten ebenfalls eine signifikante Beeinflussung durch das Substrat (**Artikel III**). So konnte eine verstärkte Bildung von Addukten und die Oxidation der abgeschiedenen Moleküle in Abhängigkeit vom Substrat beobachtet werden. Diese Reaktionen stellen einen Teil der mittels DINeC-MS untersuchten Fragmentierungs-, Metallisierungs-, und Oxidationsreaktionen verschiedener dünner Filme und Volumensproben dar.

2 | Physikalische Grundlagen

In diesem Kapitel werden die physikalischen Grundlagen der in dieser Arbeit behandelten Themen dargestellt. Zunächst wird die verwendete Methode der clusterinduzierten Desorption/Ionisation und ihre Verwendung in der Massenspektrometrie beschrieben. Anschließend werden die untersuchten Systeme, d.h. organische Farbstoffe und ionische Flüssigkeiten kurz eingeführt.

2.1 Cluster-induzierte Desorption/Ionisation

Molekulare Cluster, die aus Schwefeldioxid-Molekülen aufgebaut sind, können für die sanfte Desorption/Ionisation verschiedener organischer Moleküle eingesetzt und damit für deren massenspektrometrische Analyse verwendet werden. Die zugrundeliegenden physikalischen Prinzipien und die experimentelle Umsetzung für die MS werden im Folgenden beschrieben. Zudem erfolgt eine kurze Gegenüberstellung weiterer (fragmentationsarmer) Ionisationsmethoden.

2.1.1 Desorption- und Ionisationsmechanismus

Die für die Desorption in dieser Arbeit verwendeten neutralen SO_2-Cluster haben eine Energiedichte von ≈ 0.8 eV pro SO_2-Molekül [39]. Diese liegt unterhalb der typischen Schwelle für Sputterprozesse von organischen Proben mittels Clusterionen von ca. 1 eV [47]; es muss also ein zusätzlicher Prozess stattfinden, um Moleküle mittels dieser Cluster von einer Oberfläche zu desorbieren: Das starke permanente Dipolmoment von Schwefeldioxid (1.6 D [48]) sorgt dafür, dass sich insbesondere polare Moleküle in diesen Clustern gut lösen können. Dadurch fungiert der Cluster als Übergangsmatrix für einen Lösungsprozess der zu desorbierenden Moleküle [38, 49–51]. Dieser Prozess zeigt sich in dem in Abb. 2.1(a) gezeigten Massenspektrum (pos. Ionen) von einer ACTH 34-39 Probe, das mittels Desorption durch die SO_2-Cluster in Kombination mit einem Flugzeitmassenspektrometer aufgenommen wurde. Es zeigt neben den Peaks, die dem intakten Biomolekülen zugeordnet werden können, eine Progression von Peaks mit $\Delta m/z = 64$, die einer Anlagerung von SO_2 Molekülen an das Biomolekül zugewiesen werden können und somit auf den Desorptionsprozess mittels Lösungsprozess hindeuten [50].
Die Wechselwirkung zwischen Cluster und Adsorbat ist in Abb. 2.1(b) schematisch dargestellt: (i) Der Cluster aus 10^3 bis 10^4 Schwefeldioxidmolekülen bewegt sich mit einer Geschwindigkeit von $\approx 10^3$ m/s auf die Oberfläche zu. (ii) In dem auf der Oberfläche zerschellenden Cluster tritt für einige Pikosekunden eine Temperatur von über tausend Kelvin auf [39]. Es findet der Lösevorgang des Analyts im Cluster(fragment) statt. (iii) Das desorbierte Molekül bewegt sich in der Gasphase mit den Cluster-Rückständen von der Oberfläche weg. Obwohl die

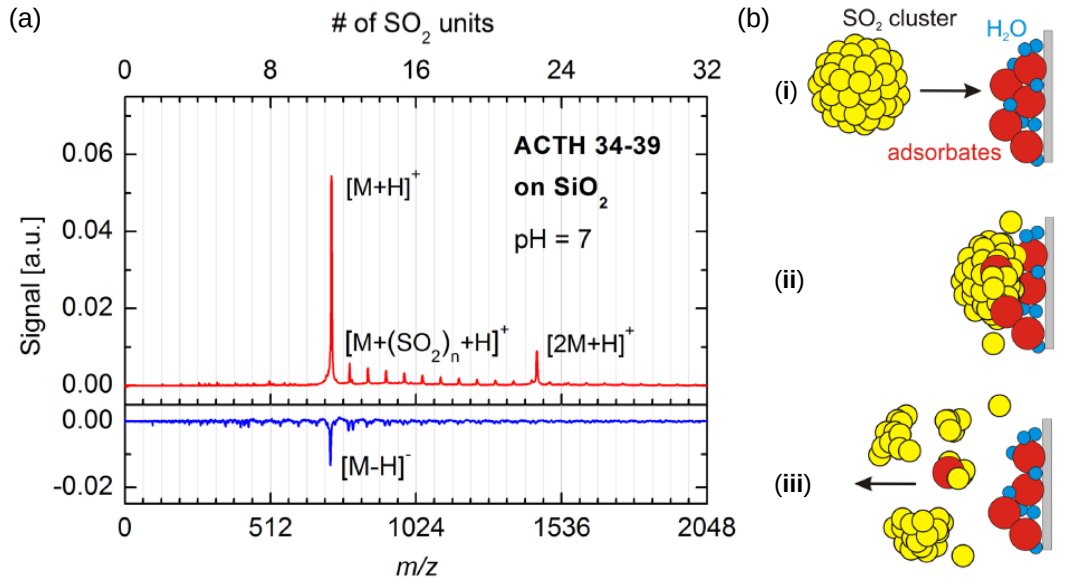

Abbildung 2.1: Desorptionsprozess von Adsorbaten durch SO_2-Cluster. (a) DINeC-Flugzeit-Massenspektren von ACTH 34-39 auf Silizium (rot: Kationen, blau: Anionen). Der Peak mit der höchsten Intensität bei $m/z = 723$ wird dem intakten Biomolekül zugeordnet. Die folgende Peakprogression mit $\Delta m/z = 64$ zeigt eine Anlagerung von SO_2 Molekülen an das Biomolekül. (b) Schematische Darstellung des Desorptionsprozesses: (i) Der neutrale Cluster bewegt sich in Richtung der Oberfläche, auf der sich das Adsorbatmolekül mit Restwasser befindet. (ii) Trifft der Cluster auf die Oberfläche auf, stellt er einerseits die Energie für die Desorption des Adsorbats zur Verfügung und fungiert andererseits als Übergangsmatrix für die Lösung des Adsorbats. (iii) Das desorbierte Molekül und die Clusterfragmente bewegen sich von der Oberfläche weg. Nachdruck aus Ref. [50], mit Genehmigung von AIP Publishing.

Cluster im DINeC-Prozess beim Auftreffen auf die Oberfläche kurzzeitig eine hohe Temperatur erreichen, werden die Moleküle durch die schnelle Abkühlung der Clusterfragmente beim Abdampfen weiterer SO_2-Moleküle nicht fragmentiert.
Zusätzlich zu dem einfach positiv geladenen Analytion $[M+H]^+$ wird im Spektrum in 2.1(a) auch das positiv geladene Dimer $[2M+H]^+$ beobachtet; es treten weiterhin auch doppelt $[M+H]^{2+}$ und dreifach $[M+H]^{3+}$ positiv geladene Ionen auf. Der Ionisationsmechanismus beruht dabei auf einer Protonenaufnahme (pos. Ionen) bzw. Abgabe (neg. Ionen). Insbesondere die H^+-Aufnahme wird durch SO_2 aus dem Cluster, das mit dem Restwasser der Probe zu schwefliger Säure reagiert, begünstigt [52, 53]. Die Ionisationseffizienz für Peptide beträgt $\eta \leq 1\%$ [49]. Über die Ionisation durch H^+-Aufnahme/Abgabe hinaus wurde auch die Ionisation z.B. über e^- Abgabe im Falle von Alkalimetallen, Porphyrinen und Tris(2-phenylpyridin)iridium(III) beobachtet [38, 41, 46, 49].

2.1.2 Verwendung in der Massenspektrometrie

Die organischen Moleküle, die durch den Desorptionsprozess mit Hilfe von neutralen Clustern desorbiert und ionisiert werden, können mit Hilfe der Massenspektrometrie analysiert werden; die schonende, matrixfreie und oberflächenempfindliche Desorptionstechnik mittels neutraler SO_2-Cluster wurde bisher zur massenspektrometrischen Untersuchung von Porphyrinen, Peptiden, Proteinen, Lipiden, ionischen Flüssigkeiten, Farbstoffen und Polymeren eingesetzt [40–45]. Die dazu verwendete Apparatur ist in Abb. 2.2 schematisch dargestellt und wird im folgenden näher beschrieben.
Zur Erzeugung der Cluster wird ein Gasgemisch (Druck $p = 15$ bar) aus SO_2 (3%) und Helium (97%) hergestellt, das durch eine gepulste Düse (Series 9 Pulse Valve, Parker Hannifin, Cleveland, USA, Öffnungsrate $f = 2$ Hz, effektive Öffnungszeit $t = 300$ ms) in eine Vakuumkammer (Basisdruck $p = 10^{-6}$ mbar) injiziert wird. Durch die adiabatische Expansion bilden sich Cluster einer Größe von 10^3 - 10^4 SO_2-Molekülen mit einer Geschwindigkeit von $v \approx 10^3$ m/s. Beim Auftreffen des Clusters auf die Oberfläche erfolgt die Desorption/Ionisation der Moleküle wie im Abschnitt 2.1.1 beschrieben. Die von den Clustern desorbierten Ionen werden durch ein elektrisches Feld zwischen Probe und Gitter in ein kommerzielles Quadrupol-Ionenfallen-Massenspektrometer (amaZon speed, Bruker Daltonik GmbH & Co. KG, Bremen) überführt. Die Zahl der eingefangenen Ionen wird in Abhängigkeit vom Masse-Ladungs-Verhältnis detektiert und im Massenspektrum aufgetragen.
Volumensproben für die massenspektrometrischen Experimente wurden durch

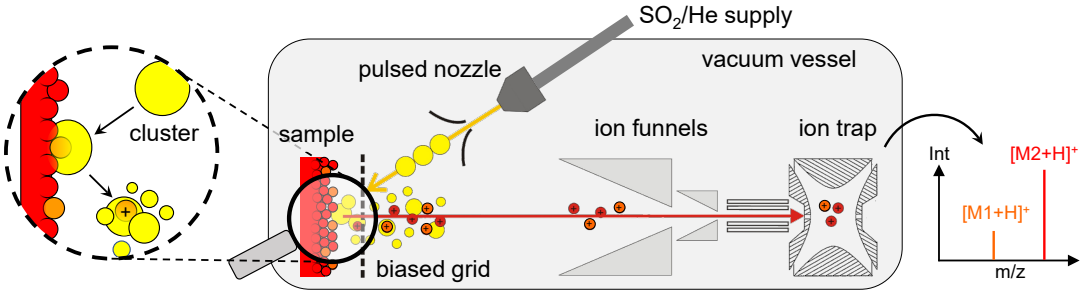

Abbildung 2.2: Schematischer Aufbau der DINeC-MS Apparatur. Der Clusterstrahl wird durch adiabatische Expansion eines SO_2/He-Gasgemisches erzeugt, das über eine gepulste Düse in die Vakuumkammer eingelassen wird. Der Skimmer, den der Clusterstrahl vor dem Auftreffen auf der Probe passiert, schneidet die äußeren Bereiche des Clusterstrahls ab. Die Cluster treffen anschließend in einem Winkel von 45° auf der Probenoberfläche auf. Nach der Desorption/Ionisation der Adsorbate werden die desorbierten Ionen über Transferoptiken in die Ionenfalle überführt. Die eingefangenen Ionen werden massenselektiv detektiert. Aus Ref. [54].

Auftropfen einer Lösung auf ein Substrat (meist Silizium mit nativer Oxidschicht) und anschließender Entfernung des Lösungsmittels im Exsikkator hergestellt. Für die Präparation von Peptid- und Farbstoffproben wurde Wasser, für Porphyrine und ionische Flüssigkeiten wurde Ethanol als Lösungsmittel verwendet. Tpyische Konzentrationen und Volumina sind $c = 1$ mM und $V = 30$ μL. Die Substrate wurden vor der Verwendung im Ultraschallbad in Ethanol und Aceton gereinigt (jeweils 15 Min.).

2.1.3 Fragmentationsarme Desorption – Vergleich unterschiedlicher Ionisationsmethoden

DINeC gilt als extrem sanfter Desorptionsprozess [55], welcher z.B. in **Artikel I** zur eindeutigen Zuordnung von Farbstoffen in Tinte und zur Identifizierung der jeweiligen Zersetzungsreaktionen verwendet wird. Am Beispiel des gelben Farbstoffs Basic Yellow 40 aus der Tinte eines gelben Textmarkers wird in Abb. 2.3 ein Vergleich der erzeugten Fragmente dreier weiterer (Desorptions-)/Ionisationsmethoden gezeigt, um den unterschiedlichen Fragmentationsgrad durch die verschiedenen Verfahren zu verdeutlichen. Gleichzeitig wird der mit den jeweiligen Molekülen verbundene Aufwand zur Präparation der Probe dargestellt.
Für die mit DINeC-MS (a), SIMS (b) und MALDI-MS (c) vermessenen Proben wurde die Tinte mit dem Stift flächig auf einen Siliziumwafer aufgetragen. Für DINeC-MS und SIMS Messungen wurde die Probe anschließend in die jeweilige Vakuumapparatur eingeschleust. Die MALDI-MS Proben wurden zusätzlich mit einer Matrix aus 2,5-Dihydroxybenzoesäure beschichtet (Vergleiche Artikel I, Supporting Information, Fig. S6). Zur Vorbereitung der ESI-MS Probe wurde die Tinte in einer Mischung aus Acetonitril, Wasser und Ameisensäure gelöst. SIMS-Messungen wurden mit $Ar_{1500}{}^{+}$-Clustern (20 keV) durchgeführt (Vergleiche Artikel I, Supporting Information, Fig. S7).
Der Hauptpeak der vier Spektren (roter Pfeil) bei $m/z = 362$ wird dem kationischen Teil des Farbstoffs Basic Yellow 40 (Vergleiche Strukturformel in Abb. 2.4(e)) zugeordnet. Der Zersetzung des Farbstoffs zugewiesene Fragmente bei $m/z = 348, 334, 318, 161, 147$ sind mit grau gestrichelten Linien gekennzeichnet. Die Signale bei $m/z = 348$ und $m/z = 334$ werden auf die Abspaltung der Ethylgruppen des Amins zurückgeführt; der Peak bei $m/z = 318$ wird der Abspaltung von CO_2 aus dem Cumarin Baustein des Molekül zugewiesen [58]. Die mit roten Linien markierten Peaks bei $m/z = 336$ und $m/z = 343$ in den Massenspektren in Abb. 2.4(a) und (d) werden anderen Inhaltsstoffen der Textmarkertinte zugeordnet. Der Peak im Inset des DINeC-Massenspektrums (schwarze Linie) bei $m/z = 155$ ist auf eine Verunreinigung in der Anlage zurückzuführen. Peaks bei geringeren Massen im Inset des Spektrums in 2.3(b) bei $m/z = 161$ und $m/z = 147$ werden Fragmenten zugeordnet, die durch eine Spaltung des Moleküls zwischen dem Imidazoliumring und der Cumarineinheit entstehen. Das Verhältnis der Summe der Peaks, die fragmentierten Molekülen zugewiesen wurden bezogen auf die Intensität aller Peaks, die Moleküle zugeordnet werden, zeigt

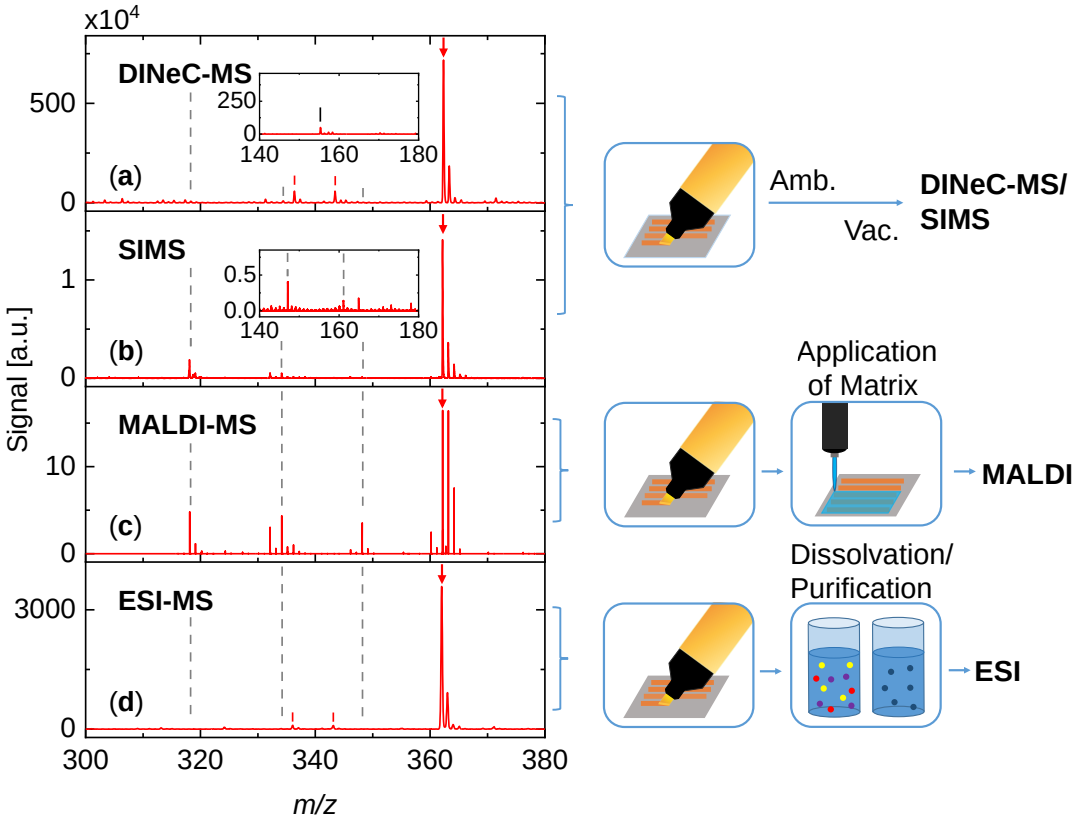

Abbildung 2.3: Vergleich der Massenspektren und Präparationsschritte verschiedener Ionisationsmethoden bei der Analyse einer Textmarkertinte. (a)-(d) Massenspektren der Tinte eines gelben Textmarkers aufgenommen mittels DINeC-MS, SIMS, MALDI-MS und ESI-MS. DINeC- und SIMS-Massenspektren sind im Inset zudem im kleineren Massenbereich dargestellt. Das Hauptsignal (roter Pfeil) bei $m/z = 362$ wird dem intakten Farbstoff (Basic Yellow 40) zugeordnet. Grau gestrichelte Linien kennzeichnen Peaks, die Fragmenten des Farbstoffs zugewiesen werden. Weitere Peaks im DINeC- und ESI-Spektrum, die mit schwarzen bzw. roten Linien markiert sind, werden Verunreinigungen bzw. weiteren Inhaltsstoffen der Textmarkertinte zugeordnet. Die Intensitätsverteilung der Peaks bei $m/z > 362$ im MALDI-Spektrum resultiert aus zusätzlich auftretenden protonierten Spezies ($[M+H]^+$) [56, 57]. Neben den Spektren ist die jeweilige Probenpräparation schematisch dargestellt.

in diesem Fall dass die meisten Fragmente durch den MALDI- ($\approx 24\%$) bzw. den SIMS-Prozess ($\approx 17\%$) induziert werden. Die Zersetzung des Farbstoffs durch MALDI-MS ist wahrscheinlich auf den laserinduzierten Farbstoffabbau zurückzuführen [59, 60], der durch das Siliziumsubstrat im Vergleich zum Papiersubstrat (Vergleiche Artikel I, Supporting Information, Fig. S6) noch gesteigert ist. Trotz der für SIMS vergleichsweise milden Desorptionsbedingungen durch Argoncluster zeigen die Spektren, dass bevorzugt CO_2 von der Cumarineinheit abgespal-

ten bzw. die Bindung zwischen den beiden Moleküleinheiten aufgebrochen wird. Die fragmentärmsten Spektren werden mit DINeC-MS und ESI-MS erzeugt. Für beide Methoden liegt der Anteil der Intensität dieser Peaks, die Fragmenten zugeordnet werden können, bei $< 2\%$ und könnte auch auf Fragmente in der Tinte zurückzuführen sein.
Die sanfte Natur der clusterinduzierten Desorption wird durch diesen Vergleich mit anderen Ionisationsmethoden deutlich. Die Technik eignet sich damit unter anderem zur Untersuchung von Fragmentierungsreaktionen organischer Moleküle (Vergleiche Abschnitt 3.2.2). Weiterführende Anwendungen könnten z.B. in der Medizin die Untersuchung strahleninduzierter Zersetzungsreaktionen von (bio)organischen Molekülen sein, die u.a. im Rahmen der Krebstherapie eine Rolle spielen [61, 62].

2.2 Untersuchte Systeme

Im Rahmen dieser Arbeit wurden organische Farbstoffe und ionische Flüssigkeiten untersucht, die im Folgenden kurz eingeführt werden.

2.2.1 Organische Farbstoffe

Farbige Gegenstände und die in ihnen enthaltenen Pigmente oder Farbstoffe begegnen uns überall im täglichen Leben. Der wahrgenommene Farbeindruck resultiert aus der Wechselwirkung von elektromagnetischer Strahlung und Materie, die verschiedene, oft auch gleichzeitig ablaufende Prozesse wie Absorption, Reflexion, Brechung, Beugung, Streuung und Fluoreszenz beinhaltet [63]. Bei den in dieser Arbeit untersuchten organischen Farbstoffen entsteht die Farbe im Wesentlichen durch Absorption, die durch Anregung der elektronischen Übergänge zwischen Molekülorbitalen hervorgerufen wird (Vergleiche Abb. 2.4(a)). Mögliche Übergänge sind z.B. $\sigma \rightarrow \sigma^*$, $\pi \rightarrow \pi^*$, $n \rightarrow \pi^*$ und $n \rightarrow \sigma^*$. Durch konjugierte π-Elektronensysteme oder auxochrome funktionelle Gruppen[1] können die Energieniveaus der Molekülorbitale relativ zueinander verschoben werden. Die Energiedifferenz der beiden elektronischen Übergange $n \rightarrow \pi^*$ und $\pi \rightarrow \pi^*$ kann dabei ausreichend verschoben werden, dass die Absorptionsbande in den sichtbaren Spektralbereich übergeht (Vergleiche Abb. 2.4(b)).
Farbstoffe können nach verschiedenen Merkmalen eingeteilt werden, z.B. nach ihrer chemischen Struktur, ihrer Herkunft (natürlich oder synthetisch), oder dem verwendeten Färbeverfahren [66]. Bei den in **Artikel I** untersuchten Farbstoffen (Vergleiche Abb. 2.4(c)-(e)) handelt es sich um kationische Farbstoffe, die für die Färbung von Stoffen mit anionischen Oberflächen wie Papier und Holz besonders gut geeignet sind. Absorption durch $\pi \rightarrow \pi^*$ Übergänge bestimmen dabei die Farbe der gezeigten Moleküle, allerdings spielen auch Fluoreszenzprozesse eine

[1] Auxochrome Gruppen sind Elektronendonatoren mit einem freien Elektronenpaar wie Ether, Amine, Sulfide und Halogene [64].

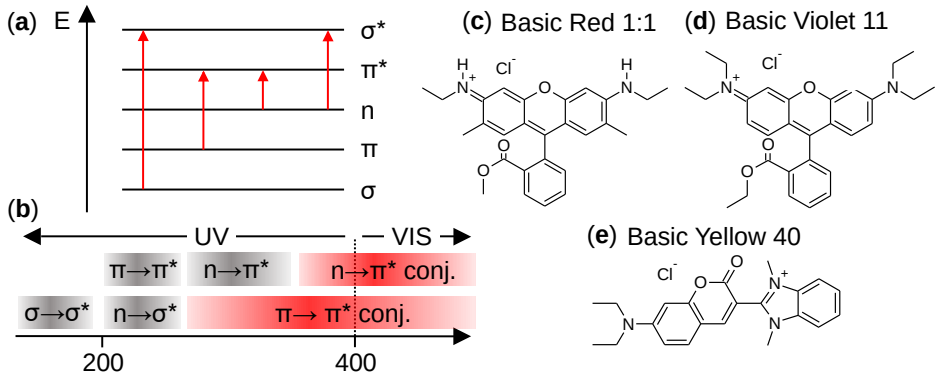

Abbildung 2.4: Farbstoffe. (a) Schematische Darstellung von Elektronenübergängen zwischen verschiedenen Molekülorbitalen in Farbstoffen (∗: antibindendes Molekülorbital, n: nichtbindendes (freies) Elektronenpaar) und (b) deren typische Absorptionsbereiche [65]. (c)-(e) Strukturformeln verschiedener Farbstoffe, die in dieser Arbeit untersucht wurden.

Rolle [67,68]. Für die folgende Untersuchung ist weiterhin wichtig, dass die Farbe verschiedener Werkstoffe, u.a. von Tinte, wird oft nicht durch einzelne Moleküle erzeugt, sondern durch eine Mischung mehrerer Moleküle [69].

2.2.2 Ionische Flüssigkeiten

Ionische Flüssigkeiten (IL) sind Salze, deren Schmelzpunkt unter 100°C liegt und die somit bei Raumtemperatur flüssig sein können [70, 71]. Dies wird durch die Delokalisierung der Ladung in den zumeist organischen Komponenten erreicht, die nicht nur im Π-Elektronensystem der organischen Kationen auftritt (Vergleiche Abb. 2.5(a)), sondern auch in kleinen Resonanzstrukturen durch Doppel- oder Dreifachbindungen in den Anionen, wie in Acetaten, Triflaten, Sulfaten, Dicyanamiden und Thiocyanaten, vorkommt (Vergleiche Abb. 2.5(b)) [72, 73].
ILs werden als „Designer-Solvents“ bezeichnet, da durch die Vielzahl der Kombinationsmöglichkeiten von Kationen und Anionen die gewünschten Eigenschaften der Flüssigkeit gesteuert werden können. Sie zeichnen sich unter anderem durch ihre Lösungseigenschaften aus, die es ermöglichen, ein ionisches Milieu zu schaffen, ohne die hohen Temperaturen und die damit verbundenen hohen Energiekosten einer Salzschmelze in Kauf nehmen zu müssen. Weitere Eigenschaften von ILs sind ihre geringe Flüchtigkeit, hohe thermische Stabilität und hohe Leitfähigkeit [74]. Die Anwendungsbereiche der ILs sind weit verbreitet, in vielen davon ist die Oberfläche der IL von Bedeutung [75,76]. Zur Untersuchung der atomaren/molekularen Oberflächeneigenschaften ionischer Flüssigkeiten wurden bisher insbesondere röntgenbasierte Methoden genutzt. Neben Elektronendichteprofilen aus Röntgenreflektometrie Messungen [77–80] gibt insbesondere auch die Photoelektronenspektroskopie (XPS) Informationen über die Zusammensetzung der Oberflächen

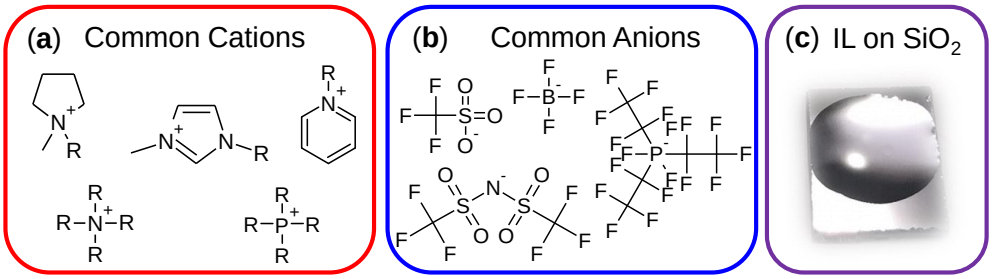

Abbildung 2.5: Ionische Flüssigkeiten. Chemische Strukturformeln von den gebräuchlichsten (a) Kationen und (b) Anionen ionischer Flüssigkeiten und (c) eine Fotografie einer ionischen Flüssigkeit auf einem Stück Silizium-Wafer wie sie für die Experimente in dieser Arbeit verwendet wurde.

von ionischen Flüssigkeiten. Durch Variation des Einfallswinkels der Röntgenstrahlung kann die Informationstiefe bei XPS verändert werden, was eine Unterscheidung der Oberflächen- und Volumeneigenschaften ermöglicht [81–85]. Massenspektrometrie wurde für die molekulare Untersuchung der Oberfläche von ILs bisher nur in wenigen Fällen verwendet [86,87]. Allgemein variiert die Zusammensetzung der Oberfläche ionischer Flüssigkeiten mit den verschiedenen Ionen [88]; so neigen stark fluorierte Ionen und Ionen mit langen Alkylketten dazu, sich an der Oberfläche anzureichern [89].

3 | Ergebnisse und Diskussion

Die Desorption mittels neutraler SO_2-Cluster wurde in dieser Arbeit vielfältig zur Präparation dünner Filme organischer Moleküle, und in Kombination mit der Massenspektrometrie, zur Analyse von Proben, die aus organischen Molekülen aufgebaut sind, eingesetzt. Im ersten Teil dieses Kapitels wird die Präparationsmethode DINeC-Depo für die Abscheidung dünner Schichten organischer Moleküle vorgestellt, die in **Artikel III** erstmals publiziert wurde. Im zweiten Teil dieses Kapitels wird die zerstörungsfreie und oberflächenempfindliche Desorptions-/Ionisationsmethode DINeC in Kombination mit der Massenspektrometrie zur Analyse der Oberflächeneigenschaften verschiedener organischer Systeme verwendet. Die eindeutige Zuordnung von Farbstoffen in Textmarkertinte und die Untersuchung ihre Zersetzungsreaktionen wurden dabei in **Artikel I** thematisiert. Die Oberflächenzusammensetzung ionischer Flüssigkeiten und weitere strukturelle Eigenschaften von ILs wurden in **Artikel II** behandelt.

3.1 Präparation organischer Schichten mittels clusterinduzierter Desorption

Die bei der Desorption mittels neutraler SO_2-Cluster desorbierten Ionen wurden bisher ausschließlich für die massenspektrometrische Analyse verschiedener Probensysteme verwendet. Wenn die desorbierten Moleküle statt in das Massenspektrometer auf ein Substrat überführt werden, können Filme der desorbierten Spezies hergestellt werden (Vergleiche Abb. 1.1(a)). Quarzkristall-Mikrowaagen-Messungen zur Dokumentation der Massenänderung des Substrats, auf dem die Moleküle abgeschieden werden, und Massenspektren von Proben dieser Filme wurden in **Artikel III** vorgestellt und zeigen qualitative und quantitative Eigenschaften der Schichten. In den folgenden Unterkapiteln wird die experimentelle Durchführung der Deposition organischer Moleküle durch die Desorption mittels neutraler SO_2 Cluster kurz beschrieben und die Analyse der so präparierten Schichten mit Hilfe der DINeC-MS diskutiert. Anschließend wird diese Abscheidungsmethode mit ähnlichen Techniken verglichen.

3.1.1 Apparativer Aufbau und Massenspektren

Die für die Depositionsexperimente verwendete Hochvakuumapparatur ist in Abb. 3.1 dargestellt. Die SO_2 Cluster werden entsprechend den Clustern der DINeC-MS-Experimente erzeugt (Vergleiche 2.1.2), wodurch sie identische Eigenschaften aufweisen. Der Clusterstrahl trifft unter einem Winkel von 45° zur Oberflächennormalen auf das Target, auf dem sich der Volumenfilm der zu de-

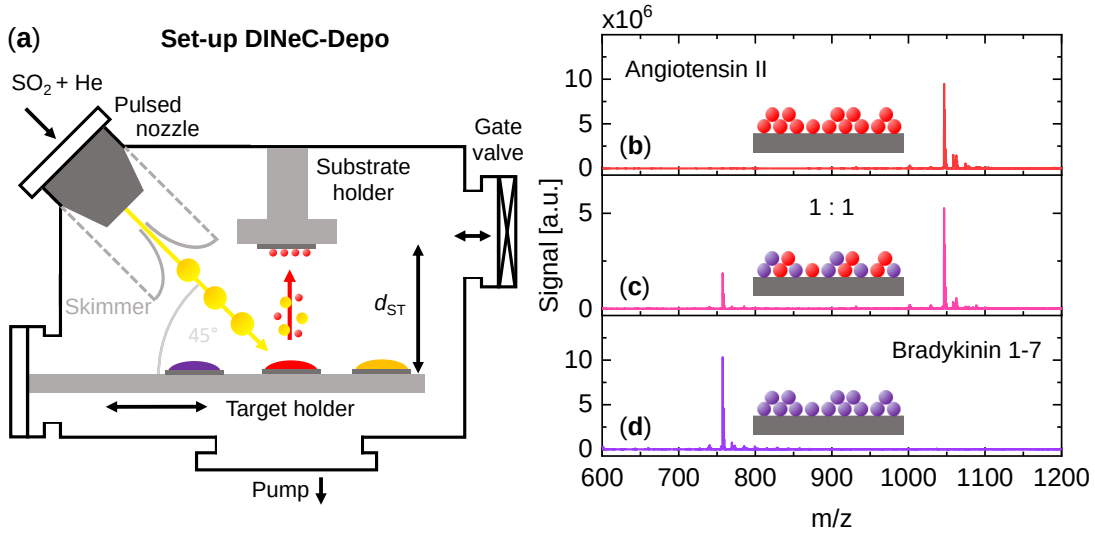

Abbildung 3.1: Schematischer Aufbau der DINeC-Depo-Apparatur und Massenspektren von DINeC-Depo Proben. (a) Der Clusterstrahl wird durch ein Gasgemisch aus SO_2 und Helium erzeugt, das über eine gepulste Düse in die Vakuumkammer eingelassen wird. Der Skimmer, den der Clusterstrahl vor dem Auftreffen auf der Probe passiert, schneidet die äußeren Bereiche des Clusterstrahls ab. Nach der Desorption der Target-Moleküle wird ein Teil der desorbierten Spezies auf dem Substrat abgeschieden. (b)-(d) DINeC-Massenspektren (pos. Ionen) reiner und gemischter Proben von Angiotensin II und Bradykinin 1-7, erzeugt durch DINeC-Depo (Depositionsdauer gesamt $t_{\mathrm{depo}} = 6$ h, $d_{\mathrm{ST}} = 12$ mm).

ponierenden Moleküle befindet. Die Targets können während des Depositionsprozesses mithilfe eines Manipulators ausgetauscht werden, um Mischproben herzustellen. Der Desorptions-/Ionisationsmechanismus erfolgt ebenfalls analog zu den DINeC-MS Experimenten (Vergleiche Abschnitt 2.1.1). Ein Teil der desorbierten Moleküle trifft auf das gegenüberliegende Substrat und wird dort abgeschieden. Das Substrat wurde mit einer Maske (perforierte Metallplatte, Lochdurchmesser $d = 6$ mm) bedeckt. Der Abstand zwischen Target und Substrat (d_{ST}) kann variiert werden. Durch ein Absperrventil kann das Substrat mit einer mobilen Vakuumkammer zur einer beliebigen anderen Vakuumkammer (meist DINeC-MS-Apparatur) transportiert werden, ohne die Probe der Umgebungsatmosphäre auszusetzen [90]. SiO_2-Substrate für DINeC-Depo wurden zusätzlich zur Reinigung im Ultraschallbad in Ethanol und Aceton (jeweils 15 min.) mit einem Reinigungsschritt entsprechend der Vorschrift „RCA Clean Typ 2“ gereinigt [91]. Das Target besteht aus einem Stück eines Siliziumwafers (2x2 cm^2), der mit der natürlichen Oxidschicht bedeckt ist. Der Volumenfilm auf der Oberfläche des Targets wird analog zu den Volumensproben der DINeC-MS-Proben präpariert, jedoch wird mehr Lösung aufgetragen ($V = 100$ μL).
In Abb. 3.1(b)-(d) sind beispielhaft die Massenspektren von reinen und gemisch-

ten Peptidproben von Angiotensin II und Bradykinin 1-7, die mittels DINeC-Depo abgeschieden wurden, dargestellt. Die reinen Angiotensin II- (b) und Bradykinin 1-7-Proben (Abb. 3.1(d)) zeigen Hauptpeaks bei $m/z = 1046$ und $m/z = 757$. Diese können den intakt abgeschiedenen Peptiden zugeordnet werden. Zusätzlich auftretende Peaks in beiden Spektren in geringer Intensität, die Addukten [92] oder Fragmenten [62, 93] zugeordnet werden können, werden in **Artikel III** ausführlich diskutiert. Für beide reinen Proben liegt der Anteil der Intensität der Peaks, die Fragmenten zugeordnet werden können, bei $< 3\%$. Dies stellt die obere Grenze für die mittels DINeC-Depo erzeugten Fragmente dar. Wahrscheinlich ist ein Teil dieser Fragmente aber auch anderen Prozessen, z.B. OF-Reaktionen, zuzuordnen.
Die Mischprobe, deren Spektrum in (c) gezeigt wird, wurde durch stündlichen Wechsel zwischen den Targets aus Angiotensin II und Bradykinin 1-7 während der sechsstündigen Deposition hergestellt. Auch in diesem Spektrum können die Hauptpeaks bei $m/z = 1046$ und $m/z = 757$ den einzelnen Peptiden ($[M+H]^+$) zugeordnet werden. Trotz vergleichbarer Intensität der Hauptpeaks in den Proben der reinen Peptide spiegelt die Mischprobe nicht das Verhältnis der Depositionsdauer wider. Unterschiedliche Desorptions-/Ionisationseffizienzen der Peptide von den Targets, wie sie bereits beobachtet wurden [42], oder Matrixeffekte [94–97], in Form einer Beeinflussung der Desorptions-/Ionisationseffizienzen durch die Anwesenheit eines anderen Moleküls, können für diese Abweichung verantwortlich sein.
Massenspektren von weiteren DINeC-Depo Proben werden in **Artikel III** diskutiert, wobei weitere Eigenschaften der hergestellten Filme und des Depositionsprozesses untersucht wurden, die zum Teil in Abschnitt 3.2 nochmals aufgegriffen werden.

3.1.2 Vergleich mit verwandten Methoden

Wie DINeC-Depo aus DINeC-MS hervorgegangen ist [98], sind viele der Methoden zur sanften Deposition von Biomolekülen aus Techniken hervorgegangen, die ursprünglich in der Massenspektrometrie verwendet wurden. Die Deposition mittels Gascluster-Ionenstrahl (GCIB) geht dabei auf die Sekundärionen Massenspektrometrie (SIMS) mittels GCIB zurück [99, 100].
Die Depositionsmethode der matrixgestützten, gepulsten Laserverdampfung (Matrix-Assisted Pulsed Laser Evaporation, MAPLE) hat Ähnlichkeiten mit der Massenspektrometrie basierend auf der Matrixgestützten Laser-Desorption/Ionisation (Matrix Assisted Laser Desorption/Ionization, MALDI) [101, 102]. Elektrospray-Ionenstrahldeposition (Electrospray Ion Beam Deposition, ES-IBD) leitet sich von der in der Massenspektrometrie verwendeten Elektrospray-Ionisation (Electrospray Ionization, ESI) ab [103–105]. Abb. 3.2 vergleicht diese vier Techniken hinsichtlich der nötigen Präparationsschritte.
Die in Abb. 3.2(a) dargestellten Methode der Deposition mittels DINeC wurde bezüglich ihrer Funktionsweise und physikalischer Grundlagen in dieser Arbeit be-

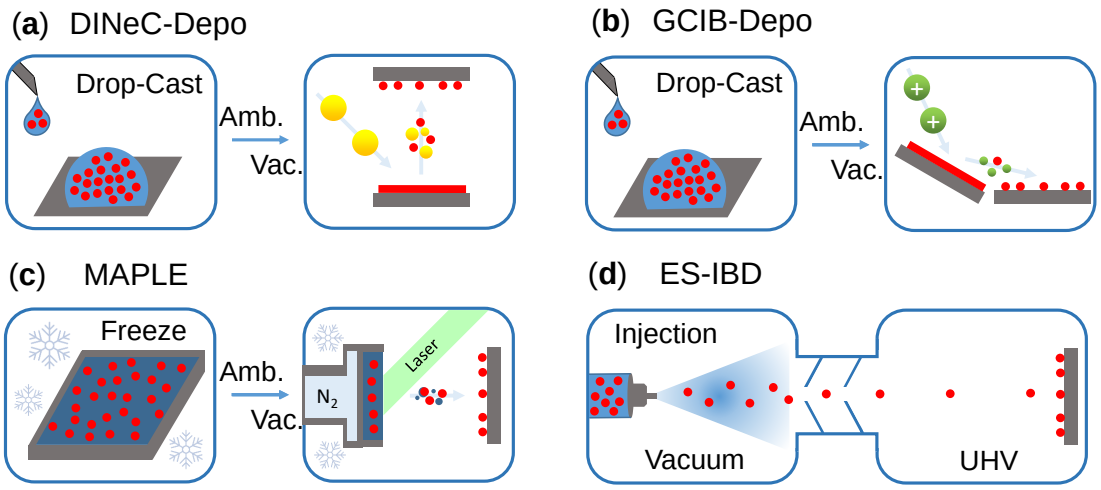

Abbildung 3.2: Schematischer Vergleich der Experimente verschiedener Depositionstechniken, die auf der Grundlage massenspektrometrischer Verfahren entwickelt wurden. Für die Präparation des Targets muss das Molekül für alle gezeigten Techniken zunächst in einem geeigneten Lösungsmittel gelöst werden. Die Targets für die Abscheidung mittels (a) DINeC-Depo und (b) GCIB-Depo werden aufgetropft und getrocknet; es sind keine weiteren Präparationsschritte erforderlich. (c) Die Matrixmoleküle im MAPLE-Verfahren werden vor dem Einfrieren zu den gelösten Molekülen hinzugefügt. Die Biomoleküle werden mit einem Laser aus der gefrorenen Matrix verdampft. Im Falle der ES-IBD (d) werden die Ionen entsprechend des ESI-Verfahrens erzeugt und getrennt und über mehrere differentielle Pumpstufen auf die (oftmals im UHV präparierten) Proben transferiert.

reits ausführlich beschrieben (Vergleiche 3.1.1). In Abb. 3.2(b) ist die Deposition mittels Desorption durch Gas-Cluster-Ionen dargestellt. Die atomaren Primärionen, die in SIMS-Experimenten bevorzugt für anorganische Proben verwendet werden, werden für die Desorption empfindlicher Biomoleküle durch geladene Edelgascluster ersetzt [106–108]. Diese kommen auch bei dieser Depositionsmethode zum Einsatz. Die Targets der GCIB-Deposition können auf die gleiche Weise hergestellt werden wie die Targets für die DINeC-Deposition. Die geladenen Edelgascluster treffen typischerweise unter einem Winkel von $> 45°$ zur Oberflächennormalen auf das Target auf [109]. Die Energiedichte der Cluster liegt mit > 1 eV/Atom über der typischen Energieschwelle für das Sputtern organischer Proben [47]. Dadurch ist die Ablöseeffizienz höher als bei DINeC-Depo, allerdings ist der Anteil fragmentierter Moleküle ($> 40\%$) auch deutlich höher [110].
Für die Deposition mittels MAPLE (Abb. 3.2(c)) werden die gelösten Moleküle zusammen mit einer Matrix aus leicht flüchtigen Substanzen eingefroren, um das Target herzustellen. Dieses wird unter weiterer Kühlung in der Vakuumkammer

eingebaut. Zur Desorption und Ionisation wird ein Laser verwendet. Der Hauptteil der Energie wird von der Matrix absorbiert, die dann verdampft. Die Matrixmoleküle, die teilweise zusammen mit den zu deponierenden Molekülen aufgetragen werden, sind so gewählt, dass sie bei Raumtemperatur wieder vom Substrat desorbieren. Moleküle bis zu 1000 kDa können auf diese Weise intakt übertragen werden; eine photokatalytische Zersetzung der Moleküle wird typischerweise nicht beobachtet [102,111,112]. Die niedrigen Temperaturen erfordern eine aufwendigere Handhabung des Targets sowie eine komplexe Anlage. Ähnlichkeiten zwischen MAPLE und DINeC-Depo zeigen sich darin, dass sowohl Matrixmoleküle als auch das SO_2 der DINeC-Cluster zunächst mit auf die Oberfläche deponiert werden. In beiden Prozessen desorbiert jedoch der Großteil der unerwünschten Bestandteile wieder.
Bei der letzten Methode, ES-IBD (Abb. 3.2(d)), wird die vorbereitete Lösung durch eine Düse direkt in die Kammer gesprüht und die Ionen entsprechend des ESI-Prozesses erzeugt und separiert. Abhängig von der kinetischen Energie, mit der die Moleküle aufgebracht werden, können $> 87\%$ der Moleküle intakt abgeschieden werden [113]. Der Depositionsprozess funktioniert jedoch ausschließlich lösungsbasiert und der Aufbau ist aufgrund der differentiellen Pumpstufen aufwendiger.
Die Deposition mittels clusterinduzierter Desorption zeichnet sich somit durch eine Kombination aus einfachem Aufbau und sehr sanfter Desorption aus. In zukünftigen Experimenten könnte durch die Selbstorganisation biomolekularer Schichten [114] und die damit verbundene Ausbildung homogener Schichten die Methode z.B. in Richtung der Herstellung von Biomembranen erweitert werden.

3.2 Analyse organischer Proben mittels DINeC-MS

Für die in dieser Arbeit durchgeführten Analysen wurde insbesondere der Aspekt der fragmentfreien Desorption des DINeC-Prozesses genutzt, welcher bereits anhand des Vergleichs der verschiedenen Desorptions-/Ionisationstechniken in Abschnitt 3.1.2 und den DINeC-Massenspektren der DINeC-Depo-Proben in Abb. 3.1 gezeigt wurde. Dabei ist zu bemerken, dass die Moleküle die zu den Spektren von den DINeC-Depo-Proben beitragen, den Desorptionsprozess sogar zweimal durchlaufen haben - zuerst bei der Deposition und dann noch einmal bei der massenspektrometrischen Analyse. Trotzdem wurde eine Obergrenze von maximal 3% fragmentierter Moleküle in den Spektren nicht überschritten, und in einigen Fällen wurden sogar deutlich niedrigere Werte erreicht [98]. Ein Teil dieser Fragmentpeaks kann darüber hinaus seinen Ursprung auch in der Fragmentierung auf der Oberfläche ohne Einfluss des Clusters haben.
Die sanfte Natur des clusterinduzierten Desorptionsprozesses wurde in dieser Arbeit nun insbesondere angewendet, um Farbstoffe in Textmarkertinten eindeutig zu identifizieren und ihre Zersetzungsreaktionen zu untersuchen. Darüber hinaus

wurden weitere Reaktionen von Molekülen auf Oberflächen, insbesondere unter Verwendung von Proben, die mittels DINeC-Depo hergestellt wurden, untersucht. Da DINeC-MS sich ebenfalls als besonders oberflächenempfindlich erwiesen hat [42], kann die Methode auch zur Untersuchung von Oberflächenzusammensetzungen genutzt werden. In dieser Arbeit wurde dies u.a. zum ersten mal auf die Oberflächen flüssiger Proben, nämlich ionischer Flüssigkeiten, angewendet.

3.2.1 Oberflächenzusammensetzung

Als Beispiel für die oberflächenempfindliche Analyse mittels DINeC-MS wurden in **Artikel I** über die Zusammensetzung von Textmarkertinte und die Zersetzungsreaktionen der Farbstoffe hinaus auch einfache Schichtsysteme auf ihre Zusammensetzung hin analysiert. Dafür wurden zwei Tinten sukzessive aufgetragen (Vergleiche 3.3(a)) und das Schichtsystem mittels DINeC-MS untersucht. In diesem Experiment kann in dem jeweiligen Massenspektrum (3.3(b)) die obere Lage entsprechend des Intensitätsverhältnisses eindeutig bestimmt werden. Im gezeigten Beispiel ist der Hauptpeak bei $m/z = 362$ (gelber Pfeil) dem Kation des gelben Farbstoffs (Basic Yellow 40, Vergleiche Strukturformel in Abb. 2.4(e)) der gelben Tinte zuzuordnen. Da die Dicke von Tinte im Mikrometerbereich liegt [115], kann dieses System als Schichtung zweier vergleichsweise dicker Filme betrachtet werden. Bei endlicher Messdauer ist daher auch nur Signal von der oberen Farbstoffschicht zu erwarten. Dass beim Auftragen der Tinten dennoch eine Vermischung stattfindet, zeigt der Peak bei $m/z = 372$ (blauer Pfeil), der der zuerst aufgetragenen blauen Kugelschreiber-Tinte zugeordnet wird.
Die hohe Oberflächenempfindlichkeit der DINeC-MS Technik wurde ebenfalls bei der Analyse von Volumensproben ionischer Flüssigkeiten (Vergleiche 3.3(c)) in **Artikel II** genutzt. Die beispielhaften Massenspektren einer ionischen Flüssigkeit in 3.3(d) zeigen die intakte Desorption kationischer $C(CA)_n^+$ bzw. anionischer $A(CA)_n^-$ Cluster (n = 0, 1, 2, ...), markiert durch graue Striche. Dabei ist auffällig, dass die Intensität der kationischen bzw. anionischen Peaks sehr unterschiedlich ist. Unter der Annahme, dass die Desorptions- und Ionisationseffizienz unabhängig von den Ionen ist, spiegelt das Intensitätsverhältnis direkt das Verhältnis der an der Oberfläche vorhandenen Ionen wider.
Trägt man das Intensitätsverhältnis I_C/I_A von Kationen und Anionen als Funktion des Massenverhältnisses m_C/m_A von Kationen und Anionen verschiedener ionischer Flüssigkeiten auf, so zeigt sich, dass die Oberflächenzusammensetzung mit der molekularen Zusammensetzung variiert (Vergleiche 3.3(e)). Kationen mit langer Alkylkette in Kombination mit kleinen Anionen neigen in Übereinstimmung mit der Literatur [83, 89, 116, 117] zur Anlagerung an der Oberfläche. Diese Tendenz nimmt ab, je größer die Anionen sind. Wenn zusätzlich die Alkylkette des Kations verkürzt wird, kann eine bevorzugte Anlagerung von Anionen an der Oberfläche beobachtet werden. Im Vergleich zu Volumensproben ist in dünnen Filmen auf SiO_2 die Tendenz der Kationen, sich an der Oberfläche anzulagern, noch ausgeprägter. Trägt man das Intensitätsverhältnis I_C/I_A von Kationen und

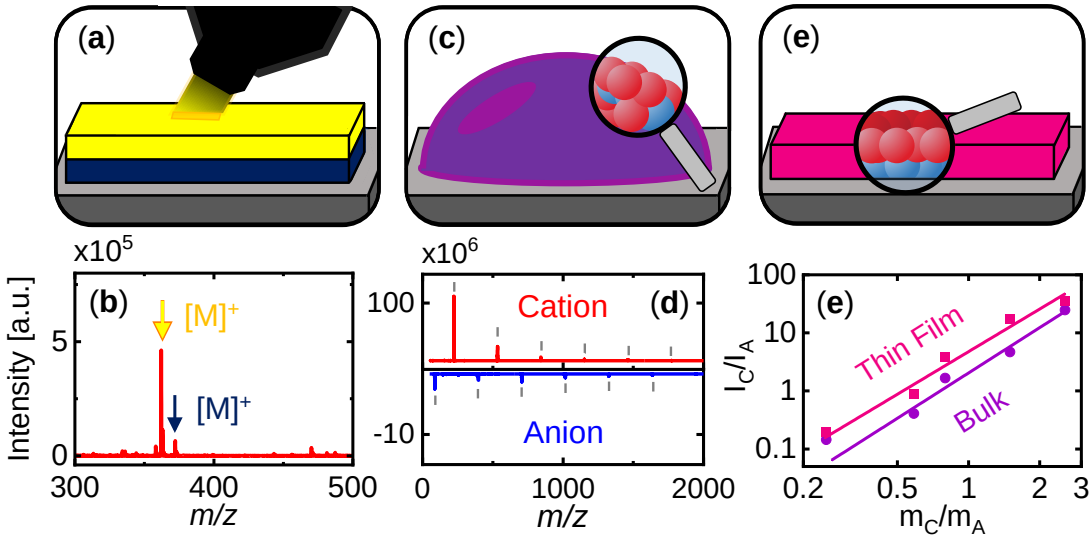

Abbildung 3.3: Schematische Darstellung verschiedener Probensysteme und zugehörige Analyse der Oberflächenzusammensetzung. (a) Schematische Darstellung des Schichtsystems zweier Tinten und (b) das entsprechende Massenspektrum (pos. Ionen). (c) Schematische Darstellung der Oberflächenzusammensetzung der Volumensprobe einer ionischen Flüssigkeit und (d) beispielhafte Massenspektren von 1-Decyl-3-methylimidazoliumtetrafluorborat (rot: pos. Ionen, blau: neg. Ionen). Graue Striche kennzeichnen pos./neg. Cluster aus den Ionen der Flüssigkeit. Die Intensität nimmt mit steigender Größe des Clusters ab. Das Verhältnis von positiven zu negativen Peaks und damit von Ionen an der Oberfläche liegt bei $I_C/I_A \approx 50$. (e) Schematische Darstellung der Oberflächenzusammensetzung des dünnen Films einer ionischen Flüssigkeit und (f) Intensitätsverhältnis I_C/I_A der kationischen und anionischen Peaks ionischer Flüssigkeiten aus DINeC-Massenspektren als Funktion des Massenverhältnisses m_C/m_A für die zwei untersuchten Probenarten (lila: Volumensproben, pink: dünne Filme).

Anionen als Funktion des Massenverhältnisses m_C/m_A von Kationen und Anionen für dünne Filme auf (Abb. 3.3(e)), so zeigt sich für die Oberflächen aller untersuchten ionischen Flüssigkeiten ein höheres Intensitätsverhältnis verglichen mit den Ergebnissen von Volumensproben. Dies wird in **Artikel II** auf den Einfluss des Substrates auf die Oberflächenzusammensetzung zurückgeführt. Aufgrund der geringen Dicke des Films begünstigt die SiO_2-Oberfläche mit ihren endständigen Hydroxylgruppen offensichtlich die Anlagerung von Kationen an der Oberfläche. Wie bereits in Abschnitt 2.2.2 beschrieben, sind herkömmliche Techniken zur Analyse der Oberflächenzusammensetzung ionischer Flüssigkeiten XPS und SIMS. Wie DINeC-MS weist XPS ebenfalls eine hohe Oberflächenempfindlichkeiten auf. Allerdings ist die molekulare Information nur indirekt über die chemische Verschiebung der XPS-Peaks zugänglich [118]. SIMS-Experimente liefern Informationen über die molekulare Struktur von Materialproben; jedoch ist die

Oberflächenempfindlichkeit geringer als bei DINeC-MS [93] und in der Literatur wurde insbesondere die Fragmentierung der Ionen der ionischen Flüssigkeit diskutiert [119].

3.2.2 Reaktionen auf Oberflächen und in organischen Filmen

Das Substrat beeinflusst nicht nur die Oberflächenzusammensetzung ionischer Flüssigkeiten, sondern spielt auch eine entscheidende Rolle bei den Depositionsexperimenten in **Artikel III**. So zeigen für diese Anwendung ungenügend gereinigte Substrate in den Massenspektren eine Adduktbildung der abgeschiedenen Moleküle mit an der Oberfläche adsorbierten Ionen. Diese Reaktion kann gezielt für Veränderungen der Moleküle auf der Oberfläche genutzt werden. Wird beispielsweise eine $CaCl_2$-Lösung auf einem SiO_2-Substrat getrocknet und das Peptid Angiotensin II mittels DINeC-Depo (Depositionsdauer $t_{\mathrm{depo}} = 6$ h, $d_{\mathrm{ST}} = 12$mm) auf der Salzoberfläche abgeschieden, so erhält man von der Probe das in Abb. 3.4(b) gezeigte DINeC-Massenspektrum. Der rote Pfeil bei $m/z = 1046$ kennzeichnet das intakte Biomolekül $[\mathrm{M+H}]^+$, während die weiteren Peaks im Spektrum bei $m/z = 1066$ ($[\mathrm{M - H_2O - H + Ca}]^+$), $m/z = 1084$ ($[\mathrm{M - H + Ca}]^+$) und $m/z = 1122$ ($[\mathrm{M - 3H + 2Ca}]^+$) Angiotensin II mit Calcium als Addukt zugeordnet wurden.
Die Wechselwirkung zwischen einem Adsorbat und einer abgeschiedenen Spezies wurde in **Artikel III** weiterhin genutzt, um die Metallisierung eines Pophyrins in einem DINeC-Depo Experiment durchzuführen und zu untersuchen. Wie in Abb. 3.4(c) dargestellt, werden dabei zwei der Protonen im Porphyrin-Ring durch ein Kupfer(II)ion ausgetauscht. Dafür wurde eine $CuCl_2$-Lösung auf einem SiO_2-Substrat getrocknet und Tetraphenylporphyrin (TPP) durch DINeC-Depo (Depositionsdauer $t_{\mathrm{depo}} = 6$ h, $d_{\mathrm{ST}} = 30$ mm) auf dem Salz deponiert. Das zu dem Versuch gehörige DINeC-Massenspektrum ist in Abb. 3.4(d) gezeigt. Der mit dem roten Pfeil bei $m/z = 615$ gekennzeichnet Peak kann dem nicht reagierten Edukt TPP ($[\mathrm{M+H}]^+$) zugeordnet werden. Peaks mit $\Delta m/z = 16$ sind mit Oxidationsreaktionen des Edukts verbunden [120]. Der mit dem orangenen Pfeil gekennzeichneten Peak geringer Intensität bei $m/z = 675$ wird einem Produkt der Reaktion von TPP mit Cu zugeordnet. Eine höhere Intensität hat der Peak bei $m/z = 692$, gekennzeichnet mit dem violetten Pfeil, der dem Produkt einer Oxidationsreaktion des deponierten Porphyrins mit eingebundenem Kupferion, $[\mathrm{M+O+H+Cu}]^+$, zugeordnet wird. Diese oxidierte Spezies ist ebenfalls das Hauptprodukt der Deposition des CuTPP auf SiO_2. Weitere Einzelheiten dieser Reaktion sind in **Artikel III** diskutiert.
Neben der bereits beschriebenen Adduktbildung durch Adsorbate auf der Oberfläche wurden auch Oxidationsreaktionen von Peptiden durch die Kombination von DINeC-Depo und DINeC-MS in **Artikel III** untersucht. Dazu wurde das Substrat chemisch modifiziert, um die abgeschiedenen Moleküle zu beeinflussen. Das SiO_2-Substrat wurde z.B. dem Reinigungsschritt „RCA Clean Typ 2“ [91] unterzogen und dabei mit Wasserstoffperoxid behandelt, was zu einer Aktivierung

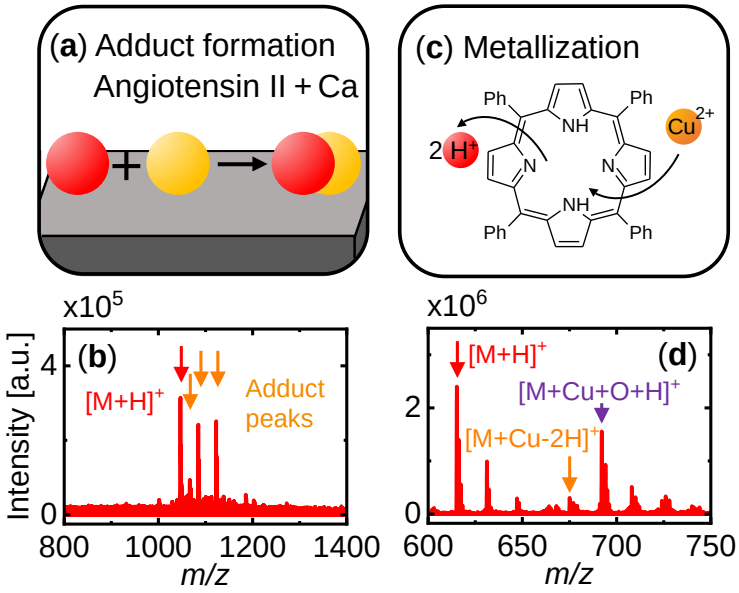

Abbildung 3.4: schematische Darstellung zu Reaktionen mittels DINeC-Depo abgeschiedener Moleküle auf Oberflächen und zugehörige DINeC-Massenspektren. (a) Schematische Darstellung der Reaktion zweier Oberflächenadsorbate und (b) das zugehörige Massenspektrum der DINeC-Depo Probe von Angiotensin II auf $CaCl_2$. Zusätzlich zum Peak des intakten Moleküls (roter Pfeil) treten Peaks auf, die Addukten von Angiotensin II und Ca zugeordnet werden. (c) Metallisierungsreaktion von Tetraphenylporphyrin durch ein Kupferion und (d) das zugehörige Massenspektrum der DINeC-Depo-Probe von Tetraphenylporphyrin (TPP) auf $CuCl_2$. Zusätzlich zum Peak des intakten Edukts (roter Pfeil) treten Peaks auf, die einer Reaktion von TPP und Cu zugeordnet werden können.

der Probenoberfläche führte. Das Massenspektrum einer solchen Probe, auf die direkt nach der Reinigung Angiotensin II-Moleküle durch DINeC-Depo (Depositionsdauer $t_{\mathrm{depo}} = 6$ h, $d_{\mathrm{ST}} = 12$ mm) abgeschieden wurden, ist in Abb. 3.5(b) dargestellt. Der rote Pfeil bei $m/z = 1046$ kennzeichnet das intakte Biomolekül $[\mathrm{M+H}]^+$. Die drei Peaks jeweils im Abstand $\Delta m/z = 16$ vom Peak des intakten Peptids (mit blauen Pfeilen markiert) sind Oxidationsprodukten des Peptids zugeordnet. Nach länger Lagerung der „aktivierten“ Substrate wird diese Reaktion nicht mehr beobachtet.
Während die Oxidation von Angiotensin II durch das aktivierte Substrat erzielt wurde, oxidiert das Peptid Bombesin nach Deposition mittels DINeC-Depo durch die enthaltenen leicht oxidierbaren Aminosäuren Methionin und Tryptophan auch ohne Aktivierung des Substrats. Das zugehörige Massenspektrum des deponierten Biomoleküls ist in Abb. 3.5(d) dargestellt. Der mit dem roten Pfeil bei $m/z = 1619$ gekennzeichnet Peak kann dem intakten Biomolekül zugeordnet werden. Die mit den blauen Pfeilen bei $m/z = 1635, 1651, 1667, 1683$ gekennzeich-

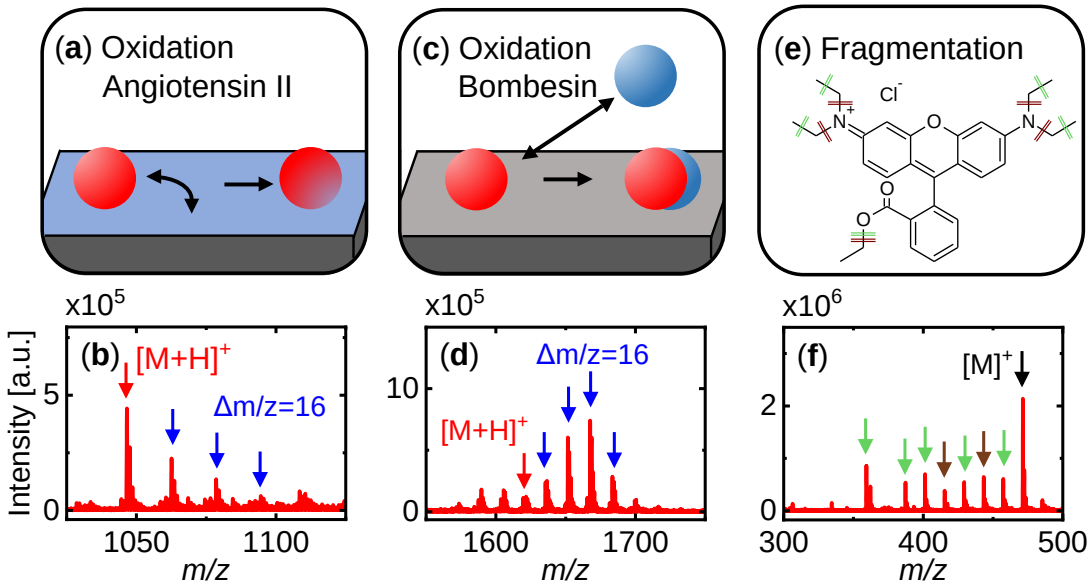

Abbildung 3.5: Schematische Darstellung verschiedener Probensysteme zur Untersuchung von Reaktionen mittels DINeC-MS und zugehörige Massenspektren. (a) Schematische Darstellung der Reaktion eines mittels DINeC-Depo abgeschiedenen Moleküls mit einer Oberfläche und (b) das zugehörige Massenspektrum der DINeC-Depo-Probe von Angiotensin II auf SiO_2, das durch Wasserstoffperoxid „aktiviert“ wurde. Die Peaks, die Oxidationsreaktionen zugeordnet werden, sind jeweils $\Delta m/z = 16$ voneinander bzw. vom Peak des intakten Moleküls getrennt. (c) Oxidation eines durch DINeC-Depo abgeschiedenen Biomoleküls auf der Oberfläche durch eine oxidative Umgebung und (d) das zugehörige Massenspektrum von Bombesin auf SiO_2. (e) Struktur des Farbstoffs Basic Violet 11 mit potentiellen Bruchstellen durch thermische (braun) oder UV-induzierte Zersetzung (grün) und (f) das zugehörige Massenspektrum des durch UV-Strahlung zersetzten Farbstoffs.

neten Peaks sind Oxidationsreaktionen des Moleküls zugeordnet. Die Mehrzahl der deponierten Biomoleküle ist mindestens einmal oxidiert. Die Probe wurde zwischen DINeC-Depo-Apparatur und DINeC-MS-Apparatur durch die Umgebungsatmosphäre transferiert, weshalb eine verstärkte Oxidation im Vergleich zu einem Transport im Vakuum beobachtet wird, wie in **Artikel III** diskutiert wird. Neben diesen Oxidationsreaktionen der mittels DINeC-Depo aufgebrachten Peptide wurden in **Artikel I** Zersetzungsreaktionen von Farbstoffmolekülen mittels DINeC-MS analysiert und verschiedene Zersetzungsprozesse unterschieden. Das Massenspektrum in Abb. 3.5(f) zeigt eine Volumensprobe des Farbstoffs Basic Violet 11, der durch UV-Strahlung teilweise zersetzt wurde. Der Hauptpeak bei $m/z = 471$ (schwarzer Pfeil) wird dem intakten Kation des Farbstoffs zugeordnet. Es gibt noch sieben weitere Peaks im Massenspektrum, die mit braunen und grünen Pfeilen gekennzeichnet sind. Die mit braunen

Pfeilen gekennzeichneten Peaks bei $m/z = 443$ und $m/z = 415$ sind die Hauptfragmente im Massenspektrum einer thermisch zersetzten Probe und entsprechen der Abspaltung von Ethylgruppen entweder an einer der Amin- oder der Estergruppe. Die potentiellen Bruchstellen im Molekül sind in Abb. 3.5(e) durch braune Linien gekennzeichnet. Mit grünen Pfeilen gekennzeichnete Peaks bei $m/z = 457, 429, 401, 387, 359$ entstehen ausschließlich durch UV-induzierte Zersetzung. Potentielle Bruchstellen im Molekül sind in Abb. 3.5(f) durch grüne Linien gekennzeichnet. Es ist also möglich, anhand der Massenspektren die zu Grunde liegende Zersetzungsmethode zu untersuchen und eindeutig zuzuordnen. Dies könnte u.a. in forensischen Anwendungen oder zur Untersuchung komplexer photoinduzierter bzw. photokatalytischer Prozesse zum Einsatz kommen.

4 | Publikationen

4.1 Artikel I

Cluster-induced desorption/ionization mass spectrometry of highlighter ink: unambiguous identification of dyes and degradation processes based on fragmentation-free desorption

K. Bomhardt, P. Schneider, M. Rohnke, C. R. Gebhardt, and M. Dürr;

Analyst **147**, 333 - 340 (2022).

Analyst

ROYAL SOCIETY OF CHEMISTRY

PAPER

Cite this: *Analyst*, 2022, **147**, 333

Cluster-induced desorption/ionization mass spectrometry of highlighter ink: unambiguous identification of dyes and degradation processes based on fragmentation-free desorption†

Karolin Bomhardt,[a] Pascal Schneider,[a] Marcus Rohnke,[b] Christoph R. Gebhardt[c] and Michael Dürr *[a]

Received 2nd September 2021,
Accepted 1st December 2021

DOI: 10.1039/d1an01588e

rsc.li/analyst

Highlighter inks were analyzed by means of soft Desorption/Ionization induced by Neutral SO_2 clusters (DINeC) in combination with mass spectrometry (MS). The dye molecules of the different inks were directly desorbed from dots of ink drawn on arbitrary substrates. Fragmentation free spectra were observed and the dyes used in the dye mixtures of the different highlighter inks were unambiguously identified. The soft nature of cluster-induced desorption was used to investigate the decomposition of the dye molecules induced by either heat or UV-light. The two processes lead to different decomposition products which are clearly distinguished in the DINeC spectra. The two different degradation processes can thus be discriminated using DINeC-MS.

1. Introduction

The analysis of a mixture of various unknown substances can be seen as the most general task to be solved in analytical chemistry.[1] Using mass spectrometry for this task, typically the mixture has to be purified and/or extractions have to be performed prior to the actual analysis.[1,2] Depending on the application, however, a direct analysis without pretreatment, *e.g.*, transfer from a substrate into a solvent, is of advantage.

Ink which was either written or printed on paper may serve as an illustrative example for such a complex mixture of chemical compounds to be analyzed by mass spectrometry directly on the original substrate without further process steps.[3–9] In particular, identification of different types of aging of the dyes used in the ink by means of a well defined correlation between the aging process and the associated decomposition products is of high interest with respect to forensic applications.[3,6,10,11] This requires a soft desorption method which does not introduce additional fragments as the latter cannot be distinguished from the products of the degradation process and hinder the discrimination of the different processes.

Desorption/Ionization induced by Neutral SO_2 Clusters (DINeC)[12] is such a soft desorption method which can be combined with mass spectrometry (MS) as an analytical tool to solve this task (Fig. 1). DINeC features matrix-free, soft desorption/ionization which comes together with simple preparation of the samples, *e.g.*, by means of drop casting.[13,14] In the case of solid samples, direct desorption from the sample surface is

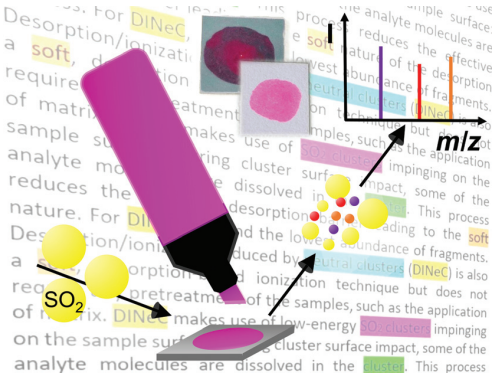

Fig. 1 Schematics of the experiment: The highlighter ink is applied *via* drawing a small dot, *e.g.*, on a SiO_2 substrate or a piece of paper (photography in the center, upper part of the figure). The SO_2 clusters desorb and ionize the dye molecules from the drawn dot for analysis by means of MS.

[a]*Institut für Angewandte Physik and Zentrum für Materialforschung, Justus-Liebig-Universität Giessen, Heinrich-Buff-Ring 16, 35392 Giessen, Germany. E-mail: michael.duerr@ap.physik.uni-giessen.de; Fax: +49641 9933409; Tel: +49 641 9933490*

[b]*Physikalisch-Chemisches Institut and Zentrum für Materialforschung, Justus-Liebig-Universität Giessen, Heinrich-Buff-Ring 17, D-35392 Giessen, Germany*

[c]*Bruker Daltonik GmbH, Fahrenheitstr. 4, D-28359 Bremen, Germany*

†Electronic supplementary information (ESI) available. See DOI: 10.1039/d1an01588e

possible[15,16] without any further treatment. The method is based on cluster-surface impact of neutral SO_2 clusters which both provide the energy for the desorption and serve as a transient matrix for the molecule to dissolve in.[17–19] The dissolvation-promoted desorption process exhibits a low desorption barrier;[19] as a consequence, the kinetic energy of the clusters can be low and desorption proceeds without fragmentation, even in the case of fragile biomolecules.[20] A variety of different classes of substances, including among others, lipids, peptides, proteins, dyes, and ionic liquids, were analyzed by means of DINeC-MS.[15,21]

Here we apply DINeC-MS for the investigation of highlighter inks with respect to chemical composition and the identification of different types of degradation, *i.e.*, thermally activated or photoinduced decomposition. As DINeC-MS does not induce any fragmentation during the measurement, even subtle differences in the degradation products can be observed and the different processes can be discriminated.

2. Experimental

Five different highlighter inks were applied on pieces of silicon wafers (1×1 cm^2, covered with a natural oxide layer) by drawing a dot of ≈5 mm in diameter (photograph shown in Fig. 1).[14] The work flow is illustrated in Fig. S1 in the ESI† where it is compared to the preparation of measurements by means of matrix assisted laser desorption/ionization (MALDI) and electrospray ionization (ESI). The mass spectrometric analysis of the highlighter inks *via* DINeC-MS was also performed on paper substrates on which a similar dot was painted and from which a piece of 1×1 cm^2 in size was cut using a scissor (photograph shown in Fig. 1). Similar results were obtained on paper and silicon wafers (Fig. S2 in the ESI†), however, for better comparability of the different samples, the experiments described in the following were mainly performed on SiO_2. Prior to sample preparation, the Si substrates were cleaned with acetone and ethanol in an ultrasonic bath.

The experimental set-up is described in detail elsewhere.[13] In brief, the cluster beam is generated *via* supersonic expansion of a gas mixture containing 3% SO_2 in He (total pressure p = 15 bar) *via* a pulsed nozzle (repetition rate f = 2 Hz, effective opening time t = 0.3 ms) into the vacuum chamber (pressure $p \approx 10^{-6}$ mbar). The resulting clusters are of 10^3 to 10^4 molecules in size and impinge on the surface with a velocity of ≈10^3 m s^{-1}.[22] This converts into an energy density below 1 eV per molecule. The desorbed molecules are transferred into a Paul-trap of a commercial ion trap mass spectrometer (amaZon speed from Bruker Daltonik GmbH, Bremen, Germany) *via* an electric field, two ion funnels, and multipole ion guides.

Reference measurements were performed with pure dyes (Basic Yellow 40 and Basic Violet 11 from Aralon Color GmbH; Basic Red 1:1 from TCI Chemicals). The reference samples were prepared from aqueous solution ($c = 1 \times 10^{-3}$ mol L^{-1}) of which 30 µL were drop-cast onto a SiO_2 substrate. For the experiments on thermal and UV-induced decomposition of the dyes, the samples were heated on a hot plate (T = 200 °C) until a noticeable change in color was observed. Alternatively, the samples were irradiated with UV-light (Camag UV-lamp Dual Wavelength λ = 254/366 nm, 8 Watts, 10 cm distance between source and samples, typical irradiation time 8 h).

3. Results and discussion

Mass spectra taken from five highlighter inks of different colors are shown in Fig. 2. Clear peaks are observed in the m/z range between 300 and 500. The three strongest peaks appear in at least three of the five spectra, but always with different relative intensity with respect to each other. Based on the m/z value, they are assigned to three well-known dye molecules: the peak at m/z = 362 is assigned to the coumarin-based fluorescent dye "Basic Yellow 40" (Fig. 3(a), m_{cation} = 362.2 u), the peak at m/z = 429 is assigned to the dye called "Basic Red 1:1", a rhodamine derivative (Rhodamine 590, Fig. 3(b), m_{cation} =

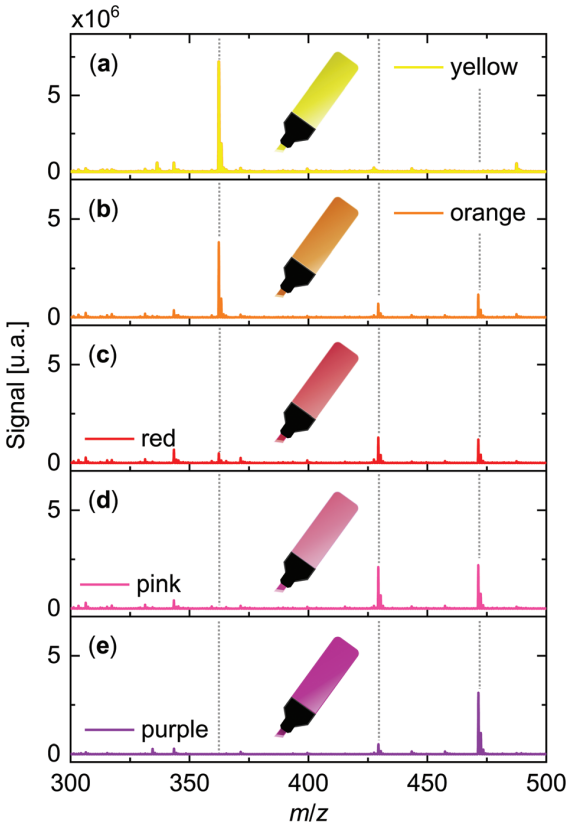

Fig. 2 Positive ion mode DINeC mass spectra from (a) yellow, (b) orange, (c) red, (d) pink, and (e) purple colored highlighter inks. Three major peaks are observed at m/z = 362, m/z = 429, and m/z = 471 in most of the spectra but with varying relative intensity. They are assigned to three dye molecules shown in Fig. 3. Peak positions of all major peaks are listed in Table S1 in the ESI.†

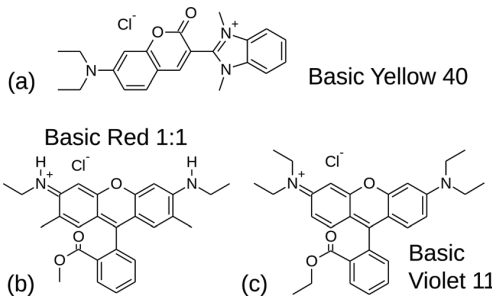

Fig. 3 Structural formulas of the three dye molecules identified in the highlighter inks. (a) Basic Yellow 40 (2-(7-(diethylamino)-2-oxo-2*H*-1-benzopyran-3-yl)-1,3-dimethyl-1*H*-benzimidazoliumchloride) (b) Basic Red 1:1 (3,6-bis(ethylamino)-9-[2-(methoxycarbonyl)phenyl]-2,7-dimethylxanthylium chloride) (c) Basic Violet 11 (3,6-bis(diethylamino)-9-(2-(ethoxycarbonyl)phenyl)xanthylium chloride).

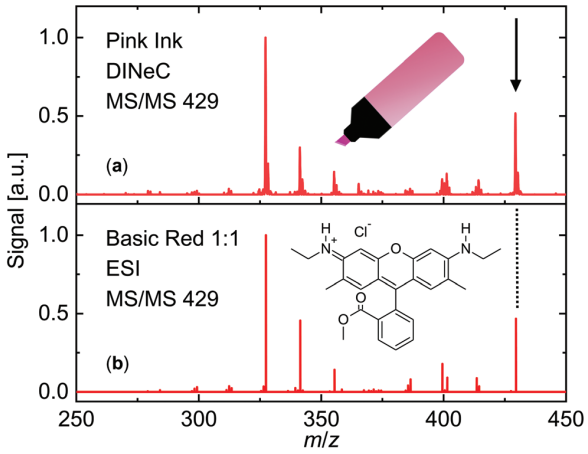

Fig. 4 (a) Positive ion mode MS/MS spectrum obtained after isolation and fragmentation of the peak at m/z = 429 in the DINeC-MS of the pink highlighter ink. The arrow indicates the peak of the intact molecule. (b) ESI MS/MS spectrum of Basic Red 1:1 as obtained from literature data.[23] For comparability, the spectra were scaled to the intensity of the most intense fragment peak. Peak positions of all major peaks are listed in Table S3 in the ESI.†

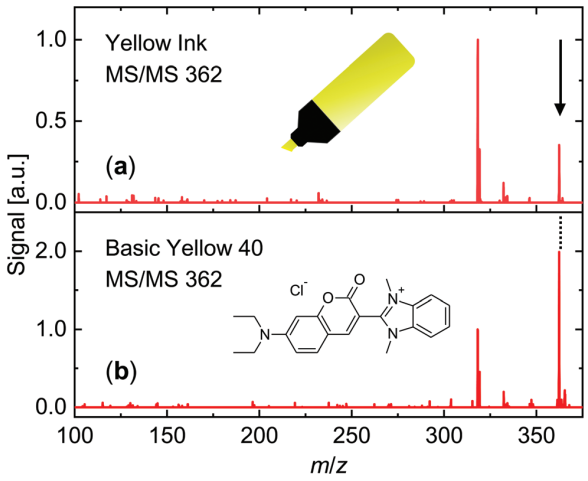

Fig. 5 (a) Positive ion mode MS/MS spectrum obtained after isolation and fragmentation of the peak at m/z = 362 in the DINeC-MS of the yellow highlighter ink. The arrow indicates the peak of the intact molecule. (b) Positive ion mode MS/MS spectrum obtained by means of DINeC-MS of the dye Basic Yellow 40. For comparability, the spectra were scaled to the intensity of the most intense fragment peak. Peak positions of all major peaks are listed in Table S4 in the ESI.†

429.2 u), and the peak at m/z = 471 is associated with the dye "Basic Violet 11", another rhodamine derivative (Rhodamine 3B, Fig. 3(c), m_{cation} = 471.3 u). The relative abundance of the three main peaks is given in Table S2 in the ESI† for each of the five highlighter inks, both for measurements performed on SiO_2 substrates as well as on paper. For a given ink, the results scatter around the mean value by a few percent, the data sets of different inks are clearly separated (Fig. S3†). Moreover, when we draw two inks on one spot, the relative abundances of the three main peaks do not match the data of one single ink and the measured values are given by the superposition of the intensity ratios of the two original inks (Table S2 and Fig. S3†).

Collision induced dissociation (CID) tandem mass spectrometry (MS^n) was used to unambiguously identify the highlighter dye molecules. The MS^n spectra from the isolated and dissociated dye molecules from the highlighter ink mixtures were either compared to literature values or to MS^n spectra which were obtained from reference dye samples.

The peak at m/z = 429, which we assign to Basic Red 1:1 based on the m/z value, was isolated in the spectrum taken from the pink highlighter and the MS/MS spectrum is compared to MS/MS data from literature (Fig. 4). The latter were obtained by electrospray ionization MS/MS.[23] Both spectra show identical peaks, which were assigned to the dye fragments.[23] Based on the agreement in peak position and relative intensity of the peaks in the MS/MS spectrum, the peak at m/z = 427 in the highlighter spectra can be clearly assigned to Basic Red 1:1.

The major peak observed in the spectrum taken from the yellow highlighter ink (m/z = 362), which was attributed to Basic Yellow 40, was isolated and the MS/MS spectrum is shown in Fig. 5. It is compared to a MS/MS spectrum of pure Basic Yellow 40 which was obtained by means of DINeC-MS from a reference sample. One intense fragment peak at m/z = 318 is observed. With a difference of $\Delta(m/z)$ = 44 to the intact dye molecule, it results from a fragment $[M_C–CO_2]^+$ due to decarboxylation of the dye molecule.[24] Further fragment peaks appear with lower intensity but show perfect agreement between the data from the yellow ink and the Basic Yellow 40 reference sample.

MS^n spectra of the peak at m/z = 471, which was isolated from the mass spectrum of the pink highlighter ink, are shown in Fig. 6. They are compared to MS^n spectra obtained from a Basic Violet 11 reference sample using DINeC-MS.

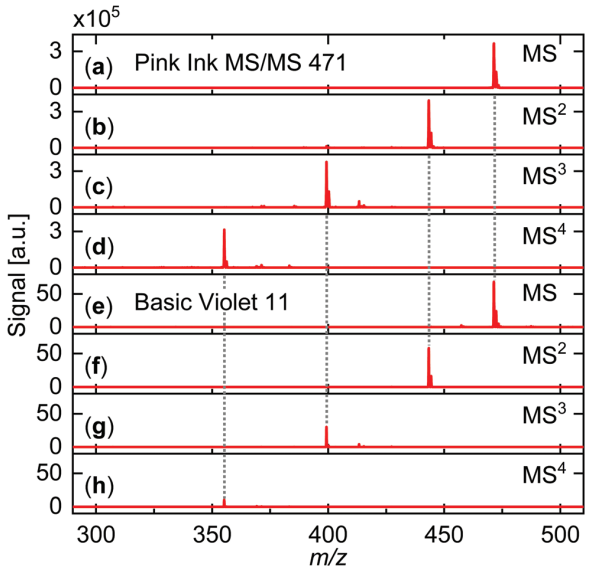

Fig. 6 (a)–(d) MS^n spectra in positive ion mode obtained after isolation and fragmentation of the peak at m/z = 471 in the DINeC mass spectrum of the pink highlighter ink. The peak in (a) is associated with the intact molecule. (e)–(h) MS^n spectra in positive ion mode obtained after cluster-induced desorption/ionization and further fragmentation of the Basic Violett 11 reference sample. Peak positions of all major peaks are listed in Table S5 in the ESI.†

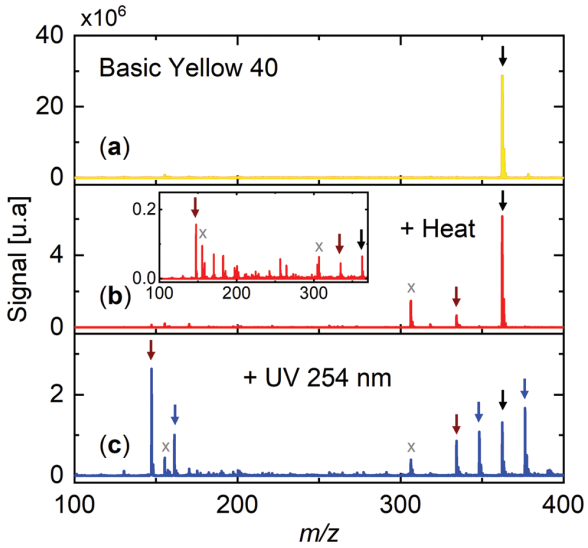

Fig. 7 (a) DINeC mass spectrum in positive ion mode of the dye Basic Yellow 40. The black arrow indicates the peak at m/z = 362 which is associated with the intact cation of the dye. (b) The spectrum from the heated dye sample shows one main additional fragment peak indicated by a brown arrow. Further decomposition with higher thermal load (intensity of the main peak reduced to less than 1% of the initial value) leads to a fragment peak at m/z = 147 (inset, 2nd brown arrow). (c) UV-light induced decomposition of the yellow dye leads to several pronounced fragment peaks in the spectrum. The peaks labeled with a blue arrow appear after UV irradiation but not after thermal decomposition. Peaks labeled with *x* are assigned to contaminations as deduced from a comparison with a bare SiO_2 substrate. Peak positions of all major peaks are listed in Table S6 in the ESI.†

Regardless the strength of the excitation amplitude during CID, the dye molecule associated with the m/z = 471 peak decomposes into one fragment with m/z = 443. Further CID leads to a fragment with m/z = 399, which can be further decomposed into a fragment with m/z = 355. Both, the peak isolated from the pink highlighter ink (Fig. 6(a)–(d)) and the major peak in the spectrum of Basic Violet 11 (Fig. 6(e)–(h)) show the same decomposition behavior, which is also reported in literature.[23,25]

Based on the MS/MS data, the main components in the highlighter inks were identified. The five colors investigated are composed of three different components which are mixed in different concentration to obtain the respective color. These results show that DINeC-MS can be used for the identification of the applied dye mixtures without further sample treatment. The relative signal intensity of the peaks associated with the different dyes is of the same order of magnitude (if present at all) within a single spectrum obtained from a sample prepared with highlighter ink; the different dyes show also comparable absolute signal intensity when the samples are prepared from pure dye solution (Fig. 7(a), 8(a), and S4(a)†). If we assume a neglectable matrix effect[15] for the investigated dyes in the polymer matrix of the highlighter ink (Fig. S2(e)†), this indicates a comparable amount of substance of the different dyes used in the highlighter inks. However, we would like to mention that some dyes, such as Brilliant Blue FCF, which is used in blue and green highlighter inks, show a strongly reduced intensity in the presence of substances with a high number of OH-groups, such as cellulose.

The full advantage of the soft nature of the DINeC process is demonstrated when we apply DINeC-MS for the investigation of degradation processes of dye molecules. Dye degradation, either caused by thermal activation or photoexcitation, is of importance with respect to the stability of the highlighter ink once applied to a given substrate, *e.g.*, paper. But also in terms of forensic applications, the discrimination of different degradation processes can be of great value with respect to the evaluation of the treatment a written document was exposed to. Only if the desorption method does not introduce fragmentation by itself, the different degradation processes can be unambiguously distinguished based on the fragments observed in the MS spectra.

We start with the thermal decomposition of Basic Yellow 40: the mass spectrum obtained from the intact dye as well as the one from a thermally treated sample are shown in Fig. 7(a) and (b), respectively. In the course of thermal decomposition, which is indicated by a reduced intensity of the peak associated with the intact molecule, a new peak at m/z = 334 appears in the mass spectrum of the yellow dye (Fig. 7(b)). With $\Delta(m/z)$ = 28, this peak can be assigned to the loss of an ethyl group of

the diethylamine group of the cation. Only further heating leads to an additional peak at m/z = 147 (Fig. 7(b), inset), which is assigned to 1,3-dimethyl-benzimidazolium. The latter peak is also observed with high intensity in the mass spectrum taken after illumination of the sample with UV-light (Fig. 7(c)). UV irradiation leads to further four additional peaks of which only one is also detected in the spectrum taken after thermal decomposition. One of the additional peaks is found at m/z = 376, *i.e.*, at a higher m/z value when compared to the intact molecule thus indicating a UV-induced reaction other than simple fragmentation. This peak was also observed with laser desorption/ionization mass spectrometry and MALDI.[3,26] It might be attributed to the reaction of a methyl group from a demethylated fragment[27] with the intact dye molecule. The demethylated fragment is also observed in the spectrum at m/z = 348. The peaks with high intensity at m/z = 147 and m/z = 161 are associated with the fragments obtained when breaking the bond between the imidazolium ring and the coumarin unit, leading to the fragment 1,3-dimethyl-benzimidazolium (m/z = 147) and the demethylated protonated 7-aminocoumarine (m/z = 161). Apparently, UV-induced degradation leads to a fragmentation pattern which is significantly different to the mass spectrum obtained from the Basic Yellow 40 molecule after thermal treatment. This is also true for increased thermal load: the respective spectrum (Fig. 7(b), inset) shows a strongly reduced intensity of the peak associated with the intact dye molecule (less than 1% of the initial intensity), but the peaks at m/z = 376, m/z = 348, and m/z = 161 do not appear; only the peak at m/z = 147 is clearly observed. The different degradation processes can thus be clearly distinguished by means of a fragmentation free desorption/ionization technique.

A very similar picture is obtained from the comparison of thermal and UV-light induced degradation of Basic Violet 11. In the mass spectrum of the thermally decomposed violet dye (Fig. 8(b)), two prominent additional peaks appear at m/z = 443 and m/z = 415. The peak at m/z = 443 is also observed with low intensity in the reference spectrum of Basic Violet 11 (Fig. 8(a)) and indicates a fragment with a missing ethyl group. It can be associated with the carboxylic acid which forms an intermediate in the synthesis of Basic Violet 11[28] and which is converted into the dye molecule by esterification. With $\Delta(m/z)$ = 56, the second fragment peak in the spectrum of the thermally decomposed violet dye might be assigned to fragments which lost two of the five ethyl groups of the dye molecule. Further heating (Fig. 8(b), inset) does not lead to further dominant fragments peaks.

In contrast, UV irradiation leads to five additional fragment peaks at m/z = 457, 429, 401, 387, and m/z = 359 (Fig. 8(c)). Including the two peaks which are also detected in the spectrum taken after thermal decomposition, the peaks follow a progression with the peaks being separated by $\Delta(m/z)$ = 14. Only the peak at the lowest m/z value, m/z = 359, is separated by $\Delta(m/z)$ = 28 from the next fragment peak. The spectrum from the sample which was decomposed with UV-light thus reflects UV-induced demethylation as reported in literature.[29–31] Again, the distribution of fragment peaks is significantly different for thermal and UV-light induced degradation and the different degradation processes can be clearly distinguished by means of DINeC-MS.

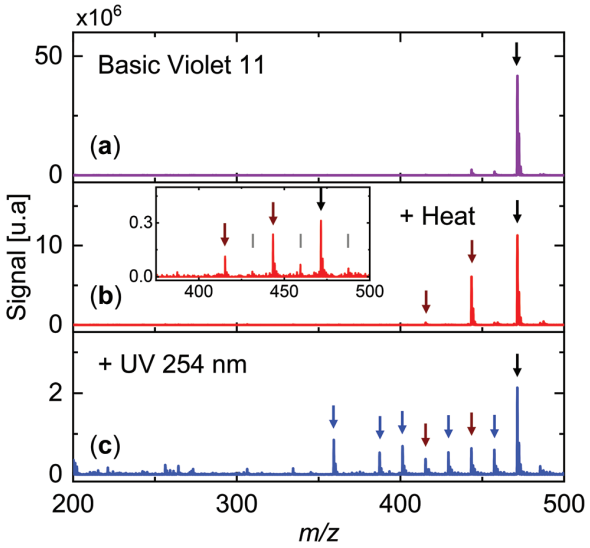

Fig. 8 (a) DINeC mass spectrum in positive ion mode of the dye Basic Violet 11. The black arrow indicates the peak at m/z = 471 associated with the intact cation of the dye. (b) The mass spectrum obtained from the heated dye sample shows two fragment peaks indicated by brown arrows. Further decomposition with higher thermal load (inset, intensity of the main peak reduced to less than 1% of the initial value) does not lead to further prominent fragment peaks. (c) Mass spectrum taken after UV-light induced decomposition of the violet dye. Additional fragment peaks are observed (labeled by blue arrows). These peaks do not coincide with the smaller peaks which are labeled by lines in the inset in (b). Peak positions of all major peaks are listed in Table S7 in the ESI.†

The same is true for the dye Basic Red 1:1, for which the products of thermal decomposition and UV degradation as analyzed by means DINeC-MS are shown in Fig. S4 in the ESI.† The prominent fragment peak observed at m/z = 373 after UV irradiation is not detected after thermal decomposition, even when high thermal load is applied. Despite the similar basic structure, clearly different fragment peaks are observed for Basic Violet 11 and Basic Red 1:1 due to their different terminal groups.

As a further example for the application of DINeC-MS as an extremely surface sensitive analysis technique, the investigation of layers of different inks is shown in Fig. 9. We compare the mass spectra derived from a paper colored with a blue ball pen (Fig. 9(a)) and a yellow highlighter (Fig. 9(d)) with mass spectra from spots colored with a blue ball pen first and then with a yellow highlighter (Fig. 9(c)) and *vice versa* (Fig. 9(b)). For the blue ball pen ink, clear peaks at m/z = 358, 372, 456, and m/z = 470 were derived which are assigned to Basic Violet 3 (including derivatives), Basic Violet 4, and Basic Blue 26, all commonly used in ball pen ink.[32] These peaks are still dominant when we wrote with the ball pen on a spot initially colored in yellow by highlighter ink (Fig. 9(b)). In reverse, the peak assigned to the highlighter ink (m/z = 362) is

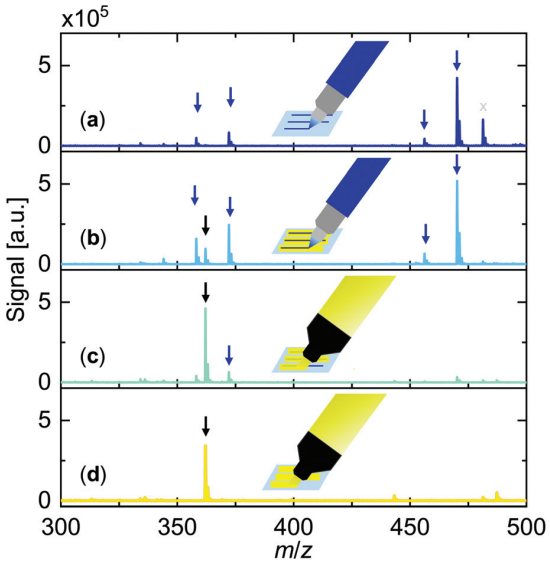

Fig. 9 DINeC mass spectrum in positive ion mode measured on a paper colored with ball pen ink (a) and yellow highlighter ink (d). The mass spectrum shown in (b) was taken from a paper spot which was first colored with yellow highlighter and afterwards with blue ball pen ink. For the mass spectrum in (c), the sampled paper spot was first colored with the ball pen and then with the highlighter. The peaks indicated with blue arrows (m/z = 358, m/z = 372, m/z = 456, and m/z = 470) are assigned to Basic Violet 3 (including derivatives), Basic Violet 4, and Basic Blue 26 as typical pigments in ball pen ink. The peak labeled with a black arrow is assigned to Basic Yellow 40 from the yellow highlighter ink. The peak indicated by an *x* is assigned to contamination. The area covered by the ball pen ink and by the highlighter ink were the same in order to avoid additional variations in intensity due to different area size sampled.

most prominent in the case when we draw the highlighter ink on top of the ball pen ink, representing the standard application. For the example shown in Fig. 9, in which it can be clearly distinguished which pen was applied first, both the bottom layer (*e.g.*, ball pen ink) and the top layer (*e.g.*, highlighter ink) covered the whole sample. The obtained spectra thus have to be considered as the most extreme cases. In reality, typically only a smaller part of the paper is covered by the ball pen ink but a larger area is covered by the highlighter ink. In that case, the relative surface areas covered by one or both inks also enter the relative intensities in the spectra; however, even in that case differences between the relative intensities can be observed depending on the sequence of application (compare Fig. S5†).

As the main results described so far rely on the soft nature of the cluster-induced desorption/ionization process, we want to briefly review the main aspects of the underlying mechanism, which was investigated in detail both experimentally[12,17,18,22] and by means of molecular dynamics (MD) simulations.[19] Most important, the desorption of surface-adsorbed molecules proceeds *via* dissolvation of these molecules in the cluster or one of the cluster fragments.[18,19] This reduces the effective desorption barrier and allows for a relatively low energy density of the clusters. With the clusters being seeded in helium, an energy density of about 0.8 eV per molecule is obtained, below the energy density threshold for sputtering processes[33] but above the heat of sublimation of SO_2, which can be seen as a rough number for the energy needed to shatter the cluster during surface impact. Shattering and further evaporation of cluster molecules from the fragment in which the desorbed molecules is dissolved first rapidly cools the system and prohibits efficient energy transfer into the molecular degrees of freedom.[12] Second, it finally leads to the bare molecules in the gas phase; if ionized, they can be employed for mass spectrometry. Although the desorption of polar molecules is additionally promoted by the stabilization of the polar molecule in the polar cluster, also non-polar molecules can be efficiently desorbed as entropy is a strong driving force for the dissolvation of the surface-adsorbed molecules in the cluster.[19] Using SO_2 as cluster constituents comes with a further advantage: as SO_2 forms sulfurous acid with water present on or in the sample, it serves as an efficient proton supply for ionization *via* proton uptake in positive ion mode leading to comparably high ionization probabilities, *e.g.*, between 10^{-3} and 10^{-2} in the case of oligopeptides.[17] For preformed ions on the surface, the ionization probability is even higher.[34]

In the following, we want to briefly discuss how these characteristics of DINeC compare to alternative ionization techniques which have been also used for the investigation of dye mixtures. We concentrate on desorption based methods, as we see one major advantage of DINeC in the most easy sample handling when applied to written ink; non-desorption based methods such as ESI always require additional preparation steps when applied to such samples (compare Fig. S1†).

If we first stay with vacuum-based techniques, MALDI is regarded as a soft method as well, but it also requires at least one additional preparation step, *i.e.*, the application of matrix (Fig. S1†). Furthermore, measurements with highlighter ink (Fig. S6†) have shown that some fragments are generated during the desorption process which is a major disadvantage when it comes to the investigation of thermal or UV-induced degradation of the dyes. In that case, it is then not clear to what extent the fragments are caused by the degradation process as such or by the desorption process. *E.g.*, for the yellow dye, both fragment peaks observed in the MALDI spectra (m/z = 334 and m/z = 348) are also present in the DINeC-MS after UV-irradiation but only the peak at m/z = 334 is observed after thermal degradation.

The same argument holds for secondary ion mass spectrometry (SIMS) measurements. For SIMS, sample treatment is comparable to DINeC, however, substantial fragmentation is typically observed.[35,36] From our results with Ar^+_{1500}-clusters (Fig. S7†), we conclude on a comparably low abundance of fragments when cluster-SIMS is applied to typical dye molecules of highlighter ink; the highest relative intensity of the fragment peaks was found to be 13% with respect to the peak associated with the intact dye molecule in the case of the yellow dye for which literally no fragments were observed with DINeC-MS. We would like to note that fragment peaks are also observed in the DINeC-MS of the violet dye (approx. 5% of the

intensity of the peak associated with the intact dye molecule, Fig. 8). However, the intensity of these peaks increases with increasing storage time of the dyes, indicating slow degradation of the dyes even in dark and at room temperature. ESI-MS show the same peaks with comparable intensity as in the DINeC mass spectra (Fig. S8†).

Desorption electrospray ionization (DESI) as a soft *ambient* desorption/ionization technique has been also applied for the investigation of highlighter and other inks;[4,9,37] it also features simple sample treatment. As with modern load lock techniques sample transfer into vacuum does not represent a major drawback any more, the work flow for sample preparation is similar for DESI and DINeC and we see the main differences between the two methods in terms of the types of experiments which can be performed: DESI can be performed on samples not suitable for high vacuum conditions; the spray of charged solvent droplets efficiently erodes the sample material from the surface.[38] DINeC is performed at high vacuum conditions, which is of advantage, *e.g.*, when it comes to reactive samples or the investigation at cryogenic temperatures. A low desorption rate ensures monolayer resolution when applied for depth-profiling the samples;[15] DINeC-MS performs also very well in the presence of large excess of salt in the sample.[39] Both methods can be applied to a wide variety of different molecules[38,40,41] and exact experimental requirements will decide on which method is to be chosen.

For the discussed application, sensitivity or limit of detection (LOD) do not play a major role; for documents written or labelled with highlighter ink, the amount of substance available is typically much higher than the LOD of all the methods compared.

4. Conclusions

In conclusion, soft cluster-induced desorption/ionization was used to identify dye molecules in various highlighter inks by means of mass spectrometry. The method can be directly applied to printed or written ink on paper or any other substrate. Furthermore, the fragmentation-free desorption method allows for the discrimination of different degradation processes, *e.g.*, thermally activated or photoinduced decomposition. The clear identification of such processes can give information on the treatment of the respective documents which can be of interest, among others, in forensic science.

Conflicts of interest

There are no conflicts to declare.

Acknowledgements

The authors acknowledge financial support from BMBF through Grant No. 05K19RG1, as well as by the Helmholtz International Center for FAIR (HICforFAIR) and the Helmholtz Graduate School for Hadron and Ion Research (P. S.). We thank Dr Simeon Vens-Cappell and Dr Corinna Henkel from Bruker Daltonik for performing the MALDI measurements and Aralon Color GmbH for providing the dyes Basic Yellow 40 and Basic Violet 11.

References

1 G. D. Christian, P. K. Dasgupta and K. A. Schug, in *Analytical Chemistry*, John Wiley & Sons, Hoboken, NJ, 2002.
2 J. McCullagh, in *Mass Spectrometry*, Oxford University Press, Oxford, 2019.
3 C. Weyermann, D. Kirsch, C. Costa-Vera and B. Spengler, *J. Am. Soc. Mass Spectrom.*, 2006, **17**, 297–306.
4 D. R. Ifa, L. M. Gumaelius, L. S. Eberlin, N. E. Manicke and R. G. Cooks, *Analyst*, 2007, **132**, 461–467.
5 J. Coumbaros, K. P. Kirkbride, G. Klass and W. Skinner, *Forensic Sci. Int.*, 2009, **193**, 42–46.
6 P. M. Lalli, G. B. Sanvido, J. S. Garcia, R. Haddad, R. G. Cosso, D. R. J. Maia, J. J. Zacca, A. O. Maldaner and M. N. Eberlin, *Analyst*, 2010, **135**, 745–750.
7 R. W. Jones and J. F. McClelland, *Forensic Sci. Int.*, 2013, **231**, 73–81.
8 R. Liu, Z. Yin, Y. Leng, W. Hanga and B. Huang, *Talanta*, 2018, **176**, 116–123.
9 G. Lee and S. Cha, *J. Am. Soc. Mass Spectrom.*, 2021, **32**, 315–321.
10 J. H. Bügler, H. Buchner and A. Dallmayer, *J. Forensic Sci.*, 2008, **53**, 982–988.
11 M. Ezcurra, J. M. G. Góngora, I. Maguregui and R. Alonso, *Forensic Sci. Int.*, 2010, **197**, 1–20.
12 C. R. Gebhardt, A. Tomsic, H. Schröder, M. Dürr and K.-L. Kompa, *Angew. Chem., Int. Ed.*, 2009, **48**, 4162–4165.
13 M. Baur, C. R. Gebhardt and M. Dürr, *Rapid Commun. Mass Spectrom.*, 2014, **28**, 290–296.
14 K. Bomhardt, P. Schneider, A. Portz, C. R. Gebhardt and M. Dürr, *J. Visualized Exp.*, 2020, **11**, e60487.
15 A. Portz, S. Aoyagi and M. Dürr, *Biointerphases*, 2018, **13**, 03B405.
16 P. Schneider, F. Verloh, A. Portz, S. Aoyagi, M. Rohnke and M. Dürr, *Anal. Chem.*, 2020, **92**, 15604–15610.
17 B.-J. Lee, M. Baur, C. R. Gebhardt and M. Dürr, *Rapid Commun. Mass Spectrom.*, 2013, **27**, 1090.
18 A. Portz, M. Baur, C. R. Gebhardt, A. J. Frank, P. Neuderth, M. Eickhoff and M. Dürr, *J. Chem. Phys.*, 2017, **146**, 134705.
19 P. Schneider and M. Dürr, *J. Chem. Phys.*, 2019, **150**, 214301.
20 A. Portz, K. Bomhardt, M. Rohnke, P. Schneider, A. Asperger, C. R. Gebhardt and M. Dürr, *Biointerphases*, 2020, **15**, 021001.
21 A. Portz, M. Baur, G. Rinke, S. Abb, S. Rauschenbach, K. Kern and M. Dürr, *Anal. Chem.*, 2018, **90**, 3328–3334.
22 F. Eusepi, A. Tomsic and C. R. Gebhardt, *Anal. Chem.*, 2003, **75**, 5124–5128.

23 M. W. Forbes and R. A. Jockusch, *J. Am. Soc. Mass Spectrom.*, 2011, **22**, 93–109.
24 Z. Ren, B. Nie, T. Liu, F. Yuan, F. Feng, Y. Zhang, W. Zhou, X. Xu, M. Yao and F. Zhang, *Molecules*, 2016, **21**, 1511.
25 B. R. V. Ferreira, D. N. Correa, M. N. Eberlin and P. H. Vendramini, *J. Braz. Chem. Soc.*, 2017, **28**, 136–142.
26 J. Siegel, J. Allison, D. Mohr and J. Dunn, *Talanta*, 2005, **67**, 425–429.
27 F. Khuong-Huu and D. Herlem, *Tetrahedron Lett.*, 1970, **11**, 3649–3652.
28 Taoka Chemical Co Ltd, *EU Patent*, EP0468821A1, 1990.
29 N. Tsuchiya, K. Kuwabara, A. Hidaka, K. Oda and K. Katayama, *Phys. Chem. Chem. Phys.*, 2012, **14**, 4734–4741.
30 Z. Yu and S. S. C. Chuang, *Phys. Chem. Chem. Phys.*, 2007, **111**, 13813–13820.
31 C.-C. Chen and C.-S. Lu, *Environ. Sci. Technol.*, 2007, **41**, 4389–4396.
32 C. M. Almeida, D. D. Sales, F. Tosato, N. A. dos Santos, J. F. A. Filho, C. J. Macrino, F. E. Pinto, P. R. Filgueiras and W. Romão, *Microchem. J.*, 2019, **148**, 220–229.
33 D. Rading, R. Moellers, H.-G. Cramer and E. Niehuis, *Surf. Interface Anal.*, 2013, **45**, 171–174.
34 B.-J. Lee, C. R. Gebhardt, H. Schröder, K.-L. Kompa and M. Dürr, *Chem. Phys. Lett.*, 2013, **556**, 77–81.
35 Y. Yokoyama, S. Aoyagi, M. Fujii, J. Matsuo, J. S. Fletcher, N. P. Lockyer, J. C. Vickerman, M. K. Passarelli, R. Havelund and M. P. Seah, *Anal. Chem.*, 2016, **88**, 3592–3597.
36 J. Y. Baek, C. M. Choi, S. J. Lee, B. K. Min, H. S. Kang, D. C. Choo, J. Y. Sung, J. S. Jin and M. C. Choi, *Appl. Surf. Sci.*, 2019, **507**, 144887.
37 M. Jurisch, P. H. Vendramini, M. N. Eberlin and R. Augusti, *J. Am. Soc. Mass Spectrom.*, 2020, **31**, 1000–1003.
38 T. L. Salter, F. M. Green, I. S. Gilmore, M. P. Seah and P. Stokes, *Surf. Interface Anal.*, 2011, **43**, 294–297.
39 A. Portz, M. Baur, C. R. Gebhardt and M. Dürr, *Biointerphases*, 2016, **11**, 02A316.
40 M. Baur, B.-J. Lee, C. R. Gebhardt and M. Dürr, *Appl. Phys. Lett.*, 2011, **99**, 234103.
41 J. Heep, P. H. K. Tuchecker, C. R. Gebhardt and M. Dürr, *ACS Omega*, 2019, **4**, 22426–22430.

Supporting Information for:

Cluster-induced desorption/ionization mass spectrometry of highlighter ink: unambiguous identification of dyes and degradation processes based on fragmentation-free desorption

K. Bomhardt[1], P. Schneider[1], M. Rohnke[2], C. Gebhardt[3] and M. Dürr[1,*]

[1] *Institut für Angewandte Physik and Zentrum für Materialforschung, Justus-Liebig-Universität Giessen, Heinrich-Buff-Ring 16, D-35392 Giessen, Germany*

[2] *Physikalisch-Chemisches Institut and Zentrum für Materialforschung, Justus-Liebig-Universität Giessen, Heinrich-Buff-Ring 17, D-35392 Giessen, Germany*

[3] *Bruker Daltonik GmbH, Fahrenheitstr. 4, D-28359 Bremen, Germany*

[*] *Corresponding author: michael.duerr@ap.physik.uni-giessen.de*

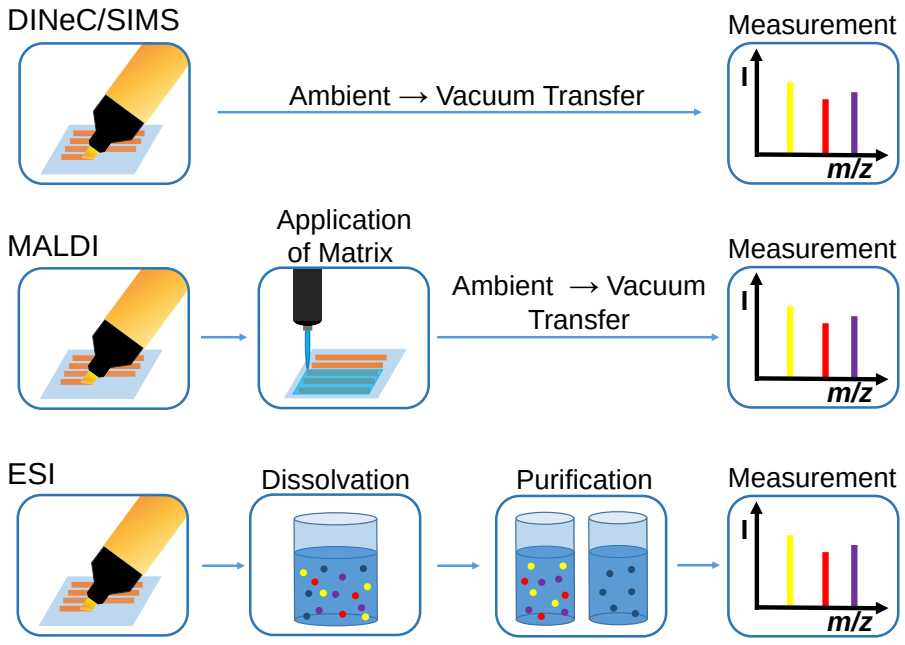

Figure S1: Schematic illustration of the workflow required for different ionization methods when applied for the investigation of inks written on paper substrates.

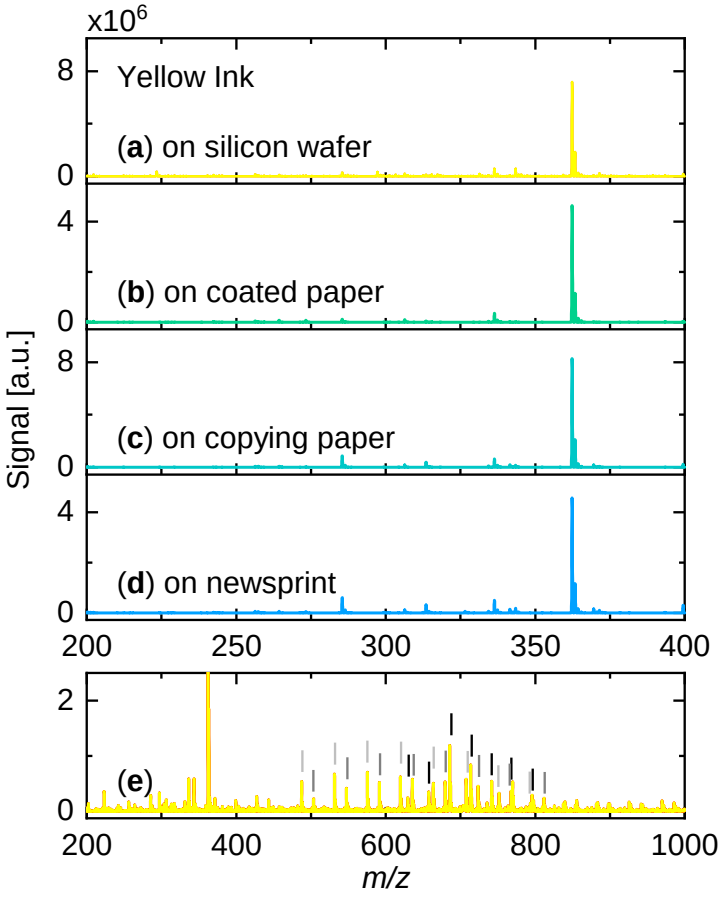

Figure S2: Positive ion mode DINeC mass spectra obtained from samples with yellow highlighter drawn on different substrates: **(a)** silicon wafer, **(b)** coated paper, **(c)** copying paper, and **(d)** newsprint. **(e)** shows the spectrum of **(a)** in an extended mass range. In addition to the peak associated with the yellow dye, three peak progressions with the peaks separated by $\Delta(m/z) = 44$ (indicated by light and dark grey lines) and $\Delta(m/z) = 28$ (black lines) are observed, which are assigned to polymer matrix in the highlighter ink.

Table S1: Ion peaks observed in the spectra shown in Figure 2 obtained by means of DINeC-MS

m/z	Intensity [a.u.]				
	(a)	**(b)**	**(c)**	**(d)**	**(e)**
471.4	35401	1170803	1192156	2198989	2518462
429.4	34588	688925	1303573	2105223	454977
362.3	7178677	3773461	494993	21871	7489

Table S2: Relative peak intensities of peaks associated with the three dye molecules of the highlighter inks investigated by means of DINeC-MS.

Color	**Substrate**	**BY40**	**BR1:1**	**BV11**
Yellow	Si	100	0	0
	paper	100	0	0
Red	Si	17	43	40
	paper	11	43	46
Purple	Si	0	15	85
	paper	0	10	90
Orange	Si	68	12	20
	Si	65	14	21
	Si	78	11	11
	Si	68	13	19
	Si	76	10	14
	paper	72	11	17
	average	**71±4**	**12 ±1**	**17±3**
Pink	Si	0	49	51
	Si	0	52	48
	Si	0	62	38
	Si	0	59	41
	Si	0	56	44
	paper	0	52	48
	average	**0 ±0**	**55 ±5**	**45±4**
Mix Orange + Pink	Si	47	29	24
	Si	27	37	36
	Si	32	35	33
	Si	53	26	21
	average	**40 ±11**	**32 ±4**	**29±6**

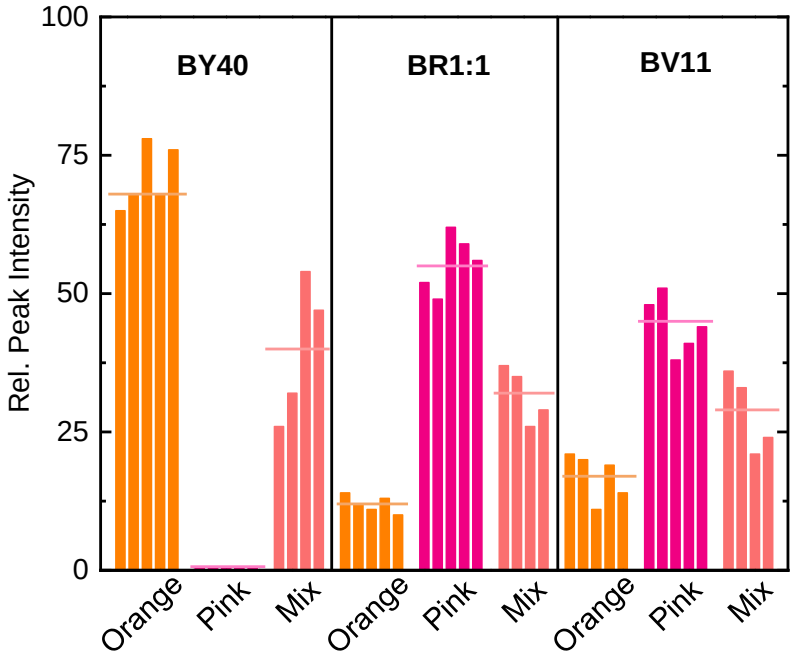

Figure S3: Relative peak intensity of the peaks associated with the three dyes Basic Yellow 40, Basic Red 1:1, and Basic Violet 11 as observed in DINeC-MS for the orange and pink highlighter inks as well as for an orange-pink highlighter ink mixture (ratio approx. 1:1). The values of the pure inks scatter slightly around the mean value (compare also Tab. S2); the distribution for the pure inks and the mixture are clearly separated.

Table S3: Ion peaks observed in the spectra shown in Figure 4 obtained by means of DINeC-MS

m/z	Intensity [a.u.]
429.3	115943
414.3	20460
401.3	12682
399.4	21832
365.3	15223
355.3	32017
341.3	67041
327.3	220820

Table S4: Ion peaks observed in the spectra shown in Figure 5 obtained by means of DINeC-MS

m/z	Intensity [a.u.]	
	(a)	**(b)**
362.3	30399	80392
347.3	2377	3867
332.3	10306	8030
318.3	86282	40389

Table S5: Ion peaks observed in the spectra shown in Figure 6 obtained by means of DINeC-MS

m/z	Intensity [a.u.]	
	(a)-(d)	**(e)-(h)**
471.4	366334	6841730
443.3	393313	5834746
399.3	377406	3045115
355.3	315823	1054573

Table S6: Ion peaks observed in the spectra shown in Figure 7 obtained by means of DINeC-MS

m/z	Intensity [a.u.]		
	(a)	**(b)** (inset)	**(c)**
376.3	64801	52294 (8953)	1670345
362.3	28684768	6149794 (64273)	1316430
348.3	50053	71441 (8110)	1085953
334.3	172624	669177 (44314)	861559
306.3		Contamination	
264.4	112327	69156 (37615)	70667
256.3	161211	91489 (56581)	83525
242.4	64613	20702 (22030)	32460
224.4	52082	28886 (20023)	27829
200.3	241682	96139 (36716)	136424
182.3	166165	54502 (66079)	82115
170.3	248930	187977 (70029)	169699
161.3	2624	11973 (6739)	1007542
155.3		Contamination	
147.3	14421	137040 (156510)	2628727

Table S7: Ion peaks observed in the spectra shown in Figure 8 obtained by means of DINeC-MS

m/z	Intensity [a.u.]		
	(a)	**(b)** (inset)	**(c)**
485.4	337919	236890 (17636)	203644
471.4	41780428	11294170 (312748)	2136593
457.4	1519330	251161 (24148)	607563
443.4	2317717	6093131 (235756)	646205
429.3	45260	24662 (9527)	547898
415.3	173562	282014 (112150)	383407
401.3	8838	5498 (2418)	699801
387.3	14077	14498 (24115)	538323
359.3	4970	2548 (4398)	854511

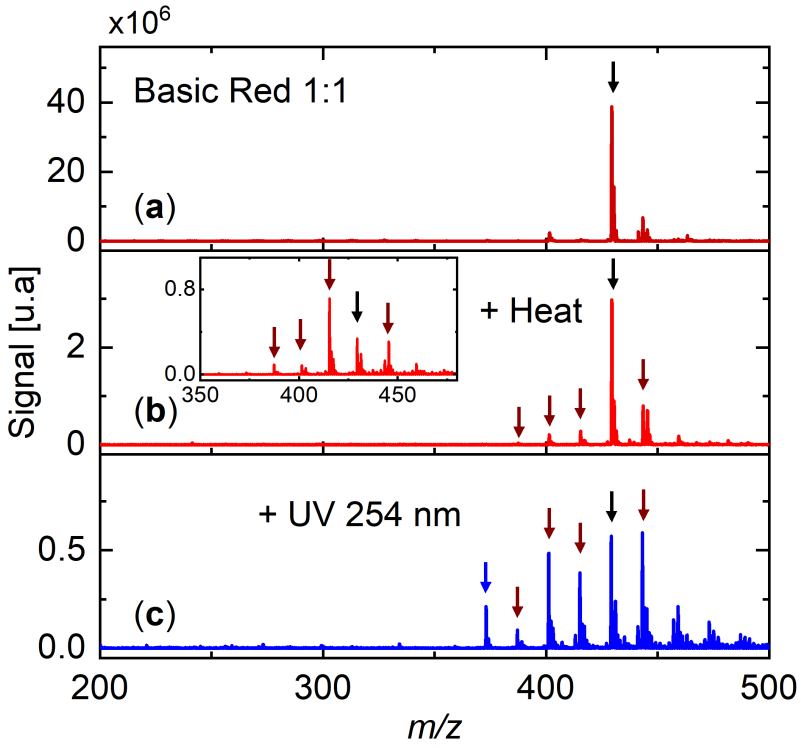

Figure S4: **(a)** DINeC mass spectrum in positive ion mode of the dye Basic Red 1:1. The black arrow indicates the peak at $m/z = 429$ associated with intact cation of the dye. **(b)** The mass spectrum obtained from the heated dye sample shows three fragment peaks indicated by brown arrows. An additional peak at $m/z = 443$, i.e., at higher m/z values when compared to the intact dye molecule, is also observed and labelled. It is attributed to a dye molecule carrying an additional methyl group, similar as observed for the Basic Yellow 40 sample after UV-light-induced decomposition (Fig. 7(c)). Further decomposition with higher thermal load (intensity of the main peak reduced to less than 2 % of the initial value) does not lead to further prominent fragment peaks. **(c)** Mass spectrum taken after UV-light induced decomposition of the red dye. An additional fragment peak is observed (labeled by a blue arrow).

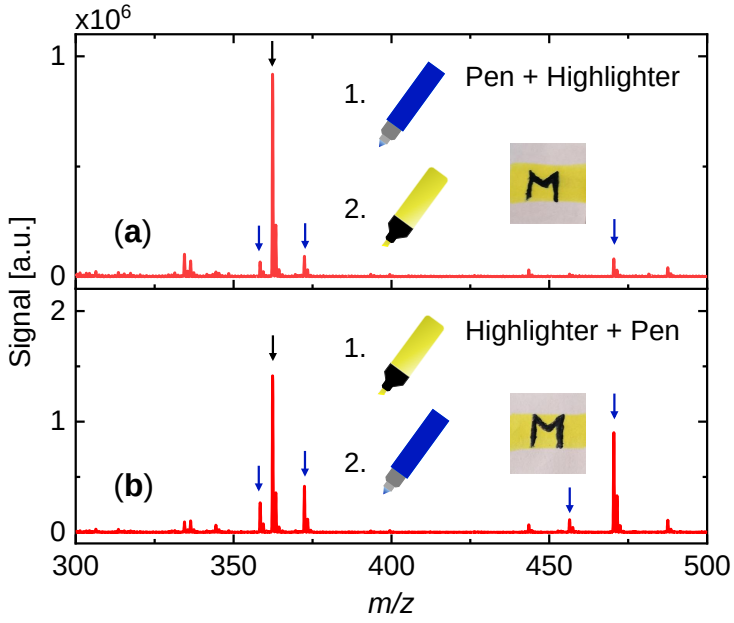

Figure S5: Positive ion mode DINeC mass spectra of **(a)** highlighter ink drawn on pen ink on a paper substrate and **(b)** strokes of pen ink drawn on the highlighter ink. Insets: Photographs of the respective samples. Black arrows indicate the peak assigned to Basic Yellow 40 from the yellow highlighter ink, blue arrows indicate the peaks assigned to the dyes used in the pen ink. If the highlighter is applied after the pen ink **(a)**, the intensity of the fluorescent dye shows highest signal intensitiy. When the order of application is reversed **(b)**, the intensity of the peaks associated with the pen ink increase in intensity. The relative intensity of the peaks is given by the intensity as measured for the pure and the completely covered ink/highlighter and highlighter/ink systems (Fig. 9) weighted by the relative area covered by the differently colored parts of the sample.

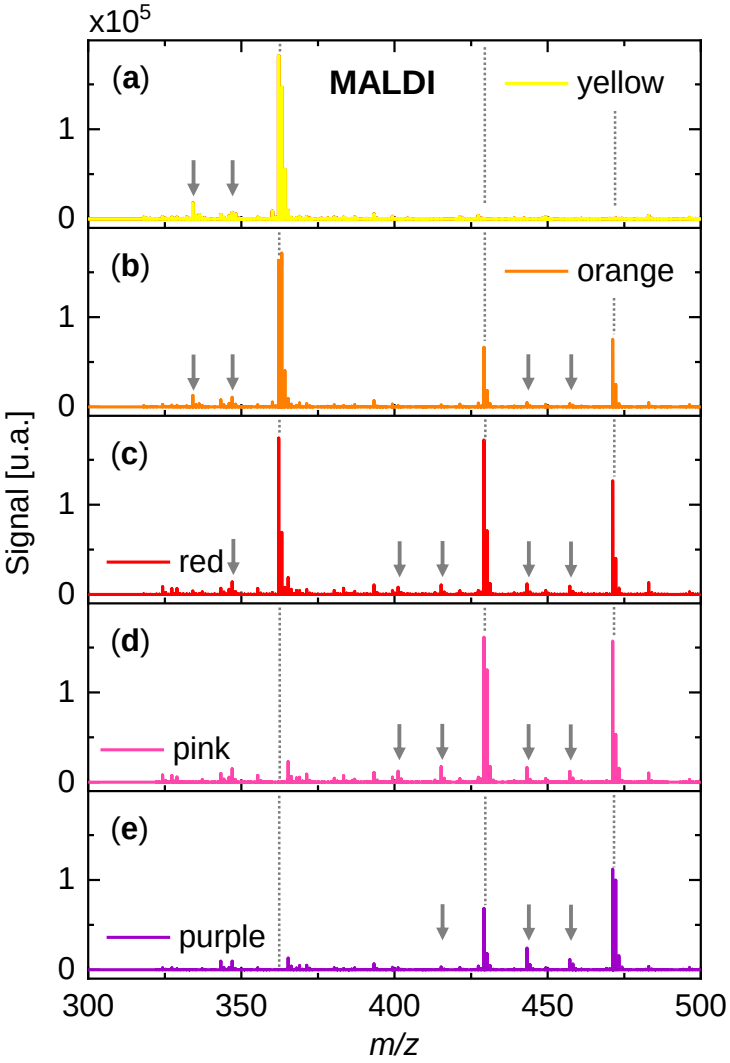

Figure S6: Positive ion mode MALDI mass spectra from **(a)** yellow, **(b)** orange, **(c)** red, **(d)** pink, and **(e)** purple colored highlighter inks from paper substrates. Three major peaks which are assigned to the dye molecules are observed at $m/z = 362$, $m/z = 429$, and $m/z = 471$ in most of the spectra but with varying relative intensity. Arrows indicate fragmentation peaks at $m/z = 334$ and $m/z = 348$ (yellow dye), $m/z = 401$ and $m/z = 415$ (red dye), and $m/z = 443$ and $m/z = 457$ (violet dye), which are also observed in DINeC spectra measured after dye degradation. The measurements were performed on a Bruker timsTOF fleX time-of-flight apparatus; 2,5-dihydroxybenzoic acid (DHB) was used as matrix. DHB was dissolved in an acetonitrile/water (90:10) mixture and sprayed (nozzle temperature 60 °C) onto the highlighter ink written on copying paper.

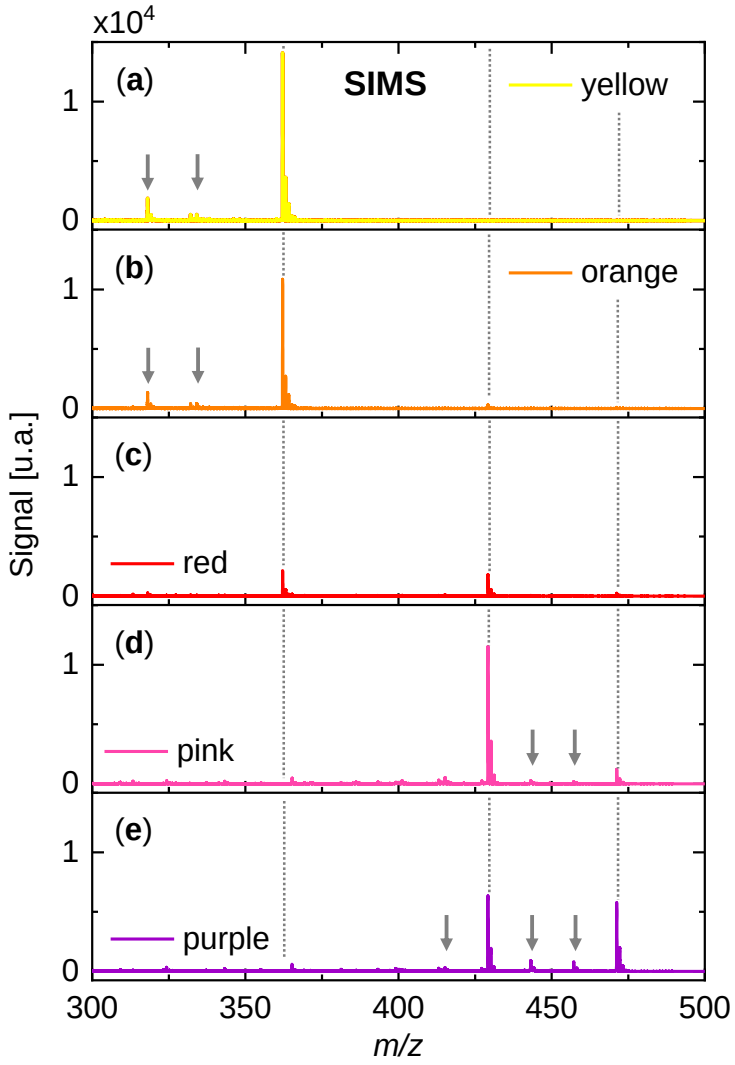

Figure S7: Positive ion mode SIMS mass spectra from **(a)** yellow, **(b)** orange, **(c)** red, **(d)** pink, and **(e)** purple colored highlighter inks applied to Si substrates. Three major peaks are which are assigned to the dye molecules observed at $m/z = 362$, $m/z = 429$, and $m/z = 471$ in most of the spectra but with varying relative intensity. Arrows indicate fragmentation peaks at $m/z = 318$ and $m/z = 334$ (yellow dye), $m/z = 415$ (red dye), and $m/z = 443$ and $m/z = 457$ (violet dye), which are also observed in DINeC spectra measured after dye degradation. The measurements were performed with a M6 Hybrid SIMS instrument (IONToF GmbH, Münster, Germany). As primary ions, 20 keV $Ar_{1500}{}^{+}$-clusters were used at a cycle time of 150 μs resulting in a primary ion current of $I = 0.07$ pA. The ion beam was rasterized with 128×128 pixels on an area of 100×100 μm^2. Total ion dose was 10^{-12} ions/cm^2 for all measurements. The obtained mass resolution (FWHM) at $m/z = 362.2$ was $m/\Delta m > 3.500$ for all spectra.

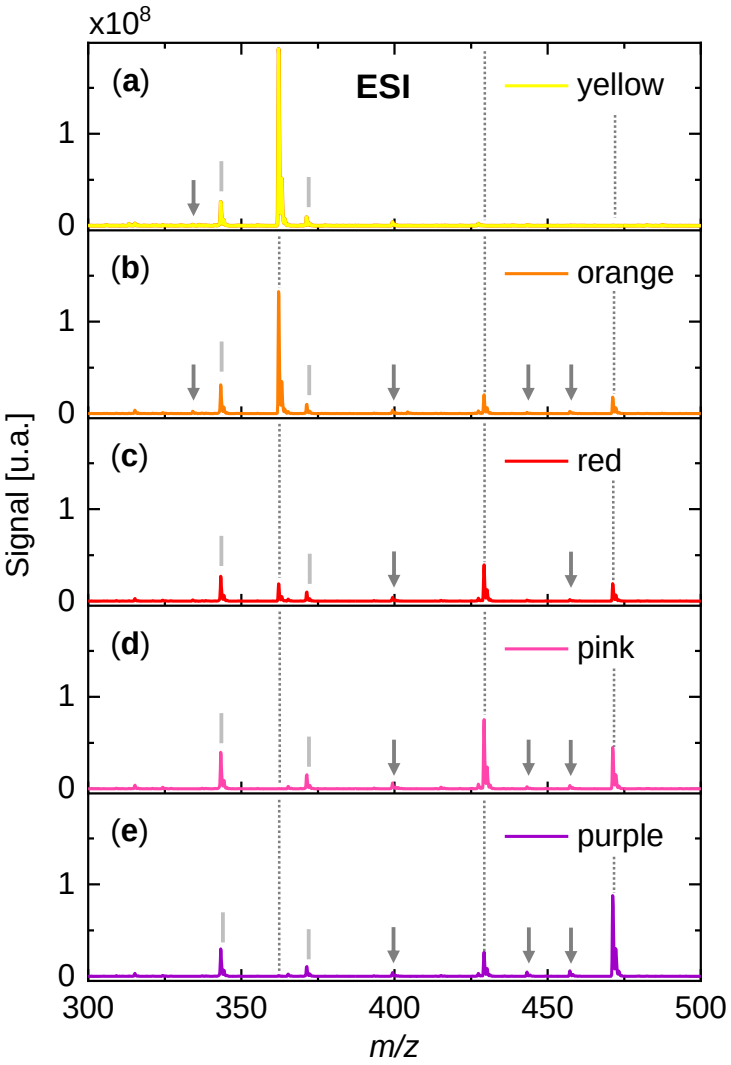

Figure S8: Positive ion mode ESI mass spectra from **(a)** yellow, **(b)** orange, **(c)** red, **(d)** pink, and **(e)** purple colored highlighter inks. For the measurements, which were performed on a Bruker amaZon speed mass spectrometer (Bruker Daltonik GmbH, Bremen, Germany), a dot of ink which was drawn on a piece of wafer, was dissolved in a mixture of acetonitrile/water (50:50) containing 0.1 Vol% formic acid. Three major peaks which are assigned to the dye molecules are observed at $m/z = 362$, $m/z = 429$, and $m/z = 471$ in most of the spectra but with varying relative intensity. Arrows indicate fragment peaks at $m/z = 334$ (yellow dye), $m/z = 399$ (red dye), and $m/z = 443$ and $m/z = 457$ (violet dye), which are also observed in DINeC mass spectra measured after dye degradation. Gray lines indicate additional peaks which are not attributed to dye fragments, they are also observed in DINeC mass spectra of the highlighter inks. They are tentatively assigned to additional compounds of the highlighter ink (Fig. 3, Tab. S1).

4.2 Artikel II

Surface Properties of Ionic Liquids: A Mass Spectrometric View Based on Soft Cluster-Induced Desorption
K. Bomhardt, P. Schneider, T. Glaser, and M. Dürr;
J. Am. Soc. Mass Spectrom. **33**, 974 - 980 (2022).

ACS Partner Journal

Journal of the American Society for Mass Spectrometry

pubs.acs.org/jasms

Research Article

Surface Properties of Ionic Liquids: A Mass Spectrometric View Based on Soft Cluster-Induced Desorption

Karolin Bomhardt, Pascal Schneider, Timo Glaser, and Michael Dürr*

Cite This: J. Am. Soc. Mass Spectrom. 2022, 33, 974−980

Read Online

ACCESS | Metrics & More | Article Recommendations | Supporting Information

ABSTRACT: Desorption/ionization induced by neutral clusters (DINeC) in combination with mass spectrometry (MS) was used for the investigation of the molecular composition of the surface of ionic liquids (IL). Based on the surface sensitivity of DINeC-MS, accumulation of either cations or anions was discriminated on the surface of bulk IL depending on the molecular structure of the IL components. In particular, cations with long alkyl chains aggregate on the surface, but this tendency is more reduced the larger the respective anion is; in the case of larger anions and smaller cations, it can be even reversed. For thin layers of IL, the ratio between cations and anions as detected in the mass spectra was found to be further influenced by the substrate surface.

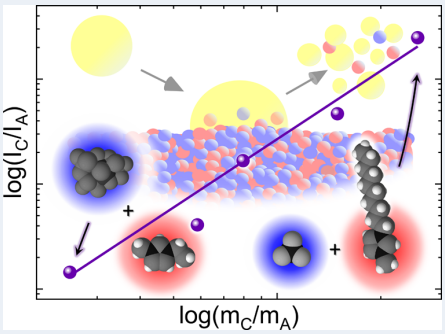

INTRODUCTION

Ionic liquids have been intensively investigated with respect to their bulk properties.[1−3] However, as for most applications the interaction proceeds via the surface, e.g., in the case of catalytic reactions,[4,5] the surface properties are of high interest, as well. Important information on the surfaces of ionic liquid (IL) has been obtained, among others, by X-ray-based methods: structural properties on the nanoscale were deduced by the electron density profile as obtained by means of X-ray reflection measurements.[6−9] X-ray photoelectron spectroscopy (XPS), in particular, angle-resolved X-ray photoelectron spectroscopy (ARXPS), contributed to the investigation of the surface composition, both with respect to the main constituents of the IL as well as with respect to (surface) contaminations.[1,10−14]

In contrast, only a very limited number of studies addressed the surface composition of ionic liquids by means of mass spectrometry. For example, crystallization of room temperature IL has been investigated at reduced temperatures using secondary ion mass spectrometry (SIMS),[15,16] but significant fragmentation of the IL constituents was induced by the primary ions in use.[15−17] With laser-desorption-based methods, the surface sensitivity required for the investigation of the surface composition of IL is typically not achieved. Thus, a soft and surface-sensitive mass spectrometric technique which directly addresses the uppermost surface region could provide additional information with respect to the actual surface structure and composition of the ionic liquid.

Desorption/ionization induced by neutral clusters (DINeC), which exhibits extreme surface sensitivity,[18] can be employed as a soft mass spectrometry (MS) technique.[19−22] DINeC is based on a low-energy beam of SO_2 clusters[19,20] in which the analyte molecules are dissolved during cluster-surface impact[23] (Figure 1). This dissolvation process reduces the effective desorption barrier,[24] thus cluster-induced desorption is operative at comparably low beam energy, leading to the fragmentation-free nature of the desorption process.[21,22]

Here, we demonstrate the application of DINeC-MS for the investigation of the surface composition of IL. Based on their negligible vapor pressure,[3,25,26] ILs allow for the investigation of liquid surfaces by means of particle-based analysis techniques such as mass spectrometry under high vacuum conditions. We find a strong tendency of cations with longer alkyl chains to accumulate on the surface, in agreement with literature.[27] With increasing size of the corresponding anion, this tendency of the cations to accumulate on the surface is reduced; in the case of larger anions and smaller cations, the anionic signal is dominant as the anions then accumulate on the surface. The composition of thin layers of IL is found to be further influenced by the surface of the substrate; structural inhomogeneities such as the formation of islands of bulk material are deduced from the temporal evolution of the mass spectra and the relative intensities of cations and anions.

Received: February 8, 2022
Revised: April 29, 2022
Accepted: May 2, 2022
Published: May 17, 2022

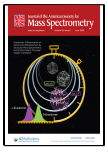

https://doi.org/10.1021/jasms.2c00038
J. Am. Soc. Mass Spectrom. 2022, 33, 974−980

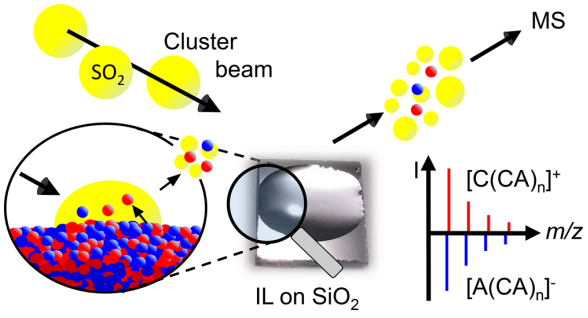

Figure 1. Schematic representation of the DINeC-MS experiment on IL. A droplet of IL is deposited on a small piece of a silicon wafer (center). During cluster-surface impact, cations and anions are desorbed from the surface via dissolvation in the shattering cluster (left). The resulting mass spectra show a series of signals both in positive and in negative ion mode, which reflects the desorption of small clusters of ionic liquid with either one cation ($[C(CA)_n]^+$; A: anion, C: cation, n = 0, 1, 2, 3, ...) or one anion ($[A(CA)_n]^-$) in excess, respectively.

EXPERIMENTAL SECTION

The SO_2 clusters used for desorption/ionization in the DINeC experiment were generated via adiabatic expansion of a gas mixture containing 3% SO_2 in He (total pressure p_{nozzle} = 15 bar, base pressure in the vacuum chamber $p_{base} \approx 10^{-6}$ mbar) using a pulsed nozzle (repetition rate f = 2 Hz, effective opening time t = 0.3 ms).[28] The clusters consist of 10^3 to 10^4 SO_2 molecules; they hit the surface with a velocity of $\approx 10^3$ m/s (mainly given by the speed of the carrier gas, i.e., He) which converts into an energy density of ≈ 0.8 eV per molecule.[29] The ions desorbed during cluster surface impact are then transferred into a commercial ion trap mass spectrometer (amaZon speed from Bruker Daltonik GmbH, Bremen, Germany) via two ion funnels and multipole ion guides.[20]

The ionic liquids investigated in this study comprise the cations and anions which are summarized in Figure 2; the cations (C1 and C2) are based on imidazolium ions, and the anions are fluorinated alkyl sulfonyl imides (A3 and A4), tetrafluoroborate (A1), trifluoromethylsulfonate (A2), and tris(pentafluoroethyl)trifluorophosphate (A5). The ionic liquids C1A1 (>98%) and C1A3 (>98%) were purchased at TCI Chemicals Deutschland GmbH, Eschborn, Germany; C1A2 (>99%) was purchased at Iolitec − Ionic Liquids Technologies GmbH, Heilbronn, Germany; C2A5 (>99%) was purchased at Sigma-Aldrich Chemie GmbH, Taufkirchen, Germany. C1A4 was synthesized by dissolving lithium bis(pentafluoroethanesulfonyl)imide (TCI >98%) in water adding 30 wt % 1-decyl-3-methylimidazolium chloride (TCI >96%). The ionic liquid was extracted with dichloromethane and washed with water, and the solvent was removed by evaporation.[30] Chemical formulas and molecular masses of the cations C1 and C2 as well as of the anions A1−A5 are summarized in Table S1 in the Supporting Information.

The SiO_2 substrates were cleaned with acetone and ethanol using an ultrasonic bath. For measurements on the surface of ionic liquid bulk material, small substrates (4 × 4 mm^2) were completely covered with a droplet of the ionic liquid. Thin films were prepared by drop-casting the IL solution (c = 1 mM in ethanol, V = 5 μL) on a SiO_2 substrate of 1 cm^2 in size,[31] and the solvent was evaporated under ambient conditions. All samples were heated at 100 °C for 30 min before mounting

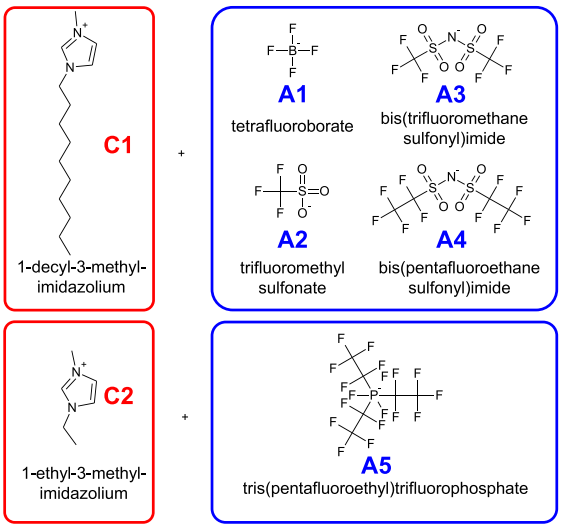

Figure 2. Structural formulas of the investigated ionic liquids. The cation C1 was combined with anions of increasing size (A1−A4). In addition, the cation C2 was combined with the anion A5.

them in the vacuum chamber in order to evaporate water accumulated on and in the ionic liquid.

RESULTS AND DISCUSSION

Positive and negative ion mode spectra from the surface of a droplet of the ionic liquid C1A3 are shown in Figure 3. Both in

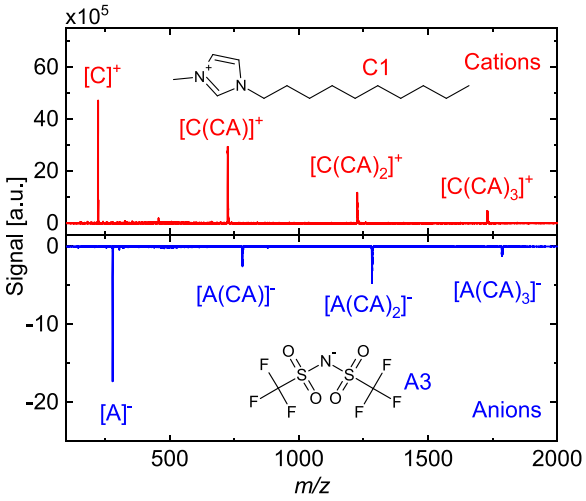

Figure 3. DINeC mass spectra in positive and negative ion mode as obtained from the surface of a bulk sample of C1A3.

positive and in negative ion mode, four distinct peaks are observed. The peaks are separated by $\Delta(m/z)$ = 503, which corresponds to a C1A3 cation−anion unit; the peak at the lowest m/z value (m/z = 223) in the positive ion mode spectrum is assigned to $[C]^+$, and the peak at the lowest m/z value (m/z = 280) in the negative ion mode spectrum is assigned to $[A]^-$. All further peaks thus represent clusters of the ionic liquid, i.e., $[C(CA)_n]^+$ for the cationic clusters and

https://doi.org/10.1021/jasms.2c00038
J. Am. Soc. Mass Spectrom. 2022, 33, 974−980

$[A(CA)_n]^-$ with n = 1−3 for the anionic clusters. The peak intensity of the IL cluster peaks is always lower than that of the peaks assigned to the bare anions and cations, respectively; overall, it decreases with increasing m/z values.

DINeC mass spectra from the other ionic liquids of this investigation (Figure S1 in the Supporting Information) are very similar to the spectra of C1A3 shown in Figure 3; they all show the peak associated with the single molecular ion (highest intensity) and in most cases IL cluster ions with in general decreasing peak intensity with increasing m/z value both in positive and negative ion mode. In some cases, minor deviations from this general trend are observed; in particular, the intensity of the peak associated with the $[A(CA)_n]^-$ cluster with n = 1 can be lower than the intensity of the peak associated with the respective cluster with n = 2. The latter observation is attributed to the existence of clusters with a particularly large/small binding energy at a given number of cluster constituents.[32] Most important, however, the intensity ratio between the cationic and anionic signal, I_C/I_A, strongly varies with varying composition of the IL.

In Figure 4, I_C/I_A is plotted for five different ILs as a function of the ratio of the mass of the cation and the mass of the anion, m_C/m_A. The latter can be seen as a most simple measure of the size and complexity of the molecular constituents of the IL. For cation C1, the relative cationic signal intensity increases with decreasing size of the anion (A4−A1); for A1, the smallest anion employed, a large excess of cationic signal intensity is observed. On the other hand, when the largest anion A5 is combined with the small cation C2, a strong excess of anionic signal intensity is observed.

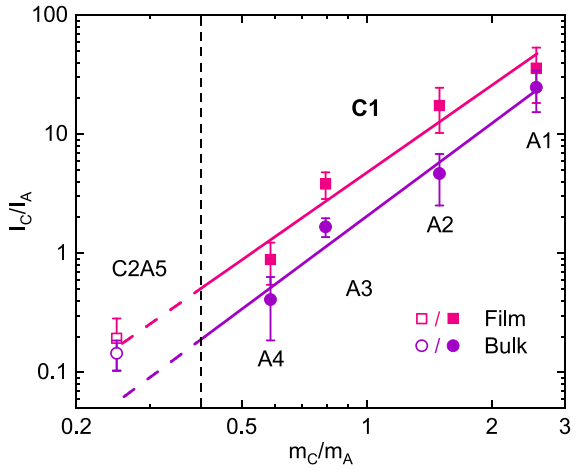

Figure 4. Intensity of the cationic mass peaks with respect to the intensity of the anionic mass peaks, I_C/I_A, as a function of the mass ratio of cations and anions, m_C/m_A. Data are shown for bulk IL (dots) and thin film samples (squares). Intensity was summed over all peaks associated with IL observed in the respective spectra; the data points represent the average value over at least three measurements. A1−A4 were measured in combination with C1 as cation; A5 was measured with C2 as cation. Straight lines are linear fits in the double-logarithmic plot, taking into account the data for A1−A4, i.e., the same cation C1.

Based on previous investigations on the desorption and ionization efficiency of the DINeC process,[18,24,33] we interpret the observed change in signal intensity as a direct result of the surface composition of the respective IL: First, the desorption efficiency of the DINeC process has been shown to be largely independent of the analyte molecule.[18,24,33] Second, the constituents of the ILs are ions; i.e., the ionization probability is unity and does not change from sample to sample either. Our observation then goes along the results of previous investigations of the surface composition of IL in terms of a change of the surface composition with different combinations of cations and anions:[5,9,11,12,34] depending on the molecular structure of the constituents of the IL, one or the other component may accumulate at the surface. Although we use the mass of the cations and anions as a simple measure for their size and complexity, we would like to point out that the actual molecular structure, which is very different for the different anions used in this study, will finally determine the composition of the ionic liquid at the surface. This difference may cause the deviations from the simple trend indicated by the straight lines in Figure 4; furthermore, it might be the origin for the different IL cluster progressions observed for the different ILs (Figures 3 and S1).

As an example, the combination of C1, which contains an alkyl chain of 10 hydrocarbon units in length, with the smallest anion, A1, leads to a suppression of the anionic signal by 1−2 orders of magnitude. This is intuitively explained by the formation of a dense layer of the alkyl chains at the IL/vacuum interface with the small anions located closer to the charged headgroup of the cations. This interpretation is in agreement with previous studies on the influence of the alkyl chain on the surface composition of IL;[6−8,12,35] the situation is illustrated in Figure 5a. The decrease in I_C/I_A with decreasing m_C/m_A then indicates that the density of the packing and/or the order of the cationic layer is reduced with increasing mass and thus size of the anions. Indeed, the size of the larger anions used (examples shown in Figure 5b) is comparable to or larger than the cationic counterpart in the IL investigated. For C2A5, the effect of accumulation is clearly reversed, and the anionic signal is predominant (Figure 4). In addition to the increased size, substantial parts of A4 and A5 consist of fluorinated groups which are also known for their tendency to accumulate at the surface of IL.[5,7,12,27,35]

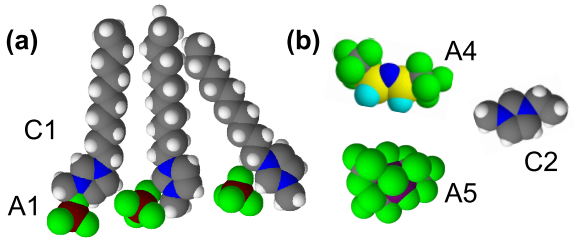

Figure 5. (a) Sketch of the arrangement of the IL C1A1 (cation with long hydrocarbon chain combined with a small anion) at the IL surface (space-filling models; white, hydrogen; dark blue, nitrogen; gray, carbon; green, fluorine; brown, boron; yellow, sulfur; light blue, oxygen; purple, phosphorus). The hydrocarbon chains are expected to point toward the vacuum, and the cations aggregate closer to the surface than the anions. (b) Space-filling models of the larger, fluorinated anions A4 and A5 and the smaller cation C2.

As we do not observe significant changes of the intensity ratio with increasing measuring time, we conclude that the surface composition is constant despite the preferential

https://doi.org/10.1021/jasms.2c00038
J. Am. Soc. Mass Spectrom. 2022, 33, 974−980

removal of the uppermost species. This can be explained by the high mobility of the ions in the IL,[36] which ensures continuous resupply of the removed ions at the surface.

In addition to the surfaces of bulk ionic liquids, the surfaces of thin films of IL were investigated, as well. In Figure 6,

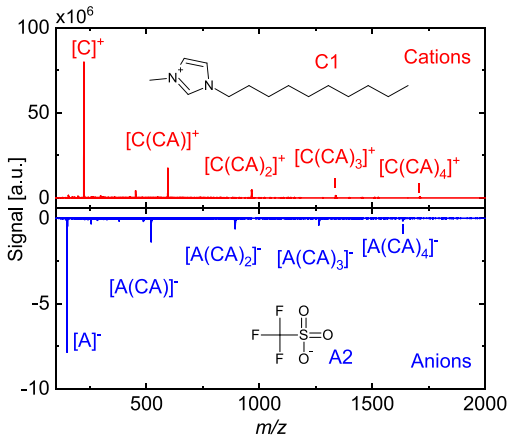

Figure 6. DINeC mass spectra in positive and negative ion mode as obtained from the surface of a thin film sample of C1A2.

DINeC-MS, which were obtained from the surface of a thin film of C1A2, are shown in positive and negative ion mode. The films were prepared by drop-casting a solution of IL in ethanol (compare the Experimental Section). Again, the most intense peaks are assigned to the single molecular ions, $[C]^+$ and $[A]^-$. They come together with up to five peaks all separated by $\Delta(m/z) = 372$, corresponding to the mass of a C1A2 cation/anion unit. They are thus associated with small IL clusters, in close resemblance to the spectra obtained from the surfaces of bulk IL (Figures 3 and S1).

However, in general, a higher ratio between cationic and anionic signal intensity, I_C/I_A, is observed for the surfaces of the thin films when compared to the surfaces of the respective bulk IL (Figures 4 and S2). This is attributed to the influence of the substrate's surface on the film composition. Apparently, the hydroxyl groups typically terminating the SiO_2 surface favor the accumulation of the cations when compared to the ratio on the surface of the bulk IL. One would expect such an influence only for a thin film of a few layers in thickness. Furthermore, for such a thin film, a decrease of signal intensity with measuring time is expected as the film is quantitatively removed by the cluster-induced desorption process.[18]

Indeed, when we record the cationic signal intensity as a function of measuring time, it shows a fast drop to a low but finite level during the first 30 min (Figure 7a). This initial drop is then followed by a very slow decrease of signal intensity during the following hours (compare Figure S3, Supporting Information). For the anionic signal, the signal drop is much less pronounced (Figures 7a and S3). The initial signal drop is associated with the removal of the thin film from the substrate; it is quantified by means of cluster-induced desorption from a thin film of IL prepared on a quartz crystal microbalance (QCM, Stanford Research SR560) measuring the mass of the film as a function of time (Figure 7b). Although the substrates are different, a similar shape of the two curves is observed in Figure 7a,b, giving direct evidence that the signal drop in

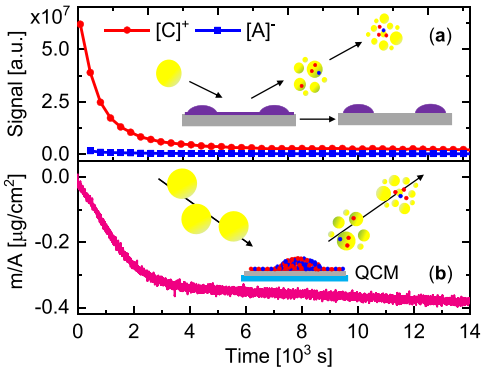

Figure 7. (a) Signal intensity of $[C]^+$ and $[A]^-$ of the thin IL film composed of C1A2. For the $[C]^+$ signal, an initial, fast drop followed by a slower decrease in intensity is observed (compare Figure S3, Supporting Information). For the whole time, the $[A]^-$ signal is lower than the $[C]^+$ signal; the drop of the $[A]^-$ signal with increasing measuring time is much less pronounced than the drop of the $[C]^+$ signal (Figure S3). Inset: The two regimes are associated with the desorption from both thin film and islands in the initial stage (left) and removal from the islands only once the film is completely desorbed (right). (b) Change in mass of an IL thin film sample as directly prepared on and measured with a QCM (compare inset).

Figure 7a is related to the removal of IL material. From the initial decrease in mass observed in Figure 7b during the first hour, an average film thickness of 3 nm is deduced when assuming the density of bulk IL material, also in good agreement with a thin film of which the composition can be influenced by the substrate surface. However, why are the integrals of cationic and anionic signals not the same? What is the origin of the finite signal intensity and the continuous decrease in mass following the initial fast drop?

As a consequence of the preparation scheme, islands of bulk material of IL are formed on the substrate in addition to the thin film between these islands,[37] in analogy to a Stranski-Krastanov mode of thin film growth (Figure S4); the situation is sketched in the left inset of Figure 7a. Although the main contribution to the initial signal originates from the thin film, which exhibits a much larger surface area exposed to the cluster beam, a minor contribution can be attributed to the IL islands. Once the film is completely removed by cluster-induced desorption, the contribution of the islands to the signal remains and drops only slowly, as these islands are slowly reduced in size by cluster-induced desorption.[37] The different relative contributions of film and islands to the total signal are also reflected in the ratio between cationic and anionic signal and its change with measuring time: The initial signal is dominated by the film contribution which apparently shows a lower relative intensity of the anionic signal when compared to that of the islands, which consist of bulk IL material with the surface composition expected to be similar to the observation on macroscopic IL droplets (Figure 4). As only a small amount of the total material is allocated in the thin film, an unbalanced ratio between cations and anions in the film can also be explained in this picture.

The film/island picture is further backed by the observation that the initial situation with respect to the ratio of the signal intensities and the temporal evolution with measuring time can be recovered when we heat the thin film samples after a first measurement cycle. In Figure 8b, the signal intensity from such

https://doi.org/10.1021/jasms.2c00038
J. Am. Soc. Mass Spectrom. 2022, 33, 974−980

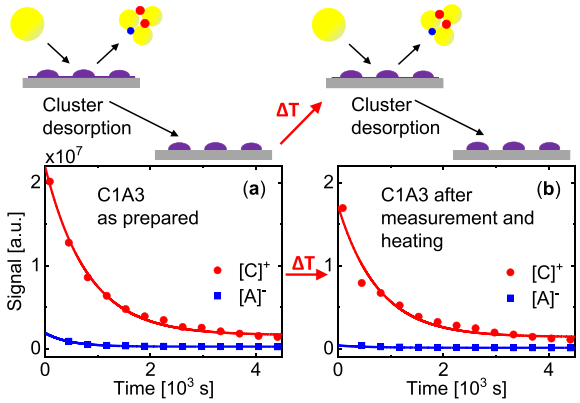

Figure 8. Signal intensity of $[C]^+$ and $[A]^-$ as a function of time measured from a thin IL film (C1A3) (a) directly after preparation and (b) after the measurement shown in (a) and an additional heating cycle up to 100 °C for 2 h. Lines are guides for the eye. The sketches in the upper part of the figure illustrate initial desorption of the thin film during cluster bombardment, redistribution of IL material from the islands to the thin film upon heating the sample, and repeated removal of the thin film by means of cluster-induced desorption.

a premeasured and heated sample is compared to the first measurement cycle (Figure 8a). Both the I_C/I_A ratio and the temporal evolution compare very well for the two measurements. Within the picture of the coexistence of thin film and islands on the substrate, this can be explained by the re-formation of the thin film through thermally activated diffusion from the islands onto the substrate. This re-formation is in part also observed at room temperature but on a much longer time scale, i.e., when we store the samples in vacuum for several days.

Comparison of Figures 7a and 8a furthermore shows that the drop of signal intensity is comparable for the two different IL samples, although the details of island formation might depend on the structure of the IL constituents (Figure S4a,b). In any case, the area covered by the film is significantly larger than the area covered by the islands, and the time constant does not depend on the coverage (first-order desorption kinetics). On the other hand, with an increasing amount of substance on the sample, e.g., using a higher concentration of IL in the solution, more material is allocated in the droplets and the relation between the contribution of thin film and bulk material is shifted toward the latter one (Figure S4).

When we compare the spectra for film and bulk IL (Figures S1 and S2), we observe in most cases in total higher signal intensity from the thin films when compared to that of the surface of bulk material, which indicates a desorption efficiency greater than that of the thin films. As the DINeC process relies on the efficient shattering of the cluster and reflection of the cluster fragments (including the dissolved analyte) from the sample surface, a liquid surface is expected to lead to less efficient desorption as more of the cluster's energy will be dissipated in the substrate by deformation of the soft substrate rather than redistributed within the cluster's constituents.

Finally, we want to briefly discuss alternative desorption-based mass spectrometry techniques and their use for the investigation of IL in comparison to DINeC-MS. Matrix-assisted laser desorption ionization (MALDI) is one of the most common desorption-based MS techniques; it is known to be very soft and is thus widely applied for the analysis of organic and bioorganic molecules.[38,39] MALDI and laser desorption ionization have been also applied to ionic liquids;[40] some IL are used as matrices for the MALDI measurements of smaller molecules.[41] However, surface sensitivity as required for the investigation of the surface composition of IL is typically not achieved; furthermore, the surface properties might be influenced by the interaction between matrix and IL in the case of MALDI. SIMS, which makes use of a keV-primary-ion beam for the sputter and ionization process, can be highly surface sensitive; however, the strong interaction between the primary ions and the analyte molecules typically leads to substantial fragmentation and reorganization of the sample,[42−44] also when applied to ionic liquids.[17] Desorption electrospray ionization has been used for the detection of ionic liquids in biological samples,[45] but no study on the surfaces of pure IL has been reported so far.

CONCLUSION

In conclusion, the surface composition of different ionic liquids was determined by means of DINeC-based mass spectrometry, which reveals the intact constituents of the IL surface. On surfaces of bulk and thin film IL material, the accumulation of either cations or anions was observed, depending on the molecular structure of the IL constituents. In thin films prepared via drop-casting of ionic liquid solutions, the surface composition was found to be further influenced by the substrate material.

ASSOCIATED CONTENT

Supporting Information

The Supporting Information is available free of charge at https://pubs.acs.org/doi/10.1021/jasms.2c00038.

A table of the chemical formulas and molecular masses of the constituents of the IL investigated in this study; additional DINeC mass spectra obtained from bulk and thin film samples; cationic and anionic signal intensity measured from a thin IL film (C1A2) as a function of measuring time, as shown in Figure 8a but plotted with a magnified signal scale for better observation of the signal change at longer time scales; optical microscope images of selected thin film samples (PDF)

AUTHOR INFORMATION

Corresponding Author

Michael Dürr − *Institut für Angewandte Physik and Zentrum für Materialforschung, Justus-Liebig-Universität Giessen, D-35392 Giessen, Germany;* orcid.org/0000-0002-4676-8715; Email: michael.duerr@ap.physik.uni-giessen.de

Authors

Karolin Bomhardt − *Institut für Angewandte Physik and Zentrum für Materialforschung, Justus-Liebig-Universität Giessen, D-35392 Giessen, Germany*

Pascal Schneider − *Institut für Angewandte Physik and Zentrum für Materialforschung, Justus-Liebig-Universität Giessen, D-35392 Giessen, Germany*

Timo Glaser − *Institut für Angewandte Physik and Zentrum für Materialforschung, Justus-Liebig-Universität Giessen, D-35392 Giessen, Germany*

Complete contact information is available at: https://pubs.acs.org/10.1021/jasms.2c00038

Notes

The authors declare no competing financial interest.

■ ACKNOWLEDGMENTS

The authors acknowledge financial support from BMBF through Grant No. 05K19RG1, as well as by the Helmholtz International Center for FAIR (HICforFAIR) and the Helmholtz Graduate School for Hadron and Ion Research (P.S.).

■ REFERENCES

(1) Hayes, R.; Warr, G. G.; Atkin, R. Structure and Nanostructure in Ionic Liquids. *Chem. Rev.* **2015**, *115*, 6357−6426.
(2) Zhou, H.; Chen, L.; Wei, Z.; Lu, Y.; Peng, C.; Zhang, B.; Zhao, X.; Wu, L.; Wang, Y. Effect of Ionic Composition on Physicochemical Properties of Mono-Ether Functional Ionic Liquids. *Molecules* **2019**, *24*, 3112.
(3) Eyckens, D. J.; Henderson, L. C. A Review of Solvate Ionic Liquids: Physical Parameters and Synthetic Applications. *Front. Chem.* **2019**, *7*, 263.
(4) Zhao, D.; Wu, M.; Kou, Y.; Min, E. Ionic liquids: Applications in catalysis. *Catal.* **2002**, *74*, 157−189.
(5) Lovelock, K. R. J. Influence of the ionic liquid/gas surface on ionic liquid chemistry. *Phys. Chem. Chem. Phys.* **2012**, *14*, 5071−5089.
(6) Sloutskin, E.; Ocko, B. M.; Tamam, L.; Kuzmenko, I.; Gog, T.; Deutsch, M. Surface Layering in Ionic Liquids: An X-ray reflectivity study. *J. Am. Chem. Soc.* **2005**, *127*, 7796−7804.
(7) Jeon, Y.; Sung, J.; Bu, W.; Vaknin, D.; Ouchi, Y.; Kim, D. Interfacial Restructuring of Ionic Liquids Determined by Sum-Frequency Generation Spectroscopy and X-ray Refelctivity. *J. Phys. Chem. C* **2008**, *112*, 19649−19654.
(8) Mezger, M.; Ocko, B. M.; Reichert, H.; Deutsch, M. Surface layering and melting in an ionic liquid studied by resonant soft x-ray reflectivity. *Proc. Natl. Acad. Sci. U. S. A.* **2013**, *110*, 3733−3737.
(9) Haddad, J.; Pontoni, D.; Murphy, B. M.; Festersen, S.; Runge, B.; Magnussen, O. M.; Steinrück, H.-G.; Reichert, H.; Ocko, B. M.; Deutsch, M. Surface structure evolution in a homologous series of ionic liquids. *Proc. Natl. Acad. Sci. U. S. A.* **2018**, *115*, E1100−E1107.
(10) Kolbeck, C.; Cremer, T.; Lovelock, K. R. J.; Paape, N.; Schulz, P. S.; Wasserscheid, P.; Maier, F.; Steinrück, H.-P. Influence of different anions on the surface composition of Ionic Liquids using ARXPS. *J. Phys. Chem. B* **2009**, *113*, 8682−8688.
(11) Lockett, V.; Sedev, R.; Harmer, S.; Ralston, J.; Horne, M.; Rodopoulos, T. Orientation and mutual location of ions at the surface of ionic liquids. *Phys. Chem. Chem. Phys.* **2010**, *12*, 13816−13827.
(12) Steinrück, H. P. Recent developments in the study of ionic liquid interfaces using X-ray photoelectron spectroscopy and potential future directions. *Phys. Chem. Chem. Phys.* **2012**, *14*, 5010−5029.
(13) Kolbeck, C.; Niedermaier, I.; Deyko, A.; Lovelock, K. R. J.; Taccardi, N.; Wei, W.; Wasserscheid, P.; Maier, F.; Steinruck, H.-P. Influence of substituents and functional groups on the surface composition of Ionic Liquids. *Chem.—Eur. J.* **2014**, *20*, 3954−3965.
(14) Blundell, R. K.; Delorme, A. E.; Smith, E. F.; Licence, P. An ARXPS and ERXPS study of quaternary ammonium and phosphonium ionic liquids: utilising a high energy Ag Lα' X-ray source. *Phys. Chem. Chem. Phys.* **2016**, *18*, 6122−6131.
(15) Günster, J.; Höfft, O.; Krischok, S.; Souda, R. A time-of-flight secondary ion mass spectroscopy study of 1-ethyl-3-methylimidazolium bis(trifluoromethylsulfonyl)imide RT-ionic liquid. *Surf. Sci.* **2008**, *602*, 3403−3407.
(16) Souda, R. Glass-Liquid Transition, Crystallization, and Melting of a Room Temperature Ionic Liquid: Thin Films of 1-Ethyl-3-methylimidazolium Bis[trifluoromethanesulfonyl]imide Studied with TOF-SIMS. *J. Phys. Chem. B* **2008**, *112*, 15349−15354.
(17) Bundaleski, N.; Caporali, S.; Chenakin, S. P.; Moutinho, A. M.C.; Teodoro, O. M.N.D.; Tolstogouzov, A. Ion-induced fragmentation of imidazolium ionic liquids: TOF-SIMS study. *Int. J. Mass Spectrom.* **2013**, *353*, 19−25.
(18) Portz, A.; Aoyagi, S.; Dürr, M. Soft depth-profiling of mixed peptide/lipid samples by means of cluster induced desorption/ionization mass spectrometry - high depth resolution and low matrix effect. *Biointerphases* **2018**, *13*, 03B405.
(19) Gebhardt, C. R.; Tomsic, A.; Schröder, H.; Dürr, M.; Kompa, K.-L. Matrix-Free Formation of Gas-Phase Biomolecular Ions by Soft Cluster-Induced Desorption. *Angew. Chem., Int. Ed.* **2009**, *48*, 4162−4165.
(20) Baur, M.; Gebhardt, C. R.; Dürr, M. Desorption/ionization induced by neutral cluster impact as a soft and efficient ionization source for ion trap mass spectrometry of biomolecules. *Rapid Commun. Mass Spectrom.* **2014**, *28*, 290−296.
(21) Portz, A.; Bomhardt, K.; Rohnke, M.; Schneider, P.; Asperger, A.; Gebhardt, C. R.; Durr, M. Soft cluster-induced desorption/ionization mass spectrometry: How soft is soft? *Biointerphases* **2020**, *15*, 021001.
(22) Schneider, P.; Verloh, F.; Portz, A.; Aoyagi, S.; Rohnke, M.; Dürr, M. Direct analysis of ion-induced peptide fragmentation in secondary-ion mass spectrometry. *Anal. Chem.* **2020**, *92*, 15604−15610.
(23) Portz, A.; Baur, M.; Gebhardt, C. R.; Frank, A. J.; Neuderth, P.; Eickhoff, M.; Dürr, M. Influence of the Cluster Constituents' Reactivity on the Desorption/Ionization Process Induced by Neutral SO_2 Clusters. *J. Chem. Phys.* **2017**, *146*, 134705.
(24) Schneider, P.; Dürr, M. Cluster-induced desorption investigated by means of molecular dynamics simulation - Microsolvation in clusters of polar and non-polar constiutuents. *J. Chem. Phys.* **2019**, *150*, 214301.
(25) Aschenbrenner, O.; Supasitmongkol, S.; Taylor, M.; Styring, P. Measurement of vapour pressure of ionic liquids and other low vapour pressure solvents. *Green Chem.* **2009**, *11*, 1217−1221.
(26) Ahrenberg, M.; Beck, M.; Neise, C.; Keßler, O.; Kragl, U.; Verevkin, S. P.; Schick, C. Vapor pressure of ionic liquids at low temperatures from AC-chip-calorimetry. *Phys. Chem. Chem. Phys.* **2016**, *18*, 21381−21390.
(27) Welton, T. Ionic Liquids: a brief history. *Biophys. Rev.* **2018**, *10*, 691−706.
(28) Portz, A.; Baur, M.; Rinke, G.; Abb, S.; Rauschenbach, S.; Kern, K.; Dürr, M. Chemical analysis of complex surface-adsorbed molecules and their reactios by means of cluster-induced desorption/ionization mass spectrometry. *Anal. Chem.* **2018**, *90*, 3328−3334.
(29) Eusepi, F.; Tomsic, A.; Gebhardt, C. R. Analysis of solution-deposited alkali ions by cluster surface collisions. *Anal. Chem.* **2003**, *75*, 5124−5128.
(30) Suarez, P. A.Z.; Dullius, J. E.L.; Einloft, S.; De Souza, R. F.; Dupont, J. The use of new ionic liquids in two-phase catalytic hydrogenation reaction by rhodium complexes. *Polyhedron* **1996**, *15*, 1217−1219.
(31) Bomhardt, K.; Schneider, P.; Portz, A.; Gebhardt, C. R.; Dürr, M. Analysis of complex molecules and their reactions on surfaces by means of cluster-induced desorption/ionization mass spectrometry. *J. Vis. Exp.* **2020**, *11*, e60487.
(32) Zhang, J.; Baxter, E. T.; Nguyen, M.-T.; Prabhakaran, V.; Rousseau, R.; Johnson, G. E.; Glezakou, V.-A. Structure and Stability of the Ionic Liquid Clusters $[EMIM]_n[BF_4]_{n+1}^-$ (n = 1−9): Implications for Electrochemical Separations. *J. Phys. Chem. Lett.* **2020**, *11*, 6844−6851.
(33) Lee, B.-J.; Gebhardt, C. R.; Schröder, H.; Kompa, K.-L.; Dürr, M. Observation of ionic desorption channels in cluster-induced desorption of alkali halides - influence of surface electronic properties and surface configuration. *Chem. Phys. Lett.* **2013**, *556*, 77−81.
(34) Martinez, I. S.; Baldelli, S. On the arrangement of ions in imidazolium-based room temperature ionic liquids at the gas-liquid interface, using sum frequency generation, surface potential and surface tension measurements. *J. Phys. Chem. C* **2010**, *114*, 11564−11575.

https://doi.org/10.1021/jasms.2c00038
J. Am. Soc. Mass Spectrom. 2022, 33, 974−980

(35) Lockett, V.; Sedev, R.; Bassell, C.; Ralston, J. Angle-resolved X-ray photoelectron spectroscopy of the surface of imidazolium ionic liquids. *Phys. Chem. Chem. Phys.* **2008**, *10*, 1330−1335.
(36) Bester-Rogac, M.; Fedotova, M. V.; Kruchinin, S. E.; Klahn, M. Mobility and association of ions in aqueous solutions: the case of imidazolium based ionic liquids. *Phys. Chem. Chem. Phys.* **2016**, *18*, 28594−28605.
(37) Baur, M.; Lee, B.-J.; Gebhardt, C. R.; Dürr, M. Soft cluster-induced desorption and ionization of biomolecules - Influence of surface load and morphology on desorption efficiency. *Appl. Phys. Lett.* **2011**, *99*, 234103.
(38) Karas, M.; Bachmann, D.; Hillenkamp, F. Influence of the wavelenght in high-irradiance ultraviolet laser desorption mass spectrometry of organic molecules. *Anal. Chem.* **1985**, *57*, 2935−2939.
(39) Dreisewerd, K. The desorption process in MALDI. *Chem. Rev.* **2003**, *103*, 395−425.
(40) Zabet-Moghaddam, M.; Krüger, R.; Heinzle, E.; Tholey, A. Matrix-assisted laser desorption/ionization mass spectrometry for the characterization of ionic liquids and the analysis of amino acids, peptides and proteins in ionic liquids. *J. Mass Spectrom.* **2004**, *39*, 1494−1505.
(41) Kobylis, P.; Stepnowski, P.; Caban, M. Review of the applicability of ionic liquid matrices for the quantification of small molecules by MALDI MS. *Microchem. J.* **2021**, *164*, 105983.
(42) Yokoyama, Y.; Aoyagi, S.; Fujii, M.; Matsuo, J.; Fletcher, J. S.; Lockyer, N. P.; Vickerman, J. C.; Passarelli, M. K.; Havelund, R.; Seah, M. P. Peptide fragmentation and surface structural analysis by means of ToF-SIMS using large cluster ion sources. *Anal. Chem.* **2016**, *88*, 3592−3597.
(43) Baek, J. Y.; Choi, C. M.; Lee, S. J.; Min, B. K.; Kang, H. S.; Choo, D. C.; Sung, J. Y.; Jin, J. S.; Choi, M. C. ToF-SIMS of OLED materials using argon gas cluster ion Beam: A promising approach for OLED inspection. *Appl. Surf. Sci.* **2020**, *507*, 144887.
(44) Kotowska, A. M.; Trindade, G. F.; Mendes, P. M.; Williams, P. M.; Aylott, J. W.; Shard, A. G.; Alexander, M. R.; Scurr, D. J. Protein identifation by 3D OrbiSIMS to facilitate in situ imaging and depth profiling. *Nat. Commun.* **2020**, *11*, 5832.
(45) Perez, C. J.; Tata, A.; de Campos, M. L.; Peng, C.; Ifa, D. R. Monitoring Toxic Ionic Liquids in Zebrafish (Danio rerio) with Desorption Electrospray Ionization Mass Spectrometry Imaging (DESI-MSI). *J. Am. Soc. Mass Spectrom.* **2017**, *28*, 1136−1148.

https://doi.org/10.1021/jasms.2c00038
J. Am. Soc. Mass Spectrom. 2022, 33, 974−980

Supporting Information for:

Surface Properties of Ionic Liquids: A Mass Spectrometric View Based on Soft Cluster-Induced Desorption

Karolin Bomhardt, Pascal Schneider, Timo Glaser and Michael Dürr*

Institut für Angewandte Physik and Zentrum für Materialforschung,
Justus-Liebig-Universität Giessen, Heinrich-Buff-Ring 16, D-35392 Giessen, Germany
* *Corresponding author: michael.duerr@ap.physik.uni-giessen.de*

Table S1: Molecular formulas and masses of the investigated ionic liquids.

Ion	Molecular formulas	mass [Da]
C1	$C_{14}H_{27}N_2{}^+$	223.22
C2	$C_6H_{11}N_2{}^+$	111.09
A1	$BF_4{}^-$	87.00
A2	$CF_3SO_3{}^-$	148.95
A3	$C_2F_6NO_4S_2{}^-$	279.92
A4	$C_4F_{10}NO_4S_2{}^-$	379.91
A5	$C_6F_{18}P^-$	444.95

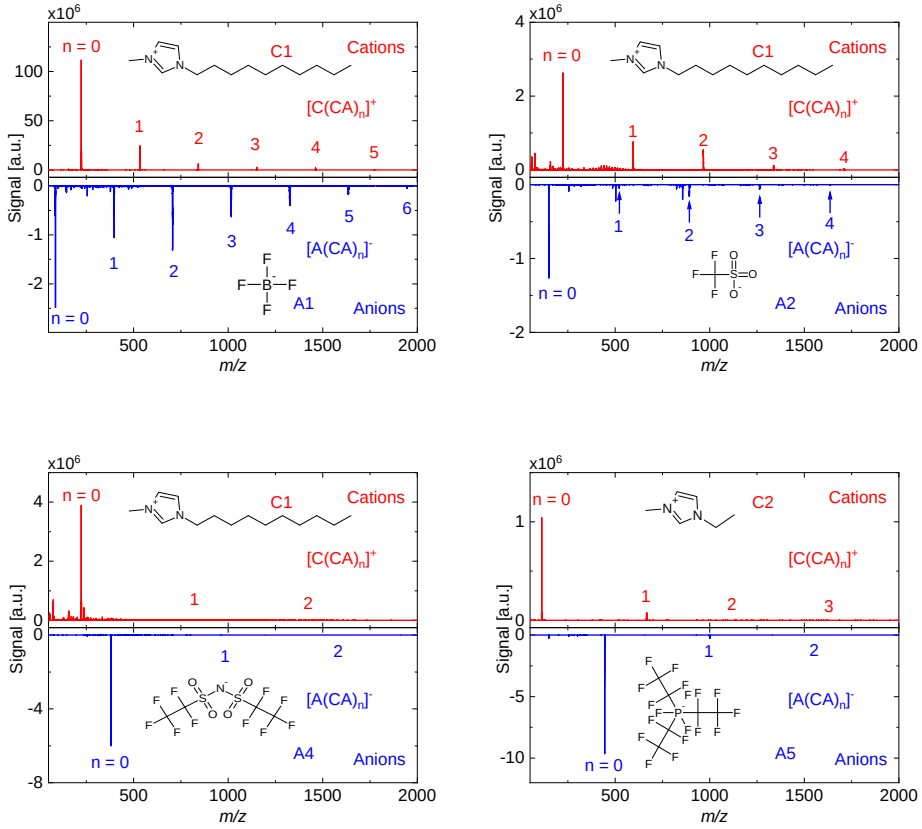

Figure S1: From left to right, top to bottom: DINeC mass spectra in positive and negative ion mode as obtained from the surface of a bulk sample of C1A1, C1A2, C1A4 and C2A5.

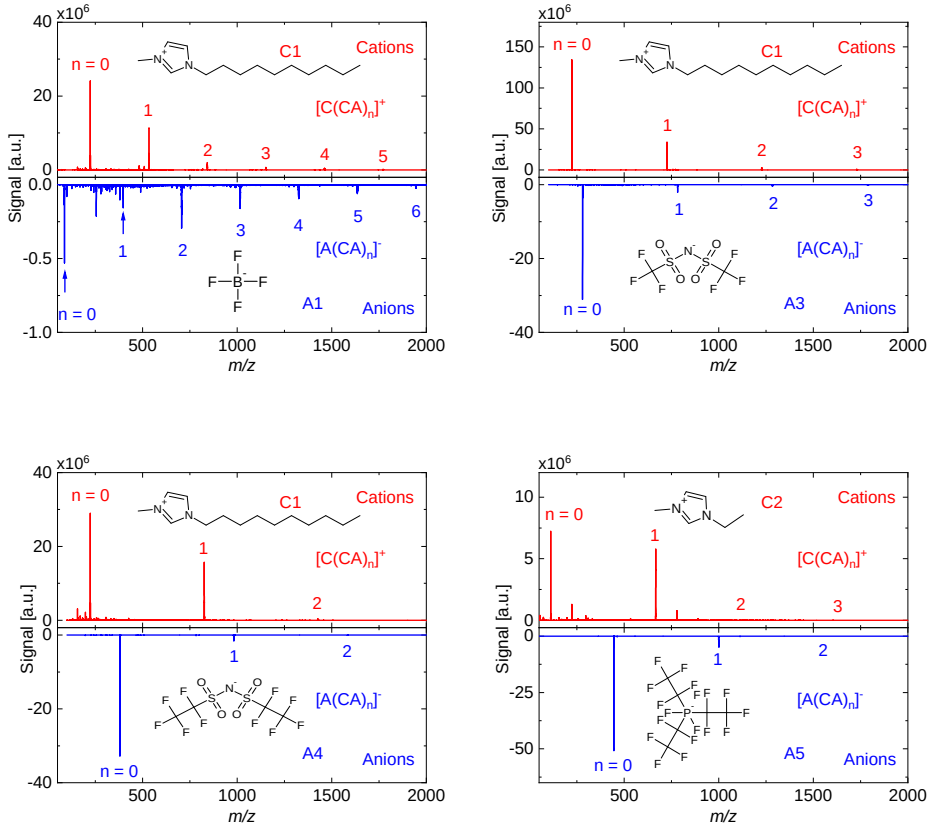

Figure S2: From left to right, top to bottom: DINeC mass spectra in positive and negative ion mode as obtained from the surface of a film sample of C1A1, C1A2, C1A4 and C2A5.

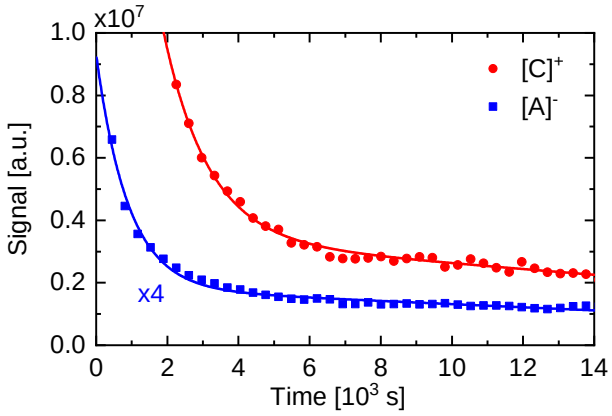

Figure S3: Signal intensity of $[C]^+$ and $[A]^-$ of the thin IL film composed of C1A2 as a function of measuring time as shown in Fig. 8 but plotted with a magnified signal scale. For the both signals, an initial fast drop followed by a slower decrease in intensity is observed. Solid lines are fits to the experimental data points. The fit functions are composed of an exponential decay superimposed by a linear decrease.

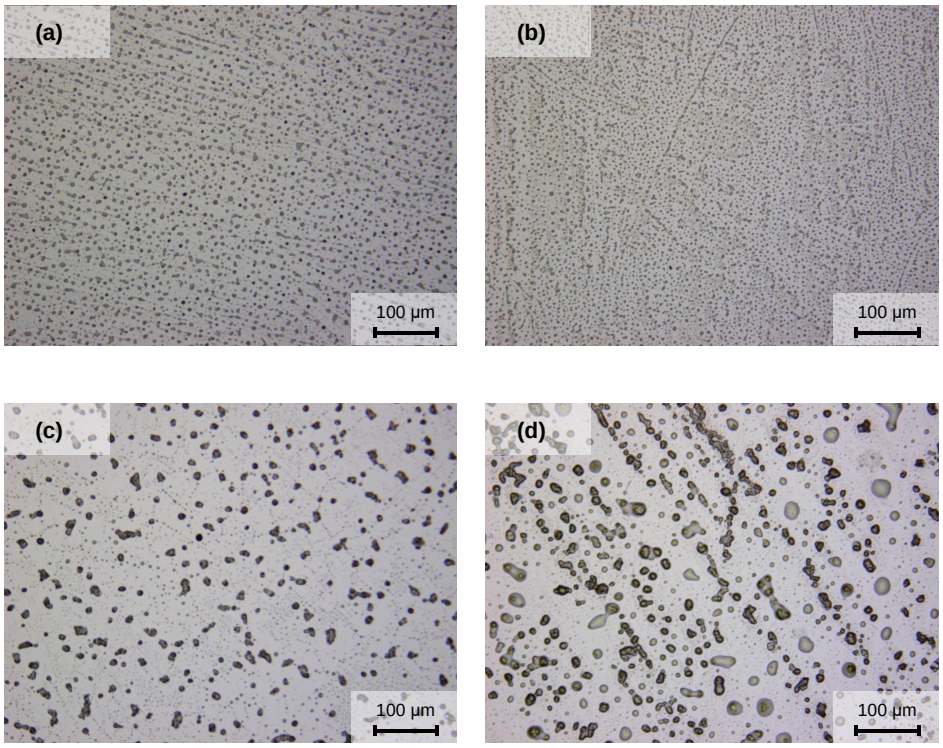

Figure S4: Microscopic image of C1A2 (a) and C1A3 (b) on Silicon prepared as described in the experimental section. With increasing concentration (5x), the proportion of C1A2 (c) and C1A3 (d) of IL islands increases.

4.3 Artikel III

Soft deposition of organic molecules based on cluster-induced desorption for the investigation of on-surface and surface-mediated reactions
K. Pluschke, A. Herrmann, and M. Dürr;
ACS Omega **8**, 40639 - 40646 (2023). Nachdruck von Referenz [98].

ACS OMEGA

Open Access

http://pubs.acs.org/journal/acsodf

Article

Soft Deposition of Organic Molecules Based on Cluster-Induced Desorption for the Investigation of On-Surface and Surface-Mediated Reactions

Karolin Pluschke, Aaron Herrmann, and Michael Dürr*

Cite This: *ACS Omega* 2023, 8, 40639−40646

Read Online

ACCESS | Metrics & More | Article Recommendations | Supporting Information

ABSTRACT: Desorption/ionization induced by neutral clusters (DINeC) was employed for the soft transfer of organic and biomolecules, such as porphyrins and peptides, from a bulk sample onto any substrate of choice. Qualitative analysis of the deposition technique was performed by means of mass spectrometry, demonstrating that the deposited molecules remained intact due to the soft nature of the transfer process. Deposition rates were studied quantitatively using a quartz crystal microbalance; layers of intact biomolecules ranging from the submonolayer regime up to a few monolayers in thickness were realized. Mixed layers of molecules were deposited when two different sources of molecules were employed. The samples which were prepared based on this soft deposition method were used for the investigation of reactions of the deposited molecules with either coadsorbates on the surface or the surface itself. Examples include adduct formation of peptides with alkali metals on SiO_2, the oxidation of peptides exposed to oxygen, as well as the metallization of porphyrins in interaction with the substrate.

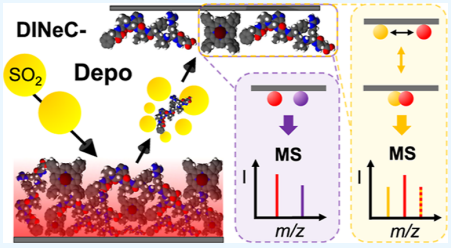

INTRODUCTION

The preparation of thin organic films by means of physical vapor deposition (PVD) is a well-established technique.[1,2] It is applied, e.g., for the preparation of thin films of metal−organic complexes, polymers, or other organic molecules, which are used, among others, in organic solar cells, organic thin film transistors, and organic light-emitting diodes.[3−5] However, PVD is only applicable to molecules that do not decompose at the elevated temperatures used to sublimate the molecules.[6,7] For the deposition of larger, more complex molecules such as biomolecules, a variety of dedicated techniques have been established; most of these techniques originate from (soft) ionization methods used in mass spectrometry (MS). For example, soft landing of molecular ions such as electrospray ion beam deposition (ES-IBD), can be used to deposit intact molecules such as peptides, proteins, and other molecules with layer thicknesses in the submonolayer to the nanometer range.[8−10] Matrix-assisted pulsed laser evaporation (MAPLE), which was derived from matrix-assisted laser desorption/ionization MS, was also applied for the deposition of larger molecules in the 10 to 1000 kDa range.[11] Noble gas cluster ion beams (GCIBs), which are typically employed for soft secondary ion MS, were also used to sputter/deposit intact biomolecules.[12,13] Whereas ES-IBD is limited to the deposition of molecular ions, MAPLE involves the codeposition of the matrix molecules if not only charged molecules are selected. In the case of the deposition induced by GCIB, a finite fraction of fragmented molecules is still expected to be deposited.[14]

In this paper, we show that desorption induced by neutral SO_2 clusters (DINeC), which is an extremely soft desorption method applied in MS,[15−17] can be employed as a deposition technique as well (short: DINeC-Depo). In this application of DINeC, the molecules are softly desorbed from a bulk sample by the SO_2 clusters and deposited directly onto a substrate that is placed opposite to the target (Figure 1a). The soft desorption of the molecules relies on a dissolution-based mechanism:[15,18,19] the impacting clusters do not only provide the energy for desorption but also serve as a transient matrix in which the desorbing molecules are dissolved.[18−20] As a result, the effective desorption barrier is reduced which enables soft desorption with low-energy clusters.[15−17] As most of the SO_2 molecules are evaporating from the desorbed molecules after cluster-surface impact and desorption,[15,20] the bare molecules can be then deposited on a target of choice; as only a minority of the desorbed molecules are ionized,[21] mainly neutral molecules are deposited. Based on the results for DINeC-MS, the DINeC-Depo method can be applied to a broad variety of molecules, e.g., lipids, peptides, proteins, dyes, polymers, and ionic liquids.[20,22−25] The coverage of the deposited layers ranges from isolated molecules in the

Received: July 28, 2023
Accepted: October 2, 2023
Published: October 19, 2023

https://doi.org/10.1021/acsomega.3c05518
ACS Omega 2023, 8, 40639−40646

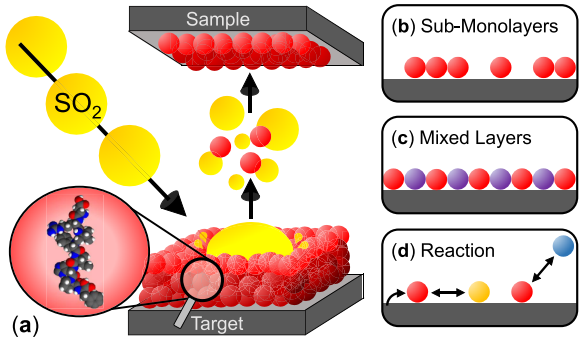

Figure 1. Schematic depiction of the DINeC-Depo experiment: (a) SO_2 clusters hit the surface and desorb the molecules that were drop-cast on the target substrate. The desorbed molecules can be deposited on any surface of choice. (b) Samples in the submonolayer to multilayer regime were prepared. (c) Mixed layers were deposited by using different target molecules. (d) Interactions of the deposited molecules with the surface or other adsorbates were investigated.

submonolayer regime (Figure 1b) to films of the thickness of several monolayers. The sample composition was controlled by changing the target material during the deposition process (Figure 1c). Samples prepared by DINeC-Depo were used to study the interaction of the deposited molecules with the surface of the substrate, with other adsorbates, or with gas phase molecules to which they were exposed (Figure 1d). In general, higher reactivity of the deposited species is observed when compared to molecules in solution or thin films.

EXPERIMENTAL SECTION

The deposition process was performed in a vacuum chamber (base pressure $p \approx 10^{-6}$ mbar), which was set up for this type of experiment (Figure S1 in the Supporting Information). The cluster beam, which was used for the desorption of the target molecules, was generated via supersonic expansion of a gas mixture containing 3% SO_2 in helium (pressure p = 15 bar) using a pulsed nozzle (repetition rate f = 2 Hz, effective opening time t = 300 ms). The clusters, consisting of 10^3 to 10^4 SO_2 molecules, hit the target surface at an angle of 45° with respect to the surface normal; the clusters' velocity $v \approx 10^3$ m/s converts into an energy density of ≈0.8 eV per molecule.[26] The clusters desorb the molecules from the target, which is positioned 90 mm from the nozzle. The substrate, on which the molecules were deposited, was mounted directly opposite to the target at a distance of d_{ST} = 8 to 30 mm. The target consisted of a piece of silicon wafer (2 × 2 cm^2) covered with its natural oxide onto which an aqueous solution ($c = 10^{-3}$ mol/L, V = 100 μL) was drop-cast. Prior to use, all substrates were cleaned in ethanol and acetone in an ultrasonic bath for 15 min each. To remove metal contamination from the silicon oxide surface, some of the substrates were additionally cleaned with the so-called "RCA cleaning procedure type 2" reported by the *Radio Corporation of America*.[27] Peptides (purity >97%) were purchased at Sigma-Aldrich Chemie GmbH, Taufkirchen, Germany, and porphyrins (purity >98%) were purchased at PorphyChem SAS, Longvic, France.

During deposition, the substrate was covered with a deposition mask (perforated metal plate, r_{hole} = 3 mm); the target and sample holder were on ground potential. The deposition rate was determined quantitatively using a quartz crystal microbalance (QCM SR560, QCM200-5 MHz Crystal Oscillator, Stanford Research Systems). Sample transfer from the deposition chamber to the vacuum chamber of the mass spectrometer was carried out through ambient conditions unless stated otherwise.

After deposition, the samples were analyzed by means of DINeC-MS. For the MS measurements, the masks were removed from the samples; the deposited molecules were desorbed by SO_2 clusters in the same way as described for the deposition procedure. In the former case, the desorbed ions were transferred into a commercial ion trap mass spectrometer (amaZon speed from Bruker Daltonik GmbH, Bremen Germany), which was equipped with a custom-built DINeC ion source; the experimental setup is described in detail elsewhere.[16]

RESULTS AND DISCUSSION

In Figure 2, the DINeC mass spectrum from an angiotensin II sample prepared by means of DINeC-Depo (Figure 2b) is

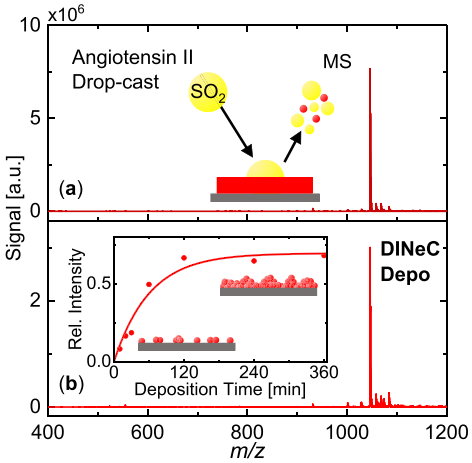

Figure 2. DINeC mass spectra in positive ion mode obtained from angiotensin II (a) drop-cast on SiO_2 and (b) deposited by DINeC-Depo (deposition time t_{depo} = 6 h, d_{ST} = 8 mm). The main peak at m/z = 1046 is assigned to the intact peptide. The intensity of this peak increases with increasing deposition time from 10 min to 6 h (inset). Further peaks occurring at m/z > 1046 are discussed in the main text. Peak positions of all major peaks are listed in Table S1 in the Supporting Information.

compared to a mass spectrum taken from a drop-cast film of angiotensin II (Figure 2a). In both cases, the main peak at m/z = 1046 is assigned to the intact angiotensin II molecule, $[M + H]^+$. Further peaks of much lower intensity are observed in the mass spectrum from the deposited sample at m/z = 1058, 1068, 1074, and 1084. Three of these peaks (m/z = 1058, 1068, and 1084) are also found in the drop-cast sample but show an increased intensity in the spectrum from the deposited sample. The peaks at m/z = 1068 and m/z = 1084 can be assigned to the adduct formation of angiotensin II with alkali metals ($[M + Na]^+$ and $[M + K]^+$, respectively). The peaks at m/z = 1058 and m/z = 1074 are associated with more complex reactions such as esterification or formylation.[28,29] For the former one, the MS/MS spectrum indicates a reaction involving the terminal aspartic acid group of the molecule (Figure S2). Peaks at m/z < 1046 are observed in even lower intensity (<3% of the main peak for both the drop-cast and the

https://doi.org/10.1021/acsomega.3c05518
ACS Omega 2023, 8, 40639−40646

DINeC-Depo sample, compare also the spectra with extended mass range in Figure S3). They can be associated with specific fragments of angiotensin II along the peptide backbone.[23] When we compare the relative intensity of these peaks (with respect to the main peak, which is associated with the intact molecule) in the spectra of the DINeC-Depo samples and in the drop-cast samples, the increase in relative intensity is ≤2%. This increase represents the upper limit for fragmentation induced by the deposition process; it might also originate, at least in part, from other processes, such as reactions on the surface. The deposition by means of DINeC-Depo can thus be seen to be close to fragmentation-free.

The signal intensity of the main peak at m/z = 1046 in the spectra from the deposited samples increases with increasing deposition time (10 min to 6 h, Figure 2b, inset). From the saturation behavior, we conclude a closed layer of angiotensin II molecules to be formed on the substrate after a deposition time of ≈1.5 h in the given configuration. Qualitatively similar mass spectra were measured from angiotensin II deposited on different substrates, e.g., on gold or HOPG substrates (Figures S4a,b in the Supporting Information, respectively).

The amount of molecules deposited by DINeC-Depo was quantified in a QCM experiment. Figure 3 shows the deposited

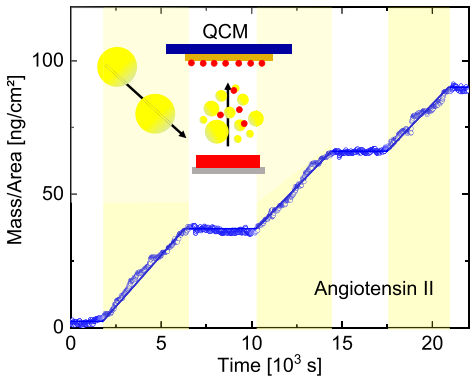

Figure 3. QCM measurement of the mass deposited during a DINeC-Depo experiment with angiotensin II. The QCM plate was installed at a distance of d_{ST} = 30 mm from the target. Yellow-labeled regions indicate that the SO_2 cluster beam was on. Blue open symbols: raw data. Blue straight lines: linear fits within the respective intervals.

mass as recorded on a QCM as a function of the deposition time. The angiotensin II molecules were deposited on the gold electrode (1.3 cm^2) of the quartz crystal resonator, which was installed at the position of the sample at a distance of d_{ST} = 30 mm from the target. When the cluster beam was switched on (t = 1800 s), a continuous increase in the mass was observed. When the beam was turned off again (t = 6300 s), the deposited mass per area was $m/A \approx 37$ ng/cm^2 and the respective deposition rate was 7.6 pg/(s·cm^2). In the following period with the beam off (until t = 10,300 s), the recorded mass remained constant. In the second and third deposition cycles, similar deposition rates of 7.1 and 7.0 pg/(s·cm^2) were recorded, respectively; the average deposition rate in this experiment was 7.3 ± 0.3 pg/(s·cm^2) which is considerably lower when compared to the desorption rate of ≈200 pg/(s·cm^2) from a drop-cast angiotensin II sample.[22] We note that the distance between the QCM-plate and the target (d_{ST} = 30 mm) was comparatively large in this experiment; with a lower distance as used in most of the reported experiments, higher deposition rates are achieved. Further improvement of the geometry beyond the current setup (reduced nozzle-target distance, optimized angle of incidence of the beam and angle of collection) is estimated to further increase the deposition rate by up to one order of magnitude. This should then allow for the preparation of real multilayers including more complex film compositions.

The signal intensity in the mass spectra from samples deposited via DINeC-Depo changes as a function of measuring time, as shown in Figure 4. For the main peak at m/z = 1046

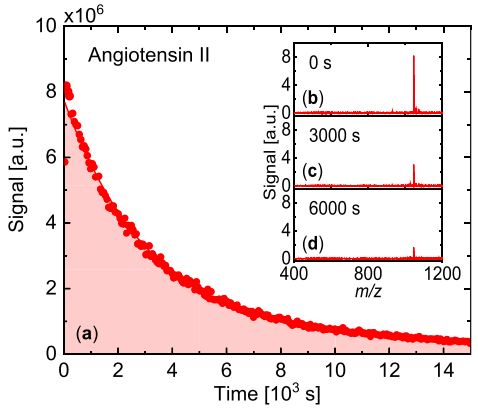

Figure 4. (a) Signal intensity of the peak at m/z = 1046 in DINeC mass spectra from a DINeC-Depo sample (angiotensin II, t_{depo} = 6 h, d_{ST} = 8 mm) as a function of desorption time. The exponential decay results from the removal of the deposited molecules from the SiO_2 surface. (b–d) Positive ion mode DINeC mass spectra were measured at different times as indicated. Peak positions of all major peaks and their intensities are listed in Table S2 in the Supporting Information.

($[M + H]^+$) as measured on a sample of angiotensin II deposited on a silicon wafer for 6 h, the continuous decrease of the signal suggests a film in the (sub-) monolayer regime. On the other hand, from the saturation of the initial signal intensity (Figure 2b, inset), one expects a closed film of several molecular layers in thickness, in accordance with the QCM measurements. We thus conclude that the amount of substance deposited, which corresponds to approximately 3–4 monolayers, is not arranged in well-ordered multilayers but a rather inhomogeneous mode of growth, including islands and clusters of molecules on the surface, is operative. The arrangement of the molecules on the surface might be further influenced by the transfer through ambient conditions, although no major difference was observed when samples that were transferred through the ambient were compared to samples that were transferred between the deposition and analysis chambers without breaking the vacuum.

As some of the molecules that are desorbed via cluster-surface impact carry additional SO_2 molecules as remainders of the cluster fragments in which they were dissolved during the desorption process,[18,19] we analyzed the amount of SO_2 on the surface after DINeC-Depo by means of X-ray photoelectron spectroscopy (XPS). If at all, a sulfur content of less than one sulfur atom per angiotensin molecule was detected on the samples (Figure S5). Indeed, the fraction of biomolecules with SO_2 adducts is typically small;[15,30] from our results, we further

https://doi.org/10.1021/acsomega.3c05518
ACS Omega 2023, 8, 40639–40646

conclude that SO_2 from the background gas does not lead to a substantial SO_2 contamination on the surface, either.

When the target substrates are exchanged during the deposition process, mixed layers can be prepared by DINeC-Depo. In the example shown in Figure 5, a mixture of two

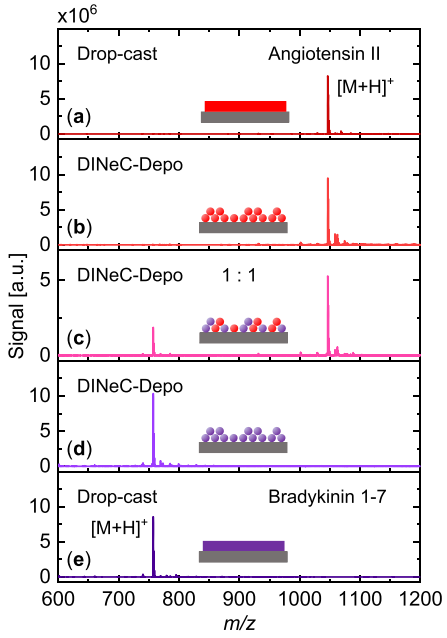

Figure 5. DINeC mass spectra in positive ion mode taken from (a) an angiotensin II sample prepared by drop-casting, (b) an angiotensin II sample prepared by DINeC-Depo, (c) a mixed sample of angiotensin II and bradykinin 1−7 prepared by DINeC-Depo, (d) a bradykinin 1−7 sample prepared by DINeC-Depo, and (e) a bradykinin 1−7 sample prepared by drop-casting. DINeC-Depo samples were prepared by 6 h of deposition (d_{ST} = 12 mm); in the case of the mixed samples, the targets were alternated every hour. The main peaks at m/z = 1046 (a,b) and m/z = 757 (d,e) are assigned to the intact angiotensin II and bradykinin 1−7 molecules, respectively. The mass spectrum from the mixed sample in (c) shows both peaks. Peak positions of all major peaks and their intensities are listed in Table S3 in the Supporting Information.

peptides, angiotensin II and bradykinin 1−7, was deposited. The DINeC-Depo samples with pure substances were prepared by deposition for 6 h from one single target; the mixed sample was prepared by alternating between the two targets every hour, adding up to a total deposition time of 6 h. In the mass spectrum from the drop-cast angiotensin II sample (Figure 5a), the most intense peak at m/z = 1046 is associated with the intact biomolecule $[M + H]^+$. The same is true for the DINeC-Depo sample with angiotensin II only. An additional peak at m/z = 1062 is observed in the mass spectrum (Figure 5b), which was not observed in the angiotensin II spectra shown previously. It is assigned to an oxidation product of the peptide. The main peak in the mass spectrum shown in Figure 5e from the drop-cast sample of bradykinin 1−7 at m/z = 757 is assigned to the intact peptide molecule $[M + H]^+$. Additional peaks of much lower intensity appear at m/z = 769, 779, 785, and 795. The peaks at m/z = 779 and m/z = 795 are assigned to the adduct formation of bradykinin 1−7 with alkali metals ($[M + Na]^+$ and $[M + K]^+$, respectively), whereas the peaks at m/z = 769 and m/z = 785 are associated with more complex reactions, in analogy to the spectrum from angiotensin II shown in Figure 2. The mass spectrum of the DINeC-Depo sample of bradykinin 1−7 (Figure 5d) again shows the most intense peak at m/z = 757 ($[M + H]^+$) indicating the transfer of the intact molecule. In comparison to Figure 5e, one additional peak is observed at m/z = 773, which can be assigned to an oxidation product of the peptide. The spectrum from the mixed sample shown in Figure 5c is dominated by the peaks at m/z = 1046 and m/z = 757, which are assigned to the two intact biomolecules, $[M1 + H]^+$ and $[M2 + H]^+$. They indicate that both molecules are present at the surface in the same order of magnitude. Although the intensity from the pure DINeC-Depo samples of bradykinin 1−7 and angiotensin II are comparable in Figure 5b,d, an intensity ratio of 1:2 is observed for the mixed sample. This deviation from the ratio expected from the ratio of the deposition times of the single components was also observed for other nominal ratios of molecules in the mixed layers (Figure S6). It might be attributed to a slightly different desorption efficiency from the targets, as observed for other peptides as well;[22] alternatively, it could indicate that in the mixed layers of molecules, the desorption/ionization efficiency of the two molecules is different. This might be attributed, e.g., to a different ionization efficiency of one of the molecules in the presence of the second (so-called "matrix effect"[31−34]).

Similar to angiotensin II, in the spectra taken from the bradykinin 1−7 samples, we find minor peaks at m/z < 757, i.e., the peak associated with the intact bradykinin molecule. They are assigned to specific fragments of the peptide (compare also the spectra with an extended mass range in Figure S7). In analogy to the angiotensin II spectra, we analyzed the increase in the intensity of these peaks, which is below 1% with respect to the main peak, i.e., even lower than in the case of angiotensin II, thus further indicating the soft nature of the desorption/deposition process. At this point, we would like to note that angiotensin II and bradykinin 1−9 have been also investigated by means of deposition via GCIBs.[35] Although experiments with Ar clusters of comparable energy density were performed (Ar^+_{5000}, 1 eV/atom), still about 40% of the molecules were found to be fragmented. The difference might be explained by the very different desorption mechanisms being operative (dissolution- versus impact-based[14,19]), the different desorption/deposition geometries, or a combination of both of them.

As the deposited molecules are in direct contact with the substrate, the cleanliness of the surface plays an important role in the DINeC-Depo experiments. Positive ion mode mass spectra from angiotensin II deposited on differently cleaned SiO_2 surfaces are shown in Figure 6b,c. For comparison, the mass spectrum from a drop-cast film of angiotensin II is shown in Figure 6a. In the latter spectrum, the main peak at m/z = 1046 is associated with the intact peptide ($[M + H]^+$), and adduct and oxidation peaks exhibit an intensity of less than 5% of the main peak. When angiotensin II was deposited on a silicon wafer that was cleaned in an ultrasonic bath (acetone and ethanol, 15 min each, Figure 6b), adduct peaks of higher intensity were observed when compared to the spectrum in Figure 6a. The peak with the highest intensity is observed at m/z = 1084. Along with the peak at m/z = 1066, it is assigned to the adduct formation of angiotensin II with potassium ($[M + K]^+$ and $[M - H_2O + K]^+$, respectively). Sodium adducts (m/z = 1068, $[M + Na]^+$) were also observed

https://doi.org/10.1021/acsomega.3c05518
ACS Omega 2023, 8, 40639−40646

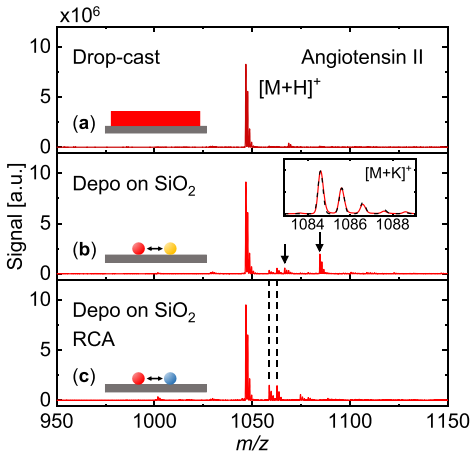

Figure 6. DINeC mass spectra in positive ion mode obtained from angiotensin II samples deposited via DINeC-Depo [(b,c), t_{depo} = 6 h, d_{ST} = 12 mm] on differently cleaned silicon substrates. The mass spectrum from a drop-cast angiotensin II sample is shown in (a) for comparison. In (b), the mass spectrum from a sample prepared by DINeC-Depo on a substrate, which was cleaned in ethanol/acetone only, is shown. Angiotensin II with adducts of potassium ions at m/z = 1084 ($[M + K]^+$) (inset) and m/z = 1066 ($[M - H_2O + K]^+$) is indicated by arrows. In (c), the mass spectrum from a sample deposited on SiO_2 which was additionally cleaned according to the RCA-2-procedure[27] is shown. The adduct peaks are suppressed, and two peaks at m/z = 1058 and m/z = 1062 occur at higher intensities than in the mass spectrum in (b). Peak positions of all major peaks and their intensities are listed in Table S4 in the Supporting Information.

in some experiments. The metal contaminations were almost completely removed from the substrate with an additional cleaning step according to the RCA-2-procedure (Figure 6c). This results in a lower intensity of adduct peaks (<3%). However, in the spectra of the samples prepared on these substrates, the peaks at m/z = 1058 (compare Figure 2) and m/z = 1062 show an increased intensity. The latter is assigned to an oxidation product of angiotensin II.[36] Both peaks are also observed from the drop-cast sample and the samples prepared by DINeC-Depo on substrates cleaned only in ethanol/acetone; however, in the mass spectrum from the samples deposited on the substrates cleaned according to the RCA-2-procedure, they appear with an increased signal intensity of up to ≈15% of the main peak. Additionally, a peak in the mass range m/z < 1046 is observed at m/z = 1001, representing a fragment of the intact peptide ($[M - COOH + H]^+$). The results demonstrate that the peptides, which are in direct contact with the clean SiO_2 surface, are much more prone to further reactions, including oxidation when compared with the molecules in solution or in a drop-cast film.

The degree of oxidation of peptides on samples prepared using DINeC-Depo depends not only on the nature of the substrate but also on handling of the sample after deposition and on the peptides themselves. The peak associated with oxidation of angiotensin II in the mass spectrum shown in Figure 6c (m/z = 1062) is only low in intensity. This changed when the molecule was deposited on a SiO_2 surface which was cleaned according to the RCA-2-procedure[27] and which was installed in the vacuum chamber directly after the cleaning process; a much stronger oxidation of the peptide was observed in this case (compare Figure S4c in the Supporting Information). In comparison, the mass spectrum from bombesin deposited on SiO_2 following the standard cleaning procedure (Figure 7b) shows four prominent peaks separated

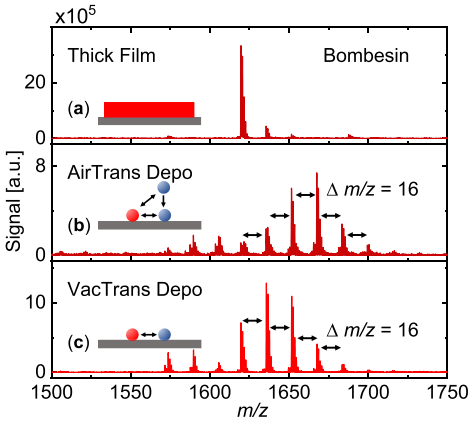

Figure 7. DINeC mass spectra in positive ion mode were obtained from bombesin samples. The mass spectrum from the drop-cast film (a) shows a major peak at m/z = 1619 associated with the intact peptide, $[M + H]^+$. The samples on which the molecules were deposited by DINeC-Depo (t_{depo} = 6 h, d_{ST} = 30 mm) were transferred to the DINeC-MS vacuum chamber via either air (b) or vacuum (c). The mass spectra from these samples show additional peaks separated by $\Delta m/z$ = 16, which are assigned to the oxidation products of the peptide. The peaks at m/z < 1619 are assigned to oxidation products of the bombesin molecule from which the oxidized side group of methionine has been cleaved off (CH_3SOH, $\Delta m/z$ = 64[37,38]). Peak positions of all major peaks and their intensities are listed in Table S5 in the Supporting Information.

by $\Delta m/z$ = 16 each starting from the intact peptide at m/z = 1619 ($[M + H]^+$). The peaks are assigned to oxidation reactions of two of the amino acids, tryptophan and methionine, which are known to be easily oxidized.[39−42] When the sample is transferred between the DINeC-Depo chamber and the DINeC-MS chamber without breaking the vacuum using a mobile vacuum transfer chamber,[43] the peak associated with the intact molecule is observed with higher intensity (Figure 7c) when compared to the spectrum from the sample which was transferred through air. Apparently, atmospheric oxygen enhances the oxidation process. Nonetheless, we also observe a substantial amount of bombesin molecules to be oxidized in the case of the sample which was transferred through vacuum. In that case, the oxidation can be most likely attributed to the influence of SO_2 from the clusters, which, together with H_2O on the sample from the residual gas in the chamber, forms H_2SO_3[18,44] which can readily oxidize the surface-adsorbed molecules during the analysis step as well. Although one might think the same process to be operative during desorption for deposition, the spectra taken from a drop-cast sample (Figure 7a) indicate that on bulk samples the process is much less important. In order to further reduce the influence of the clusters but keep the advantage of the soft desorption process by polar clusters, the use of H_2O clusters might be envisioned; however, this comes at the cost of a more complex cluster source.

So far, we have observed adduct formation and reaction with ambient gases on the surface. In the following, a more complex

https://doi.org/10.1021/acsomega.3c05518
ACS Omega 2023, 8, 40639−40646

reaction between the surface and the molecules that were deposited via DINeC-Depo is illustrated using porphyrins. Bulk samples for this experiment were prepared by drop-casting a saturated ethanolic solution (V = 5−10 μL) on SiO_2 substrates. In the mass spectrum from the drop-cast tetraphenylporphyrin (TPP) sample (Figure 8a), the main peak at m/z = 615 is assigned to the porphyrin molecule ionized by proton uptake, $[M + H]^+$. When the molecule is deposited on silicon oxide by means of DINeC-Depo (Figure 8b), additional peaks separated by $\Delta m/z$ = 16 are observed, which are associated with the oxidation products of the porphyrin. The mass spectrum shown in Figure 8e, which was obtained from a drop-cast sample of copper(II)-tetraphenylporphyrin (CuTPP), features a major peak at m/z = 675, which is assigned to the intact porphyrin $[M]^+$.[45,46] Figure 8d shows the mass spectrum from a sample of CuTPP deposited by means of DINeC-Depo onto a silicon substrate. The peak of the intact molecule is only low in intensity, but a progression of peak groups separated by $\Delta m/z$ = 16 from the most intense peak at m/z = 692 is clearly observed. Similar to the deposition experiment with TPP, these peaks are associated with an oxidation reaction. However, in contrast to oxidation of TPP, the peak progression starts at $\Delta m/z$ = 17 from the peak assigned to the intact CuTPP. This might be interpreted in terms of an additional uptake of a proton when the oxygen atom is incorporated between the copper central ion and one of the nitrogen atoms;[47−50] the oxidation thus goes along with a nominal shift of the ionization process from electron abstraction to proton uptake. Besides the copper-containing species, the peak at m/z = 615 (TPP, $[M + H]^+$) indicates that for some of the molecules copper as the central ion is removed and has been replaced by two protons.

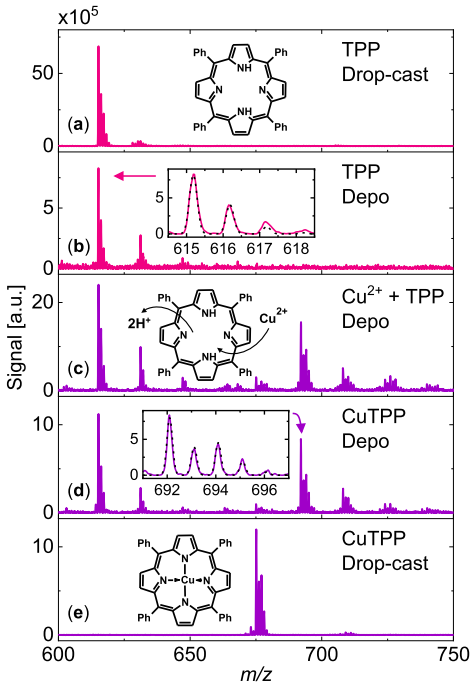

Figure 8. Positive ion mode DINeC mass spectra obtained from two different porphyrins prepared by drop-casting (a,e) or DINeC deposition [(b−d), t_{depo} = 6 h, d_{ST} = 30 mm] on SiO_2. In the mass spectrum from the drop-cast samples, two main peaks are observed at m/z = 615 (a) and m/z = 675 (e), which are assigned to TPP ($[M + H]^+$) and CuTPP ($[M]^+$), respectively.[45] The mass spectra (b−d) from samples prepared by DINeC-Depo also show peaks associated with the intact porphyrins, but additional peak progressions with $\Delta m/z$ = 16, indicating oxidation products, are observed. The mass spectrum in (c) from a sample that was prepared by DINeC-Depo of TPP on $CuCl_2$ shows peaks that are assigned to TPP and CuTPP. Peak positions of all major peaks and their intensities are listed in Table S6 in the Supporting Information.

Finally, TPP was deposited on a $CuCl_2$ surface, which was prepared by drop-casting the salt solution onto the silicon wafer before TPP was deposited via DINeC-Depo on this substrate. The corresponding mass spectrum is shown in Figure 8c; major peaks are observed at m/z = 615 and m/z = 692 accompanied by the corresponding peak progressions. The peak progression at $m/z \geq 675$ indicates the reaction of the porphyrin molecules with the substrate with Cu(II) being integrated into the porphyrin as the central ion; the integrated peak intensity of the peaks associated with CuTPP accounts for approximately 50% of the total peak intensity. Assuming comparable desorption/ionization efficiencies for all of the species investigated, this indicates that about 50% of the deposited TPP molecules were reacted in this way.

CONCLUSIONS

In conclusion, desorption/ionization induced by neutral clusters was introduced as a soft deposition method, which was employed to deposit fragile organic molecules on a variety of different substrates. The process was shown to be fragmentation-free. The amount of material that was deposited ranges from isolated molecules in the submonolayer regime to a few monolayers. As most of the molecules are in direct contact with the substrates and/or the gas phase to which the samples are exposed, reactions with the substrate and/or adsorbates were shown to play a dominant role. Samples prepared by means of DINeC-Depo can thus be used for the investigation of reactions of complex (bio)molecules on surfaces including, among others, adsorbate−adsorbate and adsorbate−surface reactions.

ASSOCIATED CONTENT

Supporting Information

The Supporting Information is available free of charge at https://pubs.acs.org/doi/10.1021/acsomega.3c05518.

Schematic drawing of the DINeC deposition chamber; MS/MS-spectra from the peaks at m/z = 1046 and m/z = 1058 from DINeC-Depo samples of angiotensin II; mass spectra from DINeC-Depo samples of angiotensin II and bradykinin 1−7 with an extended mass range; mass spectra from DINeC-Depo samples of angiotensin II deposited on Au, HOPG, and on activated SiO_2; XPS spectra taken from a DINeC-Depo sample of angiotensin II; intensity ratio of angiotensin II and bradykinin 1−7 peaks in samples mixed via DINeC-Depo as a function of the fraction of the deposition time; and tables of peak positions of all major peaks and their intensities in the shown spectra (PDF)

AUTHOR INFORMATION

Corresponding Author

Michael Dürr − *Institut für Angewandte Physik and Zentrum für Materialforschung, Justus-Liebig-Universität Giessen,*

https://doi.org/10.1021/acsomega.3c05518
ACS Omega 2023, 8, 40639−40646

35392 Giessen, Germany; orcid.org/0000-0002-4676-8715; Email: michael.duerr@ap.physik.uni-giessen.de

Authors

Karolin Pluschke − *Institut für Angewandte Physik and Zentrum für Materialforschung, Justus-Liebig-Universität Giessen, 35392 Giessen, Germany*

Aaron Herrmann − *Institut für Angewandte Physik and Zentrum für Materialforschung, Justus-Liebig-Universität Giessen, 35392 Giessen, Germany*

Complete contact information is available at: https://pubs.acs.org/10.1021/acsomega.3c05518

Notes

The authors declare no competing financial interest.

■ ACKNOWLEDGMENTS

The authors acknowledge financial support from the State of Hesse through the LOEWE Focus Group PriOSS. We thank Jan-Luca Dornseifer and Dr. Joachim Sann for their support in carrying out the XPS measurements.

■ REFERENCES

(1) Catania, F.; de Souza Oliveira, H.; Lugoda, P.; Cantarella, G.; Münzenrieder, N. Thin-film electronics on active substrates: review of material, technologies and application. *J. Phys. D: Appl. Phys.* **2022**, *55*, 323002.

(2) Abegunde, O. O.; Akinlabi, E. T.; Oladijo, O. P.; Akinlabi, S.; Ude, A. U. Overview of thin film deposition technique. *AIMS Mater. Sci.* **2019**, *6*, 174−199.

(3) Zschieschang, U.; Klauk, H. Organic transistors on paper: a brief review. *J. Mater. Chem. C* **2019**, *7*, 5522−5533.

(4) Zou, S.-J.; Shen, Y.; Xie, F.-M.; Chen, J.-D.; Li, Y.-Q.; Tang, J.-X. Recent advances in organic light-emitting diodes: toward smart lighting and displays. *Mater. Chem. Front.* **2020**, *4*, 788−820.

(5) Li, Y.; Huang, W.; Zhao, D.; Wang, L.; Jiao, Z.; Huang, Q.; Wang, P.; Sun, M.; Yuan, G. Recent Progress in Organic Solar Cells: A Review on Materials from Acceptor to Donor. *Molecules* **2022**, *27*, 1800.

(6) Herndon, L. R.; Reid, E. The decomposition of organic compounds at high temperatures and pressures. *J. Am. Chem. Soc.* **1928**, *50*, 3066−3073.

(7) Bank-Srour, B.; Becker, P.; Krasovitsky, L.; Gladkikh, A.; Rosenberg, Y.; Barkay, Z.; Rosenman, G. Physical vapor deposition of peptide nanostructures. *Polym. J.* **2013**, *45*, 494−503.

(8) Rauschenbach, S.; Stadler, F. L.; Lunedei, E.; Malinowski, N.; Koltsov, S.; Costantini, G.; Kern, K. Electrospray Ion Beam Deposition of Clusters and Biomolecules. *Small* **2006**, *2*, 540−547.

(9) Johnson, G. E.; Hu, Q.; Laskin, J. Soft Landing of Complex Molecules on Surfaces. *Annu. Rev. of Anal. Chem.* **2011**, *4*, 83−104.

(10) Portz, A.; Baur, M.; Rinke, G.; Abb, S.; Rauschenbach, S.; Kern, K.; Dürr, M. Chemical analysis of complex surface-adsorbed molecules and their reactios by means of cluster-induced desorption/ionization mass spectrometry. *Anal. Chem.* **2018**, *90*, 3328−3334.

(11) Piqué, A. The matrix-assisted pulsed laser evaporation (MAPLE) process: origins and future directions. *Appl. Phys. A: Mater. Sci. Process.* **2011**, *105*, 517−528.

(12) Lorenz, M.; Shard, A. G.; Counsell, J. D. P.; Hutton, S.; Gilmore, I. S. Angular Distribution of Molecules Sputtered by Gas Cluster Ion Beams and Implications for Secondary Neutral Mass Spectrometry. *J. Phys. Chem. C* **2016**, *120*, 25317−25327.

(13) Delmez, V.; Degand, H.; Poleunis, C.; Moshkunov, K.; Chundak, M.; Dupont-Gillain, C.; Delcorte, A. Deposition of intact and active proteins in vacuo using large argon cluster ion beams. *J. Phys. Chem. Lett.* **2021**, *12*, 952−957.

(14) Delcorte, A. A Microscopic View of Macromolecule Transfer in the Vacuum Using Gas and Bismuth Clusters. *J. Phys. Chem. C* **2022**, *126*, 7307−7318.

(15) Gebhardt, C.; Tomsic, A.; Schröder, H.; Dürr, M.; Kompa, K. Matrix-free formation of gas-phase biomolecular ions by soft cluster-induced desorption. *Angew. Chem., Int. Ed.* **2009**, *48*, 4162−4165.

(16) Baur, M.; Gebhardt, C. R.; Dürr, M. Desorption/ionization induced by neutral cluster impact as a soft and efficient ionization source for ion trap mass spectrometry of biomolecules. *Rapid Commun. Mass Spectrom.* **2014**, *28*, 290−296.

(17) Portz, A.; Bomhardt, K.; Rohnke, M.; Schneider, P.; Asperger, A.; Gebhardt, C. R.; Dürr, M. Soft cluster-induced desorption/ionization mass spectrometry: How soft is soft? *Biointerphases* **2020**, *15*, 021001.

(18) Portz, A.; Baur, M.; Gebhardt, C. R.; Frank, A. J.; Neuderth, P.; Eickhoff, M.; Dürr, M. Influence of the cluster constituents' reactivity on the desorption/ionization process induced by neutral SO_2 clusters. *J. Chem. Phys.* **2017**, *146*, 134705.

(19) Schneider, P.; Verloh, F.; Portz, A.; Aoyagi, S.; Rohnke, M.; Dürr, M. Cluster-induced desorption investigated by means of molecular dynamics simulations - Microsolvation in clusters of polar and non-polar constituents. *J. Chem. Phys.* **2019**, *150*, 214301.

(20) Schneider, P.; Verloh, F.; Dürr, M. Cluster-Induced Desorption/Ionization of Polystyrene: Desorption Mechanism and Effect of Polymer Chain Length on Desorption Probability. *J. Am. Soc. Mass Spectrom.* **2022**, *33*, 832−839.

(21) Lee, B.-J.; Gebhardt, C. R.; Schröder, H.; Kompa, K.-L.; Dürr, M. Observation of ionic desorption channels in cluster-induced desorption of alkali halides − influence of surface electronic properties and surface configuration. *Chem. Phys. Lett.* **2013**, *556*, 77−81.

(22) Portz, A.; Aoyagi, S.; Dürr, M. Soft depth-profiling of mixed peptide/lipid samples by means of cluster induced desorption/ionization mass spectrometry − High depth resolution and low matrix effect. *Biointerphases* **2018**, *13*, 03B405.

(23) Schneider, P.; Keller, P.; Schubert, I.; Bender, M.; Trautmann, C.; Dürr, M. Bond-specific fragmentation of oligopeptides via electronic stopping of swift heavy ions in molecular films. *Sci. Rep.* **2022**, *12*, 17975−17983.

(24) Bomhardt, K.; Schneider, P.; Rohnke, M.; Gebhardt, C. R.; Dürr, M. Cluster-induced desorption/ionization mass spectrometry of highlighter ink: unambiguous identification of dyes and degradation processes based on fragmentation-free desorption. *Analyst* **2022**, *147*, 333−340.

(25) Bomhardt, K.; Schneider, P.; Glaser, T.; Dürr, M. Surface Properties of Ionic Liquids: A Mass Spectrometric View Based on Soft Cluster-Induced Desorption. *J. Am. Soc. Mass Spectrom.* **2022**, *33*, 974−980.

(26) Eusepi, F.; Tomsic, A.; Gebhardt, C. R. Analysis of Solution-Deposited Alkali Ions by Cluster Surface Collisions. *Anal. Chem.* **2003**, *75*, 5124−5128.

(27) Kern, W.; Puotinen, D. Cleaning solutions based on hydrogen peroxide for use in silicon semiconductor technology. *RCA Rev.* **1970**, *31*, 187.

(28) Hesselberth, J. R. Peptide identification and sequenicng by single-molecule detection of peptides undergoing degradation. US Patent, US 20,150,087,526 A1, 2013.

(29) Lecchi, P.; Olson, M.; Brancia, F. L. The role of esterfication on detection of protonated and deprotonated peptide ions in Matrix Assisted Laser Desorption/Ionization (MALDI) Mass Spectrometry (MS). *J. Am. Soc. Mass Spectrom.* **2005**, *16*, 1269−1274.

(30) Baur, M.; Lee, B.-J.; Gebhardt, C. R.; Dürr, M. Soft cluster-induced desorption and ionization of biomolecules—Influence of surface load and morphology on desorption efficiency. *Appl. Phys. Lett.* **2011**, *99*, 234103.

(31) Deline, V. R.; Katz, W.; Evans, C. A.; Williams, P. Mechanism of the SIMS matrix effect. *Appl. Phys. Lett.* **1978**, *33*, 832−835.

(32) Shard, A. G.; Spencer, S. J.; Smith, S. A.; Havelund, R.; Gilmore, I. S. The matrix effect in organic secondary ion mass spectrometry. *Int. J. Mass Spectrom.* **2015**, *377*, 599−609.

(33) Takahashi, K.; Aoyagi, S.; Kawashima, T. TOF-SIMS matrix effects in mixed organic layers in Ar cluster ion depth profiles. *Surf. Interface Anal.* **2017**, *49*, 721−727.
(34) Nakano, S.; Yamagishi, T.; Aoyagi, S.; Portz, A.; Dürr, M.; Iwai, H.; Kawashima, T. Evaluation of matrix effects on TOF-SIMS data of leu-enkephalin and 1, 2-dioleoyl-sn-glycero-3-phosphocholine mixed samples. *Biointerphases* **2018**, *13*, 03B403.
(35) Delmez, V.; Tomasetti, B.; Daphnis, T.; Poleunis, C.; Lauzin, C.; Dupont-Gillain, C.; Delcorte, A. Gas Cluster Ion Beams as a Versatile Soft-Landing Tool for the Controlled Construction of Thin (Bio)Films. *ACS Appl. Bio Mater.* **2022**, *5*, 3180−3192.
(36) Lloyd, J. A.; Spraggins, J. M.; Johnston, M. V.; Laskin, J. Peptide ozonolysis: Product structures and relative reactivities for oxidation of tyrosine and histidine residues. *J. Am. Soc. Mass Spectrom.* **2006**, *17*, 1289−1298.
(37) Guan, Z.; Yates, N. A.; Bakhtiar, R. Detection and characterization of methionine oxidation in peptides by collision-induced dissociation and electron capture dissociation. *J. Am. Soc. Mass Spectrom.* **2003**, *14*, 605−613.
(38) Reid, G. E.; Roberts, K. D.; Kapp, E. A.; Simpson, R. J. Statistical and Mechanistic Approaches to Understanding the Gas-Phase Fragmentation Behavior of Methionine Sulfoxide Containing Peptides. *J. Proteome Res.* **2004**, *3*, 751−759.
(39) Davies, M. J. The oxidative environment and protein damage. *Biochim. Biophys. Acta Gen. Subj.* **2005**, *1703*, 93−109.
(40) Morand, K.; Talbo, G.; Mann, M. Oxidation of peptides during electrospray ionization. *Rapid Commun. Mass Spectrom.* **1993**, *7*, 738−743.
(41) Jeong, K.-H.; Seo, J.; Yoon, H.-J.; Shin, S. K. Focused Electrospray Deposition for Matrix-Assisted Laser Desorption/Ionization Mass Spectrometry. *Bull. Korean Chem. Soc.* **2010**, *31*, 2293−2298.
(42) Schweikart, F.; Hulthe, G. HPLC-UV-MS analysis: A source for severe oxidation artifacts. *Anal. Chem.* **2019**, *91*, 1748−1751.
(43) Länger, C.; Ernst, P.; Bender, M.; Severin, D.; Trautmann, C.; Schleberger, M.; Dürr, M. Single-ion induced surface modifications on hydrogen-covered Si(001) surfaces - significant difference between slow highly charged and swift heavy ions. *New J. Phys.* **2021**, *23*, 093037.
(44) Lee, B.-J.; Baur, M.; Gebhardt, C. R.; Dürr, M. Quantification of the ionization probability during desorption/ionization of oligopeptides induced by neutral cluster impact. *Rapid Commun. Mass Spectrom.* **2013**, *27*, 1090−1094.
(45) Portz, A.; Gebhardt, C. R.; Dürr, M. Real-time investigation of the H/D exchange kinetics of porphyrins and oligopeptides by means of neutral cluster induced desorption/ionization mass spectrometry. *J. Phys. Chem. B* **2017**, *121*, 11031−11036.
(46) Herritsch, J.; Kachel, S. R.; Fan, Q.; Hutter, M.; Heuplick, L. J.; Münster, F.; Gottfried, J. M. On-surface porphyrin transmetalation with Pb/Cu redox exchange. *Nanoscale* **2021**, *13*, 13241−13248.
(47) Yang, F.-A.; Guo, C.-W.; Chen, Y.-J.; Chen, J.-H.; Wang, S.-S.; Tung, J.-Y.; Hwang, L.-P.; Elango, S. ESR, zero-field splitting, and magnetic exchange of exchange-coupled copper(II)-copper(II) pairs in copper(II) tetraphenylporphyrin N-oxide. *Inorg. Chem.* **2007**, *46*, 578−585.
(48) Prigge, S. T.; Eipper, B. A.; Mains, R. E.; Amzel, L. M. Dioxygen Binds End-On to Mononuclear Copper in a Precatalytic Enzyme Complex. *Science* **2004**, *304*, 864−867.
(49) Lewis, E. A.; Tolman, W. B. Reactivity of Dioxygen-Copper Systems. *Chem. Rev.* **2004**, *104*, 1047−1076.
(50) Liu, Y.; Han, Y.; Zhang, Z.; Zhang, W.; Lai, W.; Wang, Y.; Cao, R. Low overpotential water oxidation at neutral pH catalyzed by a copper(II) porphyrin. *Chem. Sci.* **2019**, *10*, 2613−2622.

https://doi.org/10.1021/acsomega.3c05518
ACS Omega 2023, 8, 40639−40646

Supporting Information for:

Soft deposition of organic molecules based on cluster-induced desorption for the investigation of on-surface and surface-mediated reactions

K. Pluschke, A. Herrmann, and M. Dürr*

Institut für Angewandte Physik and Zentrum für Materialforschung, Justus-Liebig-Universität Giessen, Heinrich-Buff-Ring 16, D-35392 Giessen, Germany

** Corresponding author: michael.duerr@ap.physik.uni-giessen.de*

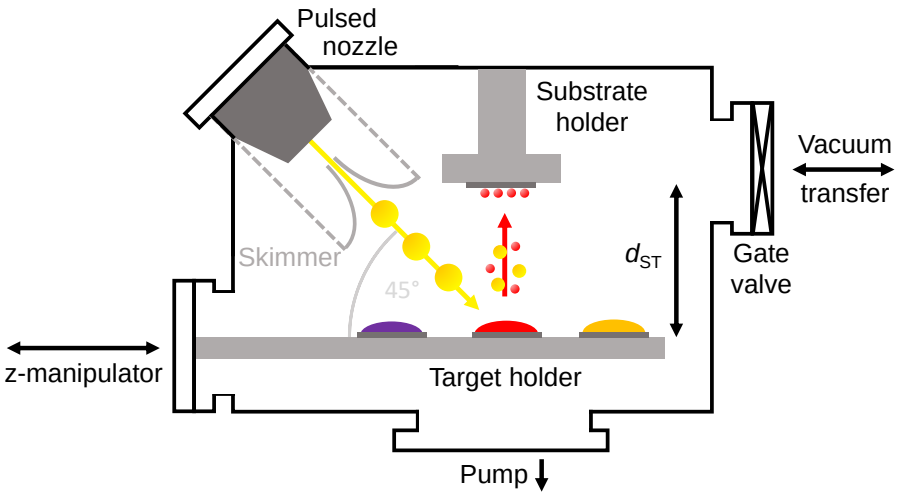

Figure S1: Schematic drawing of the chamber used for soft deposition by means of cluster-induced desorption. The SO_2 cluster beam is generated via supersonic expansion using a pulsed nozzle. The beam hits the surface at an angle of 45° after passing the skimmer. The clusters desorb the molecules applied on the target by means of drop-casting; a fraction of the desorbed molecules is deposited onto a substrate which is mounted at variable distance d_{ST} from the target. In the experiments reported in this paper, d_{ST} was between 8 and 30 mm. By moving the z-manipulator, the target molecules for the deposition process can be changed. The substrate on which the molecules were deposited can be transfered to any vacuum chamber of choice, which in the experiment reported in this paper was a DINeC-MS chamber, either through ambient or without breaking the vacuum using a mobile vacuum transfer chamber. The DINeC-Depo vacuum chamber was pumped by a turbomolecular pump with a pumping speed of $S = 120$ L/s.

Table S1: Ion peaks observed in the mass spectra shown in Figure 2 obtained by means of DINeC-MS.

m/z	Intensity [a.u.]	
	(a)	**(b)**
931.5	146641	53604
1001.5	78944	79496
1028.5	42800	88868
1046.5	7672775	2999608
1058.5	411566	242248
1068.5	398403	205835
1074.5	93344	152983
1084.5	233393	269742

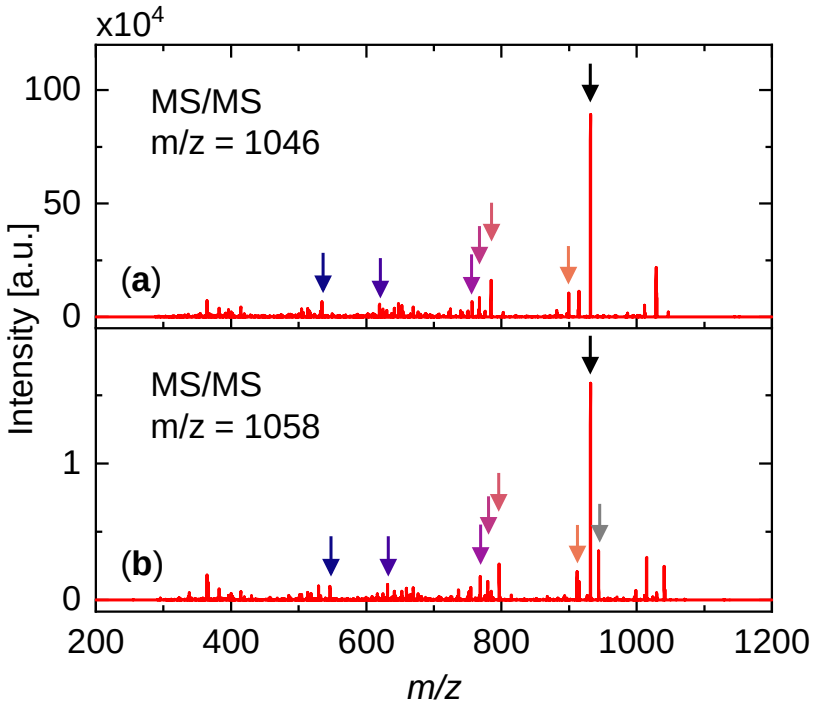

Figure S2: Positive ion mode MS/MS spectra obtained from an angiotensin II DINeC-Depo sample ($t_{\mathrm{depo}} = 6$ h, $d_{\mathrm{ST}} =$ 12 mm) after isolation and fragmentation of the peaks at (a) $m/z = 1046$ and (b) $m/z = 1058$. The main peak at $m/z = 931$ (black arrow) can be assigned to the fragment 2-8 after cleavage of the aspartic acid from the intact peptide. The dominant presence of the peak in both spectra indicates a reaction at the cleaved aspartic acid to be responsible for the peak at $m/z = 1058$. The peaks labelled with colored arrows in (a) can be assigned to further fragments of angiotensin II and occur also in (b) but shifted by $\Delta m/z = 12$. All of these fragments still include the aspartic acid. The peak at $m/z = 943$ (gray arrow), which is related to the peak at $m/z = 931$ ($\Delta m/z = 12$) indicates that the reaction in part also occurs at other amino acids in angiotensin II.

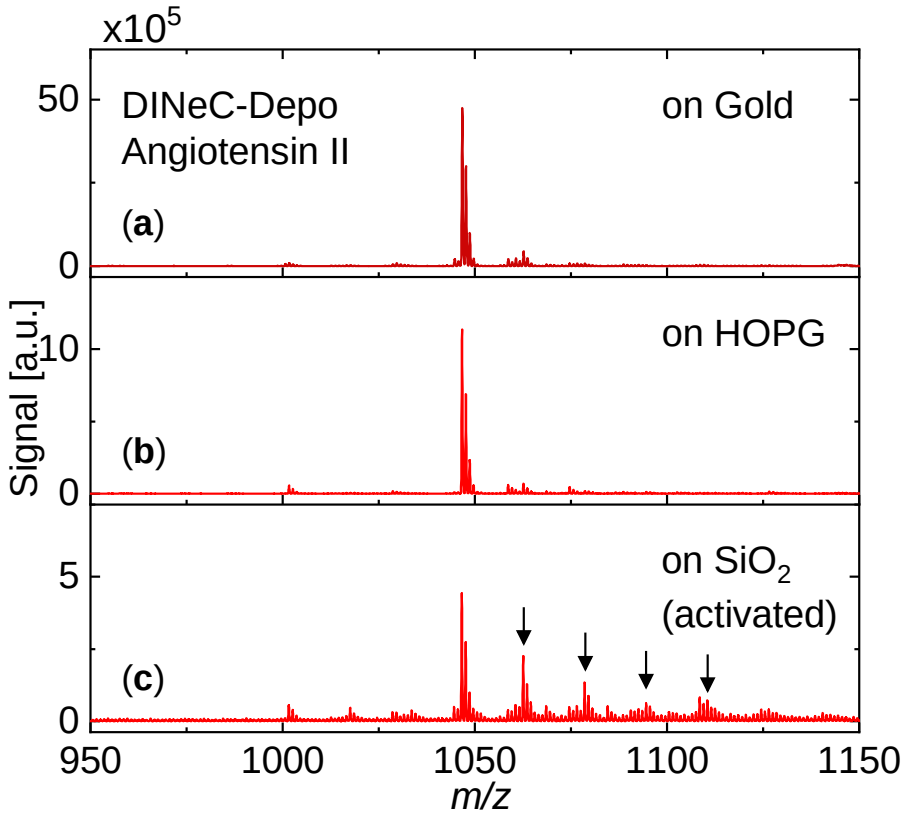

Figure S3: DINeC mass spectra in positive ion mode obtained from angiotensin II samples deposited via DINeC-Depo ($t_{\mathrm{depo}} = 6$ h, $d_{\mathrm{ST}} = 12$ mm) on (a) gold, (b) HOPG, and (c) "activated" SiO_2. The activation is a result of the treatment with hydrogen peroxide as an ingredient of the RCA-2-procedure. The substrate was mounted in the chamber directly after the cleaning procedure. The main peak in all three spectra at $m/z = 1046$ is assigned to the intact peptide, $[M+H]^+$. In the mass spectra from the gold and HOPG samples, the additional peaks are of low intensity. In the spectrum taken from the activated substrate, four additional peak groups, which are separated by $\Delta m/z = 16$ each, are observed (arrows). They indicate oxidation of the peptide on the activated surface.

Table S2: Ion peaks observed in the mass spectra shown in Figure 4 obtained by means of DINeC-MS.

m/z	Intensity [a.u.]		
	(a)	**(b)**	**(c)**
931.5	238031	105436	68233
1001.5	261154	137672	95376
1028.5	203471	401172	348672
1046.5	8181660	3034386	1602192
1058.5	663817	328500	184819
1062.5	155020	483691	22288
1068.5	53895	33184	31796
1074.5	495547	184674	121835

Table S3: Ion peaks observed in the mass spectra shown in Figure 5 obtained by means of DINeC-MS.

m/z	Intensity [a.u.]				
	(a)	**(b)**	**(c)**	**(d)**	**(e)**
739.3	4984	14943	89827	307361	143958
757.3	5453	16842	1848579	10328425	8518563
769.3	1204	7566	111359	746019	159246
773.3	164	2554	23351	393534	16165
779.3	0	5331	11630	25364	202303
785.3	15170	32524	114217	385664	108814
795.3	997	1558	16620	25541	268302
931.5	59334	174051	127921	13706	7459
1001.5	19557	337452	200791	10915	1007
1028.5	84259	108377	160791	6853	1106
1046.5	8242034	9489328	5277106	5787	2382
1058.5	106516	1492254	354237	5449	1062
1062.5	58293	1441831	551377	5323	1346
1068.5	397891	21458	36458	12644	785
1074.5	16185	566263	122408	4498	2004

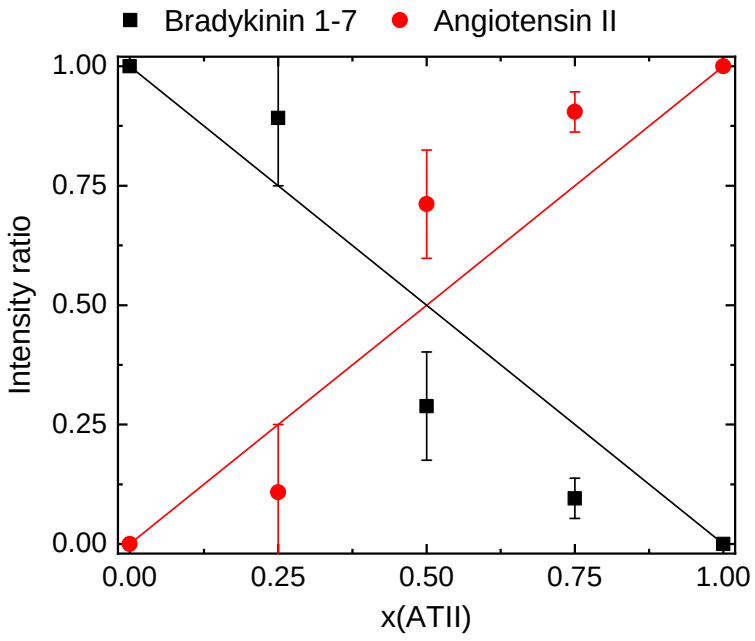

Figure S4: Intensity ratio of the main peaks assigned to the intact peptides bradykinin 1-7 and angiotensin II (m/z = 757 and m/z = 1046, respectively) of mixed samples prepared by DINeC-Depo (t_{depo} = 6 h, d_{ST} = 12 mm) measured by DINeC-MS as a function of the fraction of the deposition time of angiotensin II, x(ATII). Each data point represents 8-12 measurements. The intensity of the peaks entering the intensity ratio is normalized to the average signal intensity as measured from pure DINeC-Depo samples of bradykinin 1-7 and angiotensin II.

Table S4: Ion peaks observed in the mass spectra shown in Figure 6 obtained by means of DINeC-MS.

m/z	Intensity [a.u.]		
	(a)	**(b)**	**(c)**
931.5	59334	162579	174051
1001.5	19557	71222	337452
1028.5	84259	113925	108377
1046.5	8242034	9133217	9489328
1058.5	106516	326215	1492254
1062.5	58293	534105	1441831
1066.5	18963	559870	27506
1074.5	16185	60488	566263
1084.5	111643	1954896	25903

Table S5: Ion peaks observed in the mass spectra shown in Figure 7 obtained by means of DINeC-MS.

m/z	Intensity [a.u.]		
	(a)	**(b)**	**(c)**
1571.8	17544	38267	100099
1573.8	89279	66162	218453
1587.8	17737	95937	68263
1589.8	9118	180989	321105
1603.8	24918	102779	33281
1605.8	30613	173109	112248
1619.8	3324112	113458	597756
1635.8	438719	238764	1251395
1651.8	150683	602683	1092171
1667.8	25321	741127	405189
1683.8	3300	281889	110161
1699.8	2849	90463	30136

Table S6: Ion peaks observed in the mass spectra shown in Figure 8 obtained by means of DINeC-MS.

m/z	Intensity [a.u.]				
	(a)	**(b)**	**(c)**	**(d)**	**(e)**
615.2	6865211	827525	2401350	1121330	1557
631.2	352561	275971	990430	283397	1038
647.2	42649	88623	295265	63370	320
663.2	18502	23267	103532	57592	278
675.2	6883	26583	304580	99017	1197107
692.2	8392	15172	1554755	656830	1987
708.2	16987	3023	512563	275009	8283
724.2	2510	7058	251961	101597	1935
740.2	1675	1031	149022	55612	400

Literaturverzeichnis

[1] J. F. Rusling. *Biomolecular Films: Design, Function and Applications*, *CRC Press*, Volume 1. New York (2003).

[2] B. Kasemo. *Biological surface science.* Surf. Sci. **500**, 656–677 (2002).

[3] M. Morra. *Biomolecular modification of implant surfaces.* Expert Rev. Med. Devices **4**, 361–372 (2007).

[4] V. Shubina, L. Gaillet, T. Chaussadent, T. Meylheuc, and J. Creus. *Biomolecules as a sustainable protection against corrosion of reinforced carbon steel in concrete.* J. Clean. Prod. **112**, 666–671 (2016).

[5] K. Y. Cheong, I. A. Tayeb, F. Zhao, and J. M. Abdullah. *Review on resistive switching mechanisms of bio-organic thin film for non-volatile memory application.* Nano Rev. **10**, 680–709 (2021).

[6] S. Martić, M. Labib, and H.-B. Kraatz. *Enzymatically modified peptide surfaces: towards general electrochemical sensor platform for protein kinase catalyzed phosphorylations.* Analyst **136**, 107–112 (2011).

[7] M. D. Sonawane and S. B. Nimse. *Surface Modification Chemistries of Materials Used in Diagnostic Platforms with Biomolecules.* J. Chem. 9241378 (2016).

[8] C. Homma, M. Tsukiiwa, H. Noguchi, M. Tanaka, M. Okochi, H. Tomizawa, Y. Sugizaki, A. Isobayashi, and Y. Hayamizu. *Designable peptides on graphene field-effect transistors for selective detection of odor molecules.* Biosens. Bioelectron. **224**, 115047 (2023).

[9] A. W. G. Nijhuis, S. C. G. Leeuwenburgh, and J. A. Jansen. *Wet-Chemical Deposition of Functional Coatings for Bone Implantology.* Macromol. Biosci. **10**, 1316–1329 (2010).

[10] J. J. Richardson, J. Cui, M. Björnmalm, J. A. Braunger, H. Ejima, and F. Caruso. *Innovation in Layer-by-Layer Assembly.* Chem. Rev. **116**, 14828–14867 (2016).

[11] K. A. Kravanja and M. Finšgar. *A review of techniques for the application of bioactive coatings on metal-based implants to achieve controlled release of active ingredients.* Mater. Des. **217**, 110653 (2022).

[12] T. Franklin and R. Yang. *Vapor-Deposited Biointerfaces and Bacteria: An Evolving Conversation.* ACS Biomater. Sci. Eng. **6**, 182–197 (2020).

[13] A. Khlyustova, Y. Cheng, and R. Yang. *Vapor-deposited functional polymer thin films in biological applications.* J. Mater. Chem. B **8**, 6588–6609 (2020).

[14] G. M. Aparna and K. K. R. Tetala. *Recent Progress in Development and Application of DNA, Protein, Peptide, Glycan, Antibody, and Aptamer Microarrays.* Biomolecules **13**, 602 (2023).

[15] R. de la Rica and H. Matsui. *Applications of peptide and protein-based materials in bionanotechnology.* Chem. Soc. Rev. **39**, 3499–3509 (2010).

[16] B. Bank-Srour, P. Becker, L. Krasovitsky, A. Gladkikh, Y. Rosenberg, Z. Barkay, and G. Rosenman. *Physical vapor deposition of peptide nanostructures.* Polym. J. **45**, 494–503 (2013).

[17] L. R. Herndon and E. Reid. *The decomposition of organic compounds at high temperatures and pressures.* J. Am. Chem. Soc. **50**, 3066–3073 (1928).

[18] M. Fang, J. Ivanisevic, H. P. Benton, C. H. Johnson, G. J. Patti, L. T. Hoang, W. Uritboonthai, M. E. Kurczy, and G. Siuzdak. *Thermal Degradation of Small Molecules: A Global Metabolomic Investigation.* Anal. Chem. **87**, 10935–10941 (2015).

[19] N. N. Ivanov, D. A. Shulga, and V. A. Palyulin. *Decomposition of Small Molecules for Fragment-Based Drug Design.* Biophysica **3**, 362–372 (2023).

[20] J. Thomson. *XLII. Rays of positive electricity.* Lond. Edinb. Dublin Phil. Mag. **19**, 424–435 (1910).

[21] J. J. Thomson. *Bakerian Lecture: Rays of positive electricity.* Proc. Math. Phys. **89**, 1–20 (1913).

[22] A. J. Dempster. *A new Method of Positive Ray Analysis.* Phys. Rev. **11**, 316–325 (1918).

[23] F. Aston. *LXXIV. A positive ray spectrograph.* Lond. Edinb. Dublin Phil. Mag. **38**, 707–714 (1919).

[24] P. Liigand, J. Liigand, K. Kaupmees, and A. Kruve. *30 Years of research on ESI/MS response: Trends, contradictions and applications.* Anal. Chim. Acta **1152**, 238117 (2021).

[25] G. Famiglini, P. Palma, V. Termopoli, and A. Cappiello. *The history of electron ionization in LC-MS, from the early days to modern technologies: A review.* Anal. Chim. Acta **1167**, 338350 (2021).

[26] M. Karas, D. Bachmann, U. Bahr, and F. Hillenkamp. *Matrix-Assisted Ultraviolet Laser Desorption of Non-Volatile Compounds.* Int. J. Mass Spectrom. Ion Processes **78**, 53 – 68 (1987).

[27] N. Tarfeen, K. U. Nisa, and Q. Nisa. *MALDI-TOF MS: application in diagnosis, dereplication, biomolecule profiling and microbial ecology.* Proc. Indian National Sci. Acad. **88**, 277–291 (2022).

[28] I. Domínguez, A. Garrido Frenich, and R. Romero-González. *Mass spectrometry approaches to ensure food safety.* Anal. Methods **12**, 1148–1162 (2020).

[29] L. Mattoli, M. Gianni, and M. Burico. *Mass spectrometry-based metabolomic analysis as a tool for quality control of natural complex products.* Mass Spec. Rev. **42**, 1358–1396 (2023).

[30] X. Zhu, T. Xu, C. Peng, and S. Wu. *Advances in MALDI Mass Spectrometry Imaging Single Cell and Tissues.* Front. Chem. **9**, 782432 (2022).

[31] P. Sousa, L. Silva, C. Luís, J. S. Câmara, and R. Perestrelo. *MALDI-TOF MS: A Promising Analytical Approach to Cancer Diagnostics and Monitoring.* Separations **10**, 453 (2023).

[32] Y. Chen, Y. Xie, L. Li, Z. Wang, and L. Yang. *Advances in mass spectrometry imaging for toxicological analysis and safety evaluation of pharmaceuticals.* Mass Spec. Rev. **42**, 2207–2233 (2023).

[33] C. Uetrecht and A. J. R. Heck. *Modern Biomolecular Mass Spectrometry and its Role in Studying Virus Structure, Dynamics, and Assembly.* Angew. Chem. Int. Ed. **50**, 8248–8262 (2011).

[34] K. M. Engel, P. Prabutzki, J. Leopold, A. Nimptsch, K. Lemmnitzer, D. N. Vos, C. Hopf, and J. Schiller. *A new update of MALDI-TOF mass spectrometry in lipid research.* Prog. Lipid Res. **86**, 101145 (2022).

[35] L. Darie-Ion, D. Whitham, M. Jayathirtha, Y. Rai, A.-N. Neagu, C. C. Darie, and B. A. Petre. *Applications of MALDI-MS/MS-Based Proteomics in Biomedical Research.* Molecules **27**, 6196 (2022).

[36] S. Maher, F. P. M. Jjunju, and S. Taylor. *Colloquium: 100 years of mass spectrometry: Perspectives and future trends.* Rev. Mod. Phys. **87**, 113–135 (2015).

[37] K. Evans-Nguyen, A. R. Stelmack, P. C. Clowser, J. M. Holtz, and C. C. Mulligan. *Fieldable mass spectrometry for forensic science, homeland security, and defense applications.* Mass Spec. Rev. **40**, 628–646 (2021).

[38] C. R. Gebhardt, H. Schröder, and K. L. Kompa. *Surface impact ionization of polar-molecule clusters through pickup of alkali atoms.* Nature **400**, 544–547 (1999).

[39] C. Gebhardt, A. Tomsic, H. Schröder, M. Dürr, and K. Kompa. *Matrix-free formation of gas-phase biomolecular ions by soft cluster-induced desorption.* Angew. Chem. Int. Ed. **48**, 4162–4165 (2009).

[40] M. Baur, C. R. Gebhardt, and M. Dürr. *Desorption/ionization induced by neutral cluster impact as a soft and efficient ionization source for ion trap mass spectrometry of biomolecules.* Rapid Commun. Mass Spectrom. **28**, 290 – 296 (2014).

[41] A. Portz, C. R. Gebhardt, and M. Dürr. *Real-time investigation of the H/D exchange kinetics of porphyrins and oligopeptides by means of neutral cluster induced desorption/ionization mass spectrometry.* J. Phys. Chem. B **121**, 11031–11036 (2017).

[42] A. Portz, S. Aoyagi, and M. Dürr. *Soft depth-profiling of mixed peptide/lipid samples by means of cluster induced desorption/ionization mass spectrometry – High depth resolution and low matrix effect.* Biointerphases **13**, 03B405 (2018).

[43] P. Schneider, F. Verloh, and M. Dürr. *Cluster-Induced Desorption/Ionization of Polystyrene: Desorption Mechanism and Effect of Polymer Chain Length on Desorption Probability.* J. Am. Soc. Mass Spectrom. **33**, 832–839 (2022).

[44] K. Bomhardt, P. Schneider, T. Glaser, and M. Dürr. *Surface Properties of Ionic Liquids: A Mass Spectrometric View Based on Soft Cluster-Induced Desorption.* J. Am. Soc. Mass Spectrom. **33**, 974–980 (2022).

[45] K. Bomhardt, P. Schneider, M. Rohnke, C. R. Gebhardt, and M. Dürr. *Cluster-induced desorption/ionization mass spectrometry of highlighter ink: unambiguous identification of dyes and degradation processes based on fragmentation-free desorption.* Analyst **147**, 333–340 (2022).

[46] P. Keller, S. Aoyagi, and M. Dürr. *Cluster-induced desorption/ionization mass spectrometry of Ir(ppy)3.* J. Vac. Sci. Technol. **41**, 054002 (2023).

[47] D. Rading, R. Moellers, H.-G. Cramer, and E. Niehuis. *Dual beam depth profiling of polymer materials: comparison of C_{60} and Ar cluster ion beams for sputtering.* Surf. Interface Anal. **45**, 171–174 (2013).

[48] D. Patel, D. Margolese, and T. R. Dykea. *Electric dipole moment of SO2 in ground and excited vibrational states.* J. Chem. Phys. **70**, 2740–2747 (2008).

[49] B.-J. Lee, C. R. Gebhardt, H. Schröder, K.-L. Kompa, and M. Dürr. *Observation of ionic desorption channels in cluster-induced desorption of alkali halides – influence of surface electronic properties and surface configuration.* Chem. Phys. Lett. **556**, 77 – 81 (2013).

[50] A. Portz, M. Baur, C. R. Gebhardt, A. J. Frank, P. Neuderth, M. Eickhoff, and M. Dürr. *Influence of the cluster constituents' reactivity on the desorption/ionization process induced by neutral SO_2 clusters.* J. Chem. Phys. **146**, 134705 (2017).

[51] P. Schneider and M. Dürr. *Cluster-induced desorption investigated by means of molecular dynamics simulations - Microsolvation in clusters of polar and non-polar constituents.* J. Chem. Phys. **150**, 214301 (2019).

[52] M. Baur, B.-J. Lee, C. R. Gebhardt, and M. Dürr. *Soft cluster-induced desorption and ionization of biomolecules—Influence of surface load and morphology on desorption efficiency.* Appl. Phys. Lett. **99**, 234103 (2011).

[53] B.-J. Lee, M. Baur, C. R. Gebhardt, and M. Dürr. *Quantification of the ionization probability during desorption/ionization of oligopeptides induced by neutral cluster impact.* Rapid Commun. Mass Spectrom. **27**, 1090–1094 (2013).

[54] K. Bomhardt, P. Schneider, A. Portz, C. R. Gebhardt, and M. Dürr. *Analysis of Complex Molecules and Their Reactions on Surfaces by Means of Cluster-Induced Desorption/Ionization Mass Spectrometry.* J. Visualized Exp. **11**, e60487 (2020).

[55] A. Portz, K. Bomhardt, M. Rohnke, P. Schneider, A. Asperger, C. R. Gebhardt, and M. Dürr. *Soft cluster-induced desorption/ionization mass spectrometry: How soft is soft?* Biointerphases **15**, 021001 (2020).

[56] C. D. Calvano, M. A. M. Capozzi, A. Punzi, G. M. Farinola, T. R. I. Cataldi, and F. Palmisano. *1,5-Diaminonaphtalene is a Highly Performing Electron-Transfer Secondary-Reaction Matrix for Laser Desorption Ionization Mass Spectrometry of Indolenine-Based Croconaines.* ACS Omega **3**, 17821–17827 (2018).

[57] A. E. Kramell, M. García-Altares, M. Pötsch, R. Kluge, A. Rother, G. Hause, C. Hertweck, and R. Csuk. *Mapping Natural Dyes in Archeological Textiles by Imaging Mass Spectromet.* Sci. Rep. **9**, 2045–2322 (2019).

[58] Z. Ren, B. Nie, T. Liu, F. Yuan, F. Feng, Y. Zhang, W. Zhou, X. Xu, M. Yao, and F. Zhang. *Simultaneous determination of coumarin and its derivatives in tobacco products by liquid chromatography-tandem mass spectrometry.* Molecules **21**, 1511 (2016).

[59] K. Hayat, M. Gondal, M. Khaled, Z. Yamani, and S. Ahmed. *Laser induced photocatalytic degradation of hazardous dye (Safranin-O) using self synthesized nanocrystalline WO3.* J. Hazard. Mater. **186**, 1226–1233 (2011).

[60] J. Gu, C. Luo, W. Zhou, Z. Tong, H. Zhang, P. Zhang, and X. Ren. *Degradation of Rhodamine B in aqueous solution by laser cavitation.* Ultrason. Sonochem. **68**, 105181 (2020).

[61] D. Schardt, T. Elsässer, and D. Schultz-Ertner. *Heavy-ion tumor therapy: Physical and radiobiological benefits.* Rev. Mod. Phys. **82**, 383–425 (2010).

[62] P. Schneider, P. Keller, I. Schubert, M. Bender, C. Trautmann, and M. Dürr. *Bond-specific fragmentation of oligopeptides via electronic stopping of swift heavy ions in molecular films.* Sci. Rep. **12**, 17975–17983 (2022).

[63] A. Gürses, M. Açıkyıldız, K. Güneş, and M. S. Gürses. *Dyes and Pigments.* Springer International Publishing (2016).

[64] I. Klöckl. *Handbook of Colorants Chemistry : Dyes and Pigments Fundamentals*, Volume 1. De Gruyter, Berlin (2023).

[65] S. Bienz, L. Bigler, T. Fox, and H. Meier. *Spektroskopische Methoden in der organischen Chemie, Georg Thieme Verlag*, Volume 9. Stuttgart (2016).

[66] S. Nicolai, T. Tralau, A. Luch, and R. Pirow. *A scientific review of colorful textiles.* JCF **16**, 5–17 (2021).

[67] J. A. Ferreira and S. M. Costa. *Rhodamine* $3B^+ClO_4^-$ *electronic transitions: reaction field and vibrational structure.* Chem. Phys. **273**, 39–49 (2001).

[68] K. Hunger. *Industrial dyes : chemistry, properties, applications, Whiley-VCH Verlag*, Volume 9. Weinheim (2003).

[69] I. Klöckl. *Handbook of Colorants Chemistry : in Painting, Art and Inks*, Volume 2. De Gruyter, Berlin (2023).

[70] P. Walden. *Über die Molekulargröße und die elektrische Leitfähigkeit einiger geschmolzenen Salze.* Bull. Acad. Imp. Sci. Staint-Petersbourg **8**, 405–422 (1914).

[71] S. K. Singh and A. W. Savoy. *Ionic liquids synthesis and applications: An overview.* J. Mol. Liq. **297**, 112038 (2020).

[72] T. Welton. *Ionic Liquids: a brief history* . Biophys. Rev. **10**, 691–706 (2018).

[73] C. D. Rodríguez-Fernández, L. M. Varela, C. Schröder, and E. L. Lago. *Charge delocalization and hyperpolarizability in ionic liquids.* J. Mol. Liq. **349**, 118153 (2022).

[74] F. U. Shah, R. An, and N. Muhammad. *Editorial: Properties and Applications of Ionic Liquids in Energy and Environmental Science.* Front. Chem. **8**, 627213 (2020).

[75] G. Kaur, H. Kumar, and M. Singla. *Diverse applications of ionic liquids: A comprehensive review.* J. Mol. Liq. **351**, 118556 (2022).

[76] S. P. Neofotistos, A. Tzani, and A. Detsi. *Ionic Liquids: Advances and Applications in Phase Transfer Catalysis.* Catalysts **13**, 474 (2023).

[77] E. Sloutskin, B. M. Ocko, L. Tamam, I. Kuzmenko, T. Gog, and M. Deutsch. *Surface Layering in Ionic Liquids: An X-ray reflectivity study.* J. Am. Chem. Soc. **127**, 7796–7804 (2005).

[78] Y. Jeon, J. Sung, W. Bu, D. Vaknin, Y. Ouchi, and D. Kim. *Interfacial Restructuring of Ionic Liquids Determined by Sum-Frequency Generation Spectroscopy and X-ray Refelctivity.* J. Phys. Chem. C **112**, 19649 – 19654 (2010).

[79] M. Mezger, B. M. Ocko, H. Reichert, and M. Deutsch. *Surface layering and melting in an ionic liquid studied by resonant soft x-ray reflectivity.* Proc. Natl. Acad. Sci. USA **110**, 3733 – 3737 (2013).

[80] J. Haddad, D. Pontoni, B. M. Murphy, S. Festersen, B. Runge, O. M. Magnussen, H.-G. Steinrück, H. Reichert, B. M. Ocko, and M. Deutsch. *Surface structure evolution in a homologous series of ionic liquids.* Proc. Natl. Acad. Sci. USA **115**, E1100–E1107 (2018).

[81] P. J. Cumpson. *Angle-resolved XPS depth-profiling strategies.* Appl. Surf. Sci. **144-145**, 16–20 (1999).

[82] V. Lockett, R. Sedev, C. Bassell, and J. Ralston. *Angle-resolved X-ray photoelectron spectroscopy of the surface of imidazolium ionic liquids.* Phys. Chem. Chem. Phys. **10**, 1330 – 1335 (2008).

[83] H. P. Steinrück. *Recent developments in the study of ionic liquid interfaces using X-ray photoelectron spectroscopy and potential future directions.* Phys. Chem. Chem. Phys. **14**, 5010 – 5029 (2012).

[84] C. Kolbeck, I. Niedermaier, A. Deyko, K. R. J. Lovelock, N. Taccardi, W. W. P. Wasserscheid, F. Maier, and H.-P. Steinrück. *Influence of substituents and functional groups on the surface composition of Ionic Liquids.* Chem. Eur. J. **20**, 3954–3965 (2014).

[85] R. K. Blundell, A. E. Delorme, E. F. Smith, and P. Licence. *An ARXPS and ERXPS study of quaternary ammonium and phosphonium ionic liquids: utilising a high energy Ag Lα‘ X-ray source.* Phys. Chem. Chem. Phys. **18**, 6122–6131 (2016).

[86] J. Günster, O. Höfft, S. Krischok, and R. Souda. *A time-of-flight secondary ion mass spectroscopy study of 1-ethyl-3-methylimidazolium bis(trifluoromethylsulfonyl)imide RT-ionic liquid.* Surf. Sci. **602**, 3403–3407 (2008).

[87] R. Souda. *Glass-Liquid Transition, Crystallization, and Melting of a Room Temperature Ionic Liquid: Thin Films of 1-Ethyl-3-methylimidazolium Bis[trifluoromethanesulfonyl]imide Studied with TOF-SIMS.* J. Phys. Chem. B **112**, 15349 – 15354 (2008).

[88] C. Kolbeck, T. Cremer, K. R. J. Lovelock, N. Paape, P. S. Schulz, P. Wasserscheid, F. Maier, and H.-P. Steinrück. *Influence of different anions on the surface composition of Ionic Liquids using ARXPS.* J. Phys. Chem. B **113**, 8682–8688 (2009).

[89] K. R. J. Lovelock. *Influence of the ionic liquid/gas surface on ionic liquid chemistry.* Phys. Chem. Chem. Phys. **15**, 5071–5089 (2012).

[90] C. Länger, P. Ernst, M. Bender, D. Severin, C. Trautmann, M. Schleberger, and M. Dürr. *Single-ion induced surface modifications on hydrogen-covered Si(001) surfaces—significant difference between slow highly charged and swift heavy ions.* New J. Phys. **23**, 093037 (2021).

[91] W. Kern and D. Puotinen. *Cleaning solutions based on hydrogen peroxide for use in silicon semiconductor technology.* RCA **31**, 187 (1970).

[92] A. Portz, M. Baur, C. R. Gebhardt, and M. Dürr. *Mass spectrometry of oligopeptides in the presence of large amounts of alkali halides using desorption/ionization induced by neutral cluster impact.* Biointerphases **11**, 02A316 (2016).

[93] P. Schneider, F. Verloh, A. Portz, S. Aoyagi, M. Rohnke, and M. Dürr. *Direct Analysis of Ion-Induced Peptide Fragmentation in Secondary-Ion Mass Spectrometry.* Anal. Chem. **92**, 15604 – 15610 (2020).

[94] V. R. Deline, W. Katz, C. A. Evans, and P. Williams. *Mechanism of the SIMS matrix effect.* Appl. Phys. Lett. **33**, 832 – 835 (1978).

[95] K. Takahashi, S. Aoyagi, and T. Kawashima. *TOF-SIMS matrix effects in mixed organic layers in Ar cluster ion depth profiles.* Surf. Interface Anal. **49**, 721 – 727 (2017).

[96] S. Nakano, T. Yamagishi, S. Aoyagi, A. Portz, M. Dürr, H. Iwai, and T. Kawashima. *Evaluation of matrix effects on TOF-SIMS data of leu-enkephalin and 1, 2-dioleoyl-sn-glycero-3-phosphocholine mixed samples.* Biointerphases **13**, 03B403 (2018).

[97] A. G. Shard, A. Miisho, J.-L. Vorng, R. Havelund, I. S. Gilmore, and S. Aoyagi. *A two-point calibration method for quantifying organic binary mixtures using secondary ion mass spectrometry in the presence of matrix effects.* Surf. Interface Anal. **54**, 363–373 (2022).

[98] K. Pluschke, A. Herrmann, and M. Dürr. *Soft Deposition of Organic Molecules Based on Cluster-Induced Desorption for the Investigation of On-Surface and Surface-Mediated Reactions.* ACS Omega **8**, 40639–40646 (2023).

[99] N. Winograd. *Gas Cluster Ion Beams for Secondary Ion Mass Spectrometry.* Annu. Rev. Anal. Chem. **11**, 29 – 48 (2018).

[100] T. Fu, S. Della-Negra, D. Touboul, and A. Brunelle. *Internal Energy Distribution of Secondary Ions Under Argon and Bismuth Cluster Bombardments: SSoft"Versus "Hard"Desorption-Ionization Process.* J. Am. Soc. Mass Spectrom. **30**, 321 – 328 (2019).

[101] V. Califano, F. Bloisi, L. R. Vicari, P. Colombi, E. Bontempi, and L. E. Depero. *MAPLE deposition of biomaterial multilayers.* Appl. Surf. Sci. **254**, 7143–7148 (2008).

[102] A. Piqué. *The matrix-assisted pulsed laser evaporation (MAPLE) process: origins and future directions.* Appl. Phys. A **105**, 517–528 (2011).

[103] S. Rauschenbach, F. L. Stadler, E. Lunedei, N. Malinowski, S. Koltsov, G. Costantini, and K. Kern. *Electrospray Ion Beam Deposition of Clusters and Biomolecules.* Small **4**, 540 – 547 (2006).

[104] S. Rauschenbach, R. Vogelgesang, N. Malinowski, J. W. Gerlach, M. Benyoucef, G. Costantini, Z. Deng, N. Thontasen, and K. Kern. *Electrospray Ion Beam Deposition: Soft-Landing and Fragmentation of Functional Molecules at Solid Surfaces.* ACS Nano **10**, 2901 – 2910 (2009).

[105] P. Fremdling, T. K. Esser, B. Saha, A. A. Makarov, K. L. Fort, M. Reinhardt-Szyba, J. Gault, and S. Rauschenbach. *A preparative mass spectrometer to deposit intact large native protein complexes.* ACS nano **16**, 14443–14455 (2022).

[106] D. S. McPhail. *Applications of Secondary Ion Mass Spectrometry (SIMS) in Material Science.* J. Mater. Sci. **41**, 873 – 903 (2006).

[107] J. G. Son, S. Yoon, H. K. Shon, J. H. Moon, S. Joh, and T. G. Lee. *Ar-gas cluster ion beam in ToF-SIMS for peptide and protein analysis.* Biointerphases **15**, 021011 (2020).

[108] F. Jia, X. Zhao, and Y. Zhao. *Advancements in ToF-SIMS imaging for life sciences.* Frontiers in Chemistry **11**, 1237408 (2023).

[109] M. Lorenz, A. G. Shard, J. D. P. Counsell, S. Hutton, and I. S. Gilmore. *Angular Distribution of Molecules Sputtered by Gas Cluster Ion Beams and Implications for Secondary Neutral Mass Spectrometry.* J. Phys. Chem. C **23**, 25317–25327 (2016).

[110] V. Delmez, B. Tomasetti, T. Daphnis, C. Poleunis, C. Lauzin, C. Dupont-Gillain, and A. Delcorte. *Gas Cluster Ion Beams as a Versatile Soft-Landing Tool for the Controlled Construction of Thin (Bio)Films.* ACS Appl. Bio Mater. **5**, 3180–3192 (2022).

[111] B. R. Ringeisen, J. Callahan, P. K. Wu, A. Piqué, B. Spargo, R. A. McGill, M. Bucaro, H. Kim, D. M. Bubb, and D. B. Chrisey. *Novel Laser-Based Deposition of Active Protein Thin Films.* Langmuir **17**, 3472–3479 (2001).

[112] A. Bonciu, A. Vasilescu, V. Dinca, and S. F. Peteu. *Interfaces obtained by MAPLE for chemical and biosensors applications.* Sens. Actuators Rep. **3**, 100040 (2021).

[113] A. Portz, M. Baur, G. Rinke, S. Abb, S. Rauschenbach, K. Kern, and M. Dürr. *Chemical analysis of complex surface-adsorbed molecules and their reactios by means of cluster-induced desorption/ionization mass spectrometry.* Anal. Chem. **90**, 3328 – 3334 (2018).

[114] D. Pochan and O. Scherman. *Introduction: Molecular Self-Assembly.* Chem. Rev. **121**, 13699–13700 (2021).

[115] M. Myllys, H. Häkkänen, J. Korppi-Tommola, K. Backfolk, P. Sirviö, and J. Timonen. *X-ray microtomography and laser ablation in the analysis of ink distribution in coated paper.* J. Appl. Phys. **117**, 144902 (2015).

[116] R. Hayes, G. G. Warr, and R. Atkin. *Structure and Nanostructure in Ionic Liquids.* Chem. Rev. **115**, 6357–6426 (2015).

[117] S. M. Purcell, P. D. Lane, L. D'Andrea, N. S. Elstone, D. W. Bruce, J. M. Slattery, E. J. J. Smoll, S. J. Greaves, M. L. Costen, T. K. Minton, and K. G. McKendrick. *Surface Structure of Alkyl/Fluoroalkylimidazolium Ionic–Liquid Mixtures.* J. Phys. Chem. B **126**, 1962–1979 (2022).

[118] D. N. G. Krishna and J. Philip. *Review on surface-characterization applications of X-ray photoelectron spectroscopy (XPS): Recent developments and challenges.* Appl. Surf. Sci. Adv. **12**, 100332 (2022).

[119] N. Bundaleskia, S. Caporalib, S. P. Chenakinc, A. M. C. Moutinhoa, O. M. N. D. Teodoroa, and A. Tolstogouzova. *Ion-induced fragmentation of imidazolium ionic liquids: TOF-SIMS study.* Int. J. Mass Spectrom. **353**, 19 – 25 (2013).

[120] C. Brückner and N. Hewage. *Oxidation and Reduction of Porphyrins*, 303–347. John Wiley & Sons, Ltd (2022).

Abbildungsverzeichnis

Danksagung

Zunächst möchte ich mich bei Prof. Dr. Michael Dürr für die Überlassung des spannenden Themas, die gute Betreuung und die zielführenden Diskussionen bedanken.

Des Weiteren danke ich Priv.-Doz. Dr. Marcus Rohnke für die Übernahme des Zweigutachtens und Prof. Dr. André Schirmeisen sowie Priv.-Doz. Dr. Angelika Polity für die Mitarbeit in der Prüfungskommission.

Ich möchte mich zudem bei den Personen bedanken, die mir weitere Messungen mit anderen Messtechniken ermöglicht haben, darunter Priv.-Doz. Dr. Marcus Rohnke, Dr. Christoph R. Gebhardt, Dr. Simeon Vens-Cappell, Dr. Corinna Henkel, Dr. Joachim Sann, Dr. Daniel Martín-Jiménez und Jan-Luca Dornseifer.

Zudem bedanke ich mich bei Aaron Herrmann für seinen Beitrag zu meiner Forschung im Rahmen seiner Bachelorarbeit.

Ich danke allen meinen Kolleginnen und Kollegen, Dr. Christian Länger, Dr. Julian Heep, Dr. Tamam Bohamud, Dr. Pascal Schneider, Dr. Timo Glaser, Philip Keller, Mohit Jain und Sophie Göbel.

Besonderer Dank gilt meinen Eltern Ralf und Karla, meinen Brüdern Johannes und Mathias und meiner Oma Hildegard, die mich über so viele Jahre immer unterstützt haben.

Zu guter Letzt möchte ich mich bei meinem Mann Dennis bedanken. Du warst bei jedem Schritt an meiner Seite und das war wunderbar.

Eigenständigkeitserklärung

Hiermit versichere ich, die vorgelegte Dissertation selbstständig und ohne unerlaubte fremde Hilfe und nur mit den Hilfen angefertigt zu haben, die ich in der Dissertation angegeben habe. Alle Textstellen, die wörtlich oder sinngemäß aus veröffentlichten Schriften entnommen sind, und alle Angaben, die auf mündlichen Auskünften beruhen, sind als solche kenntlich gemacht. Bei den von mir durchgeführten und in der Dissertation erwähnten Untersuchungen habe ich die Grundsätze guter wissenschaftlicher Praxis, wie sie in der ‚Satzung der Justus-Liebig-Universität zur Sicherung guter wissenschaftlicher Praxis' niedergelegt sind, eingehalten. Ich stimme einer Überprüfung der Dissertation mittels Anti-Plagiatssoftware zu.

_____ _____

Ort, Datum Unterschrift